JOURNAL OF AGRICULTURAL AND FOOD CHEMISTRY

Food Safety and Toxicology

Zearalenone Exposure Induces the Apoptosis of Porcine Granulosa Cells and Changes Long Noncoding RNA Expression to Promote Anti-Apoptosis by Activating the JAK2-STAT3 Pathway

Fa-Li Zhang, Na Li, Han Wang, Jin-Mei Ma, Wei Shen, and Lan Li

J. Agric. Food Chem., **Just Accepted Manuscript** • DOI: 10.1021/acs.jafc.9b05189 • Publication Date (Web): 07 Oct 2019

Just Accepted

is published by the American Chemical Society. 1155 Sixteenth Street N.W., Washington, DC 20036

Zearalenone Exposure Induces the Apoptosis of Porcine Granulosa Cells and Changes Long Noncoding RNA Expression to Promote Anti-Apoptosis by Activating the JAK2-STAT3 Pathway

Fa-Li Zhang [&], Na Li [#], Han Wang [&], Jin-Mei Ma[+], Wei Shen[&], Lan Li [&,*]

& College of Life Sciences, Qingdao Agricultural University, Qingdao 266109, China;

 # College of Animal Science and Technology, Qingdao Agricultural University, Qingdao 266109, China;

+ Animal Husbandry and Veterinary Station of Penglai City, Yantai 265600, China

*** Correspondence and reprint requests to:**

Dr. Lan Li, E-mail: lli@qau.edu.cn; lilan9600@126.com

ABSTRACT

Zearalenone (ZEA), a pathogenic toxin produced by *Fusarium*, is widely detected in moldy feed materials. Previous studies have reported that ZEA exerts a harmful influence to animal reproductive systems, however, its effects on the changes of long noncoding RNAs (lncRNAs) remain unclear. Here, tackling this question, we performed RNA-seq on porcine granulosa cells (GCs) after being exposed to 10 μM and 30 μM ZEA *in vitro*. The results showed that ZEA exposure observably changed the expression of lncRNAs in porcine GCs and increased the rate of apoptosis. Furthermore, Gene Ontology analysis showed that ZEA exposure induced variation of the JAK2-STAT3 signaling pathway in porcine GCs. To verify our bioinformatics analysis, western blotting and immunofluorescence analysis were performed and the results demonstrated that porcine GCs after ZEA exposure increased the expression of key proteins in the JAK2-STAT3 signaling pathway. Further bioinformatics analysis found that MSTRG.22680 and MSTRG.23882 played a pivotal role in activating the JAK2-STAT3 signaling pathway. To summarize, our results throw light on the fact that ZEA exposure dramatically increases the apoptosis of porcine GCs and alters the expression of lncRNAs that play an anti-apoptotic role in porcine GCs via activating the JAK2-STAT3 signaling pathway.

Key words: Zearalenone; porcine granulosa cells; apoptosis; lncRNA; JAK2-STAT3 signaling pathway

Introduction

Zearalenone (ZEA), produced by *Fusarium*[1], tends to lead to reproductive toxicity and can be easily detected in contaminated livestock feeds[2]. It was reported that ZEA contamination was as high as 800-1,000 mg/kg in some feed materials in some regions[3]. Moreover, numerous studies reported that ZEA had a structure similar to 17β-estradiol (E2), and ZEA and estrogen combined competitively with estrogen receptors (ERs)[4], which led to ZEA exerting estrogenic effects when animals were exposed to it[5]. ZEA has been shown to perform a bad effect on the reproductive system of exposed animals, mainly influencing the ovary, uterus and so on, in which ERs tend to show high levels of expression[6]. Notably, the findings of a previous research revealed that ZEA exposure affected follicular development and oocyte maturation[7], and studies else indicated that ZEA induced oxidative stress in porcine granulosa cells (GCs)[8] and affected the progression of meiosis in mouse oocytes[9]. In addition, ZEA exposure down-regulated the expression of LIM Homeobox 8 (*Lhx8)*, in turn, impaired ovarian primordial follicle formation in mice[10]. Thus, ZEA exposure exerts negative effects on animal production systems, the research of the mechanism of ZEA exposure is necessary to alleviate the loss resulting from ZEA exposure, unfortunately, so far, it remains an unanswered question.

How does ZEA affect animal reproductive systems? There are the two primary events, such as follicular growth and atresia. During folliculogenesis, atresia largely results from the apoptosis of granulosa cells (GCs)[11]. GCs were indispensable for folliculogenesis and the studies demonstrated that GCs affected follicular development via releasing signal molecules that were essential for follicular development and maturation[12]. In addition, recent work has shown that ZEA exposure induces apoptosis of the GCs in several species[13-14]. Though we have

done many works to reveal the potential effects caused by ZEA exposure[8-9, 13-14], the exact molecular mechanism underlying ZEA induced cytotoxicity remains unclear. In fact, most studies focused on the dynamical changes at the mRNA level, while limited studies are available that investigated the mechanism of how ZEA exposure affects cellular apoptosis by the changes of long non-coding RNAs (lncRNAs).

LncRNAs are referred to cellular RNAs molecules, which length is longer than 200 bp and cannot be translated into proteins[15]. LncRNAs studies on the ovary have mainly been focused on their effects on ovarian cancers. Many lncRNAs have been shown to play the vital roles in promoting cellular proliferation and inhibiting cellular apoptosis in ovarian cancers including PVT1, LSINCT5, MEG3 and others[16-18]. A growing number of studies have illustrated that lncRNAs perform an important function in multiple biologic processes, such as apoptosis[19,20-21]. Additionally, one of the mechanisms by which lncRNAs regulate cellular apoptosis is the silencing of microRNA[22]. Currently, lncRNAs are emerging as new participants in gene regulation but the mechanism of how lncRNAs work to regulate growth and apoptosis in GCs remains to be fully described.

The JAK-STAT signaling pathway is relevant to many important biological processes including cellular proliferation, differentiation, apoptosis and immune regulation[23]. Compared with other signaling pathways, JAK-STAT signaling pathway is relatively simple and consists of three components, namely, tyrosine kinase associated receptor, Janus kinase (JAK) and the signal transducer and activator of transcription (STAT)[24]. One of the branches is the JAK2-STAT3 signaling pathway, which main function of it is anti-apoptosis[25]. It's worth noting that STAT3 is an anti-apoptosis transcription factor[25].

Distinct from previous reports, the aim here is to better uncover the in-depth mechanism of lncRNAs in porcine GCs after ZEA exposure. The function of lncRNAs about apoptosis of porcine GCs after ZEA exposure was preliminarily explored in this research. The findings of our research will provide a theoretical basis for the mitigation of the harmful effects of ZEA in animal husbandry.

Materials and Methods

Porcine granulosa cell culture and experimental design

Porcine ovaries were collected into saline supplemented with 1 % penicillin-streptomycin from Qingdao Wanfu Group Co., Ltd. (Qingdao, Shandong, China) and taken it back to the laboratory within 2 h. Briefly, follicular fluid in 3 to 5 mm follicles was collected by a 10 ml syringe, then the GCs were isolated and cultured in DMEM high glucose medium (HyClone, SH30022.01, Beijing, China). 10 % fetal bovine serum (FBS, Gibco, 10099-141, Australia), 1 % penicillin-streptomycin (HyClone, SV30010, Beijing, China) and 0.2 % gentamicin (BBI, EB30KA0357, Shanghai, China) were added to medium, then the GCs were cultured at 37 °C in a 5 % CO_2 atmosphere.

When primary GCs grew to about 50 % - 70 % confluency, they were treated with 10 μM or 30 μM ZEA (Sigma-Aldrich, Z2125, MO, USA), Dimethyl sulfoxide (DMSO) was adopted to dissolve ZEA and it was stored at -20 °C, meanwhile the control (Ctrl) group was treated with vehicle only. Concentrations used in this study were based on our previous finding that 10 and 30 μM of ZEA had dramatic adverse effects on porcine GCs[14]. All the animal treatment procedures in this paper have been approved by the Ethics Committee of Qingdao Agricultural

University.

Sequencing and quality control

Briefly, about total 4 μg RNA was isolated per sample and the sequencing libraries were generated according to standard protocol, then the libraries were sequenced using the Hiseq4000 platform at Novogene Co., Ltd. (Beijing, China).

FastQC (version v0.11.8) was adopted to assess the quality of the raw data. Moreover, Fastp (version v0.19.5) was used to remove low quality data, adapter and poly-N sequences. Clean data were collected, and then the basic information, including the value of GC content, Q20 and Q30, of it was calculated[26]. All analysis of downstream steps was done using the filtered clean data.

Transcriptome assembly

We downloaded porcine reference genome and gene model annotation files from the NCBI database (version Sscrofa11.1). STAR (version STAR_2.7.0b) was selected to build the index of reference genome, subsequently we utilized STAR to put paired-end clean reads aligned to the reference genome. Moreover, we utilized Stringtie (version 1.3.4d) to assemble the transcriptome of each library[27]. Stringtie run with "-rf", "FPKM=0.5", "TPM=0.5" and other options were set as default.

Filtering pipeline in order to identify lncRNAs

We selected candidate lncRNAs using the following filtering pipeline: 1) The transcripts,

annotated as “i”, “x”, “u”, “o” or “e” by the bio-software gffcompare (version v0.10.6), were left for the moreover filter. 2) The transcripts of single-exon, length ≤ 200, FPKM (Fragments Per Kilobase per Million reads) < 0.5 and TPM (Transcripts Per Kilobase Million) < 0.5 were filtered by Stringtie when merging the file of transcripts. 3) The remaining transcripts which passed above filtered steps, were assessed their coding potential by the Coding Potential Calculator 2 (CPC2), Coding-Non-Coding-Index (CNCI) and Pfamscan, and the threshold of these softwares were that score < 0 and tag as ‘noncoding’, score < 0 and tag as ‘noncoding’, tag as ‘noncoding’, respectively[28-30]. 4) The left behind was perceived as the transcriptome of lncRNA. The HTSeq software was adopted to count reads of lncRNAs for providing input for later analysis. Parameters were ‘-s yes’ and default of others.

Expression analysis

The expression of mRNA and lncRNA was confirmed with FPKM calculated by a custom script and in this study all expression of mRNA and LncRNA was used in this data. The DESeq2 software package was used to determine differentially expressed mRNAs (DEMs) and differentially expressed lncRNAs (DELs). We used the *padj* < 0.05 and | log2FoldChange | >1 as threshold to determine the differently expressed lncRNAs or mRNAs[31]. The trend of expression level and trend of lncRNAs were observed by the Chord Diagram and Heatmap.

Co-location analysis

Cis-role of lncRNA is aimed at adjacent genes[32-33]. The FEELnc (version v0.1.1) was used to search for all coding genes which located at 10 kb – 100 kb upstream or downstream of all the

confirmed lncRNAs[34]. We only made co-location analysis of the core lncRNAs. The core lncRNA that we used a step - by - step reduction scheme to determine. Briefly, we obtained the intersection of different difference groups, finally we gained the core lncRNAs.

Co-expression analysis

It was reported that the *trans*-role of lncRNAs was related to their co-expressed genes[35]. The DEMs and DELs were identified by co-expression analysis. In order to investigate the function of DELs, we calculated Pearson's correlation coefficients (r) between DELs and DEMs using R package named Hmisc (version 4.2-0, http://biostat.mc.vanderbilt.edu/Hmisc). We selected relational pair with $| r | > 0.9$ and $pvalue < 0.05$ as the co-expressed genes of lncRNAs.

Gene Ontology (GO) and Kyoto Encyclopedia of Genes and Genomes (KEGG) signaling pathway enrich analysis

The co-location and co-expression genes were performed function enrich analysis, including GO terms and KEGG signaling pathway analysis, by clusterProfiler (R package, version 3.8.1, R version 3.5.1) and ClueGo (a plugin of Cytospace, version v2.5.4, Cytospace version v3.7.1)[36-37]. GO terms with $pvalue < 0.01$ and KEGG pathways with $pvalue < 0.05$ were considered as significantly enriched.

Flow cytometry analysis of apoptosis

After porcine GCs exposed 10 μM or 30 μM ZEA for 48 h, the flow cytometry was utilized to detect the level of apoptosis of it. Briefly, GCs were collected and we utilized PBS to wash it

at least three times. Then, according to the manufacturer's instructions the Annexin V-FITC/PI kit (Tran, Fa101, Beijing, China) was added to samples. Notably, the PI has adhesion, so before flow cytometry, the GCs were filtered using 150 mesh sieves and washed clean as much as possible. Subsequently, the FACSCalibur flow cytometer detected these samples.

Immunofluorescence

Immunofluorescence analysis (IF) was performed by a standard method with minor modifications[38]. Briefly, immunofluorescence was performed with the following steps: 1) We collected the adherent GCs, which were digested with trypsin for 3 minutes at 37 °C. 2) GCs were put into 4 % paraformaldehyde at 4 °C for at least 45 minutes. 3) About 30 μl cell suspensions were smeared on slide glass. The smears were permeabilized for 10 minutes in PBST (PBS added 0.5 % Triton X-100) then blocked for 45 minutes in PBST supplemented with 10 % goat serum (BOSTER, AR0009, Wuhan, China). 4) Slides were then incubated with primary antibodies (Table S1) at 4 °C overnight. 5) Then the secondary antibodies were added and incubated for at least 45 minutes at 37 °C. 6) We used Hoechst33342 to perform nuclei staining for 5 minutes and the slides were finally mounted with Antifade Mounting Medium. The fluorescence imaging system (Olympus BX51, Tokyo, Japan) was used to take photos and performed subsequent analysis.

Western blotting

Western blotting (WB) analysis was performed by a standard method with minor modifications and was used to detect the expression of proteins [39-40]. Briefly, the SDS-PAGE separated the

total proteins and then shifted it to PVDF membranes. Subsequently, blocked the PVDF membranes carrying protein in TBST (Tris-buffered saline with Tween-20) buffer added 5 % bovine serum albumin (BSA, Solarbio, A8020, Beijing, China) at 4 °C for at least 2 h, the PVDF membranes were then incubated in TBST buffer added 10 % BSA with primary antibody (Table S2) for at least 7 h at 4 °C. The next step is that the PVDF membranes were incubated in TBST buffer with secondary antibodies for 2 h. Finally, we adopted AlphaView SA software to determine the levels of expression of proteins.

Statistical analysis

All experiments were subjected to at least three independent replicates, except for Flow cytometry analysis of apoptosis, because we only wanted to verify the repeatability of previous studies. We adopted mean ± SEM (Standard Error of Mean) to show data, used one-way ANOVA with Duncan's multiple range test to determine differences among samples and further rechecked the results by Student's t test via Graphpad Prism 8.0 software.

Results

Overview of RNA sequencing and lncRNAs identification in porcine GCs exposed to ZEA *in vitro*

Previous research has indicated that ZEA exposure causes toxic effects on animal ovarian cells [13-14], but the effect on lncRNA expression in porcine GCs has not been described. To investigate the lncRNA expression dynamics following ZEA exposure, the porcine GCs were cultured *in vitro* and exposed to different concentration ZEA, including 10 μM and 30 μM, respectively

(Fig. 1A).

As culture proceeded, cellular apoptosis increased from 24 h and 48 h groups (Fig. 1B). Annexin-V fluorescence analysis showed that after ZEA exposure for 48 h, in terms of the experimental group, the percentage of positive GCs was dramatically increased with ZEA concentration (Fig. 1C). Early apoptotic cells were slightly elevated in the Ctrl (3.28 %), 10 μM (4.72 %) and 30 μM (5.59 %) groups, respectively. A larger change was seen in the late apoptotic cells where the 30 μM ZEA exposed group (29.3 %) was significantly higher when comparing to the Ctrl (10.0 %) and the 10 μM (14.3 %) groups (Fig. 1D).

To further study the toxic effect of ZEA exposure on porcine GCs, we performed an RNA-seq study. A brief diagrammatic drawing of the porcine GCs *in vitro* culture model and experimental procedures of this study are in Fig. 1A. With the RNA-seq 64,164,686 raw reads were generated in all 6 libraries, and after quality control we gained 63,587,260 clean reads (Fig. S1A). We adopted a highly strict filtering pipeline to identify the lncRNAs, which could remove transcripts without the characteristics of lncRNA (Fig. 1E). We compared the length of mRNA and lncRNA and revealed that mRNA was located on 0 to 10,000 bp, while the lncRNA was located on 200 to 5,000 bp (Fig. 1F). This pipeline produced 3,202 lncRNA genes with 3,811 lncRNA transcripts relevant to this (Figs. 1G and S1B). To verify the stability of samples, we made the correlation analysis based on Euclidean distances and the principal components analysis (Figs. S1C and S1D).

Identification of differential expression of lncRNAs and mRNAs

To further explore the effect of ZEA on the differential expression of lncRNAs and mRNAs in

porcine GCs, DESeq2 was utilized. For lncRNAs, there were 100, 106 and 12 up-regulated lncRNAs in the Ctrl *vs.* 10 μM group, the Ctrl *vs.* 30 μM group and the 10 μM *vs.* 30 μM group, respectively; conversely, the down-regulated lncRNAs were 115, 139 and 28, respectively (Fig. 2A). For mRNAs, the up-regulated expression was 332, 442 and 11 in the different groups, respectively. Meanwhile, the down-regulated expression was 615, 837 and 24 in the different groups, respectively (Fig. 2B).

Furthermore, Chord Diagram was utilized to show the distribution and expression of each lncRNA and mRNA per chromosome (Fig. 2C). Interestingly, overall the number of DELs was less than DEMs. In chromosome 2, chromosome 3 and chromosome X, the DEMs were much more than the DELs. In chromosome 7, there was an expressional peak of lncRNAs, and in chromosome X, there was an expressional peak of mRNAs, which may be related to their respective functions.

Function overview of DELs

It has been reported that the *trans*-role of lncRNAs is related to their co-expressed genes[35]. To investigate the function of DELs, in the different treatment groups, we calculated the Pearson's correlation coefficients between DELs and DEMs using Hmisc. The results showed that 947 co-expressed mRNAs (CEMs) related to lncRNAs were differentially expressed in the Ctrl *vs.* 10 μM group, and 1,248 CEMs related to lncRNAs were differentially expressed in the Ctrl *vs.* 30 μM group (Fig. 3A).

Subsequently, we performed the GO enrich analysis of these CEMs. In the Ctrl *vs.* 10 μM group (Figs. 3B and 3D), we found that the CEMs carried 70 biological process GO terms and

we showed the top 20 according to *pvalues*. Furthermore, ClueGo, showed 26 biological process GO terms. We found that the top 3 GO terms according to *pvalues* were GO:0051607 (defense response to virus), GO:0009615 (response to virus) and GO:0043330 (response to exogenous dsRNA), using clusterProfiler. Moreover, ClueGo also showed the biological process GO term, GO:0043330. In the Ctrl *vs.* the 30 μM group (Figs. 3C and 3E) we found that the CEMs carried 54 biological process GO terms and we showed the top 20 according to *pvalues*. ClueGo, showed 11 biological process GO terms. We found that the top 3 GO terms according to *pvalues* were GO:0051607, GO:0043604 (amide biosynthetic process), and GO:0006412 (translation). Moreover, ClueGo also showed the biological process GO term, GO:0051607.

In addition, some biological process GO terms related to the JAK-STAT signaling pathway were enriched, including GO:0033139 (regulation of peptidyl-serine phosphorylation of STAT protein), GO:0033141 (positive regulation of peptidyl-serine phosphorylation of STAT protein) and GO:0042501 (serine phosphorylation of STAT protein), which suggested that the JAK-STAT signaling pathway plays crucial roles in porcine GCs after ZEA exposure.

Further analysis of DELs

Further exploration of the function of different clustered lncRNAs was performed. We explored the function of lncRNAs, including the intersection between the differentially expressed lncRNA in the Ctrl *vs.* 10 μM group and the Ctrl *vs.* 30 μM group (Fig. 4A).

We found the Chord Diagram and Heatmap showed dynamic expression patterns (Figs. 4B-4C). Subsequently, GO and KEGG signaling pathway enrichment analysis of CEMs were

283 performed in the Ctrl *vs.* 10 μM group. We found 936 CEMs and in the Ctrl *vs.* 30 μM group
284 co-expression of mRNAs was 1,248 (Fig. 4D). Similarly, we utilized the two software
285 platforms, clusterProfiler and ClueGO, to perform GO and KEGG signaling pathway
286 enrichment analysis. We identified GO terms related to the JAK-STAT signaling pathway,
287 including GO:0033141 and GO:0033139 (Figs. 4E and 4F). KEGG signaling pathway
288 enrichment analysis showed that many terms related to disease, such as ssc05414 (dilated
289 cardiomyopathy (DCM)) were enriched (Figs. S2A and S2B).

290 Next, we performed the same analysis for the following lncRNAs, including the
291 intersection between the DELs in the Ctrl *vs.* 10 μM group and the 10 μM *vs.* 30 μM group
292 (Figs. S3) and the intersection between the DELs in the Ctrl *vs.* 30 μM group and the 10 μM
293 *vs.* 30 μM group (Figs. S4).

294

295 **Identification of the core lncRNA cluster**

296 In order to identify the core lncRNA cluster, we believed that the intersections between the
297 differentially expressed lncRNA in the Ctrl *vs.* 10 μM group, the Ctrl *vs.* 30 μM group and the
298 10 μM *vs.* 30 μM group would identify the core lncRNA cluster. To identify the function of
299 this cluster of lncRNAs (Fig. 5A), the Chord Diagram and Heatmap showed dramatically
300 dynamic expression patterns in this cluster (Figs. 5C and 5E). *Cis*-regulation analysis and
301 *trans*-regulation analysis were performed.

302 On the one hand, lncRNA could serve as trans-regulatory elements and control the
303 expression of adjacent genes, here we detected 780, 1,101 and 26 CEMs in the Ctrl *vs.* 10 μM
304 group, the Ctrl *vs.* 30 μM group and the 10 μM *vs.* 30 μM group, respectively (Fig. 5B). Two

methods, GO and KEGG signaling pathway enrichment analysis, were used to predict the function of the lncRNAs.

In the Ctrl *vs.* 10 μM groups we found that the CEMs carried 30 biological process GO terms while ClueGo showed 17 biological process GO terms (Figs. 5G and 5I). In these GO terms, many were related to the JAK2-STAT3 signaling pathway, including GO:0033139, GO:0033141, GO:0042501 and so on. For KEGG signaling pathway terms in this group, the results indicated that many terms were related to disease, such as ssc05414 (Fig. S5A). In the Ctrl *vs.* 30 μM group, we found that the CEMs carried 48 biological process GO terms while ClueGO showed 14 Biological process GO terms (Figs. 5H and 5J). Many of the GO terms were related to the JAK-STAT signaling pathway by further analysis, including GO:0033139, GO:0046425 (regulation of JAK-STAT cascade), GO:1904892 (regulation of STAT cascade), and so on. We analyzed all biological process GO terms and the Venn diagram showed a relationship between the different group, including 7 shared terms (Fig. 5D)**.** We analyzed the 7 shared terms and found that some terms were related to the JAK-STAT signaling pathway, including GO:0033139, GO:0033141 and GO:0042501, this GO terms hinted that it was related to regulation STAT protein.

The results of KEGG signaling pathway analysis in this group showed that this part of lncRNA (Fig. 5A) may be related to disease, such as ssc05414 (Fig. S5B). One the other hand, we searched for all coding genes, which were located at 10 kb-100 kb upstream and downstream of this part of lncRNAs (Fig. 5A). The results showed that MSTRG.26353, MSTRG.26354 and MSTRG.26355 were next to *TOP2A* (Fig. 5F). It had been reported that *TOP2A* was related to cell cycle, cell survival and so on[41-43].

Based on the above analysis, we chose to verify the core proteins of the JAK-STAT signaling pathway by WB and IF analysis, such as JAK2 and STAT3. The results of IF analysis showed that porcine GCs significantly up-regulated the expression of STAT3 after ZEA exposure (Figs. 6A and 6C). Porcine GCs also up-regulated the expression of JAK2 after ZEA exposure, however it was not as obvious as STAT3 (Figs. 6B and 6D). The results of WB analysis showed that porcine GCs up-regulated the expression of JAK2 and STAT3 after ZEA exposure, meanwhile the functional STAT3 protein, p-STAT3, was also up-regulated though not significantly (Figs. 6E-6G).

Prediction of the key lncRNA of regulating JAK-STAT signaling pathway

In order to find which lncRNA played a core role in regulating the JAK-STAT signaling pathway, we performed hierarchical cluster analysis. The results showed that for the left branch, the correlation between MSTRG.26353 and MSTRG.26355 was strongest, and for the right, the correlation between MSTRG.22680 and MSTRG.23882 was strongest (Fig. 7A). We hypothesize that either MSTRG.26353 and MSTRG.26355 or MSTRG.22680 and MSTRG.23882 played pivotal role in regulating JAK-STAT signaling pathway.

We then performed co-expression analysis of MSTRG.26353 and MSTRG.26355 or MSTRG.22680 and MSTRG.23882. The results showed that in the Ctrl *vs.* 10 μM groups MSTRG.26353 and MSTRG.26355 carried 3 CEMs, and in the Ctrl *vs.* 30 μM group it carried 9 (Fig. 7A). For MSTRG.22680 and MSTRG.23882, it carried 587 CEMs in the Ctrl *vs.* 10 μM groups and 994 in the Ctrl *vs.* 30 μM groups (Fig. 7A). We performed GO enrichment analysis for co-expression. There were no GO terms enriched in the CEMs of MSTRG.26353

and MSTRG.26355. However, these CEMs of MSTRG.22680 and MSTRG.23882 showed GO terms related to the JAK2-STAT3 signaling pathway (Fig. 7B), which indicated that MSTRG.22680 and MSTRG.23882 may play a vital role in regulating JAK2-STAT3 signaling pathway.

Discussion

ZEA, a harmful toxin commonly found in contaminated feedstuffs, played negative influences in the development of GCs. Consistent to previous studies[10, 13-14], we also found that ZEA exposure was able to induce the apoptosis of porcine GCs. Based on this, the study of porcine GCs after ZEA exposure carries a certain significance, which may provide the theoretical basis to reduce the loss resulting from ZEA exposure to the animal industry.

Recently, studies of ZEA exposure have been mainly focused on mRNAs rather than on lncRNAs[10, 14]. In this paper, for the first time we focused on the changes of lncRNA in porcine GCs after ZEA exposure. To obtain a better comprehension of regulation of lncRNAs in porcine GCs after ZEA exposure, we adopted RNA-seq technology in this research. Moreover, RNA-seq also revealed that porcine GCs after ZEA exposure had altered lncRNAs and mRNAs expression. Notably, the potential coding capability was the key to distinguish the non-coding and protein-coding genes. In this research, we performed a highly rigorous filtering workflow to maximize the identification of positive candidate lncRNAs. We selected Stringtie to perform transcriptome assembly and identified 3202 candidate lncRNAs[27]. In agreement with similar studies, the candidate lncRNAs had these basic characteristics, compared with the protein-coding genes, they had fewer exon numbers and their transcript lengths were shorter[44-45]. Our

data showed that the expression of lncRNA was dramatically changed. In general, there were more up-regulated lncRNAs in porcine GCs after ZEA exposure, which indicated that porcine GCs after ZEA exposure caused changes in genomic expression[14].

In order to better understand the functional mechanism of lncRNAs, we took the function of the DELs after exposure to ZEA into consideration. The GO terms of CEMs were related to the JAK-STAT signaling pathway. Moreover, through further analysis of the GO terms we specifically identified the JAK2-STAT3 signaling pathway, which was a branch of JAK-STAT signaling pathway, playing a major role. Interestingly, JAK2-STAT3 signaling pathway is related to anti-apoptosis mechanism[25]. The above analysis seems to be at odds with previous studies[14], but may be interpreted that it is a self-protection mechanism. In order to explore this, we analyzed the intersection of differentially expressed lncRANs in different groups. We found that some lncRNAs were indeed related to the regulation of the JAK2-STAT3 signaling pathway. In addition, we determined the core lncRNA cluster showing that its function was related to regulating the JAK2-STAT3 signaling pathway. Many studies illustrated that the JAK2-STAT3 signaling pathway exerts a vital role in regulating apoptosis since STAT3 has anti-apoptosis abilities[46-47]. After ZEA exposure, the expression of related proteins was up-regulated. GCs will regulate lncRNAs to activate the JAK2-STAT3 signaling pathway when their survival is threatened as an instinctive form of self-preservation. For the core lncRNA cluster, MSTRG.22680 and MSTRG.23882 played a key role in activating the JAK2-STAT3 signaling pathway, which provides guidance for subsequent studies.

In summary, our findings suggest that ZEA exposure dramatically increases the porcine GCs apoptosis and the change of lncRNAs expression promotes GCs anti-apoptosis via

activating the JAK2-STAT3 signaling pathway.

Abbreviations used

ZEA, Zearalenone; GCs, granulosa cells; JAK, Janus kinase; STAT, signal transducer and activator of transcription; RNA-seq, ribonucleic acid sequencing; FPKM, fragments per kilobase per million reads; TPM, transcripts per kilobase million; CPC2, coding potential calculator 2; CNCI, coding-non-coding-index; DMEM, Dulbecco's modified Eagle's medium; FBS, fetal bovine serum; BSA, bovine serum albumin; GO, gene ontology; KEGG, kyoto encyclopedia of genes and genomes; WB, western blotting; IF, immunofluorescence; SEM, standard error of mean; DELs, differentially expressed lncRNAs; DEMs, differentially expressed mRNAs; CEMs, co-expressed mRNAs.

Conflicts of interest

None.

Acknowledgements

This work was supported by National Natural Science Foundation of China (31572225), National Key Research and Development Program of China (2016YFD0501207) and Taishan Scholar Construction Foundation of Shandong Province. The authors would also like to thank Dr. Paul W. Dyce at the University of Auburn and Dr. Shen Yin at Qingdao Agricultural University for their careful edits to the manuscript.

References

1. Caldwell, R. W.; Tuite, J.; Stob, M.; Baldwin, R., Zearalenone production by Fusarium species. *Appl Microbiol* **1970,** *20* (1), 31-4.
2. Kuiper-Goodman, T.; Scott, P. M.; Watanabe, H., Risk assessment of the mycotoxin zearalenone. *Regul Toxicol Pharmacol* **1987,** *7* (3), 253-306.
3. Muller, H. M.; Reimann, J.; Schumacher, U.; Schwadorf, K., Fusarium toxins in wheat harvested during six years in an area of southwest Germany. *Nat Toxins* **1997,** *5* (1), 24-30.
4. Pang, J.; Zhou, Q.; Sun, X.; Li, L.; Zhou, B.; Zeng, F.; Zhao, Y.; Shen, W.; Sun, Z., Effect of low-dose zearalenone exposure on reproductive capacity of male mice. *Toxicol Appl Pharmacol* **2017,** *333*, 60-67.
5. Yang, D.; Jiang, X.; Sun, J.; Li, X.; Li, X.; Jiao, R.; Peng, Z.; Li, Y.; Bai, W., Toxic effects of zearalenone on gametogenesis and embryonic development: A molecular point of review. *Food Chem Toxicol* **2018,** *119*, 24-30.
6. Kuiper, G. G.; Lemmen, J. G.; Carlsson, B.; Corton, J. C.; Safe, S. H.; van der Saag, P. T.; van der Burg, B.; Gustafsson, J. A., Interaction of estrogenic chemicals and phytoestrogens with estrogen receptor beta. *Endocrinology* **1998,** *139* (10), 4252-63.
7. Lai, F. N.; Ma, J. Y.; Liu, J. C.; Wang, J. J.; Cheng, S. F.; Sun, X. F.; Li, L.; Li, B.; Nyachoti, C. M.; Shen, W., The influence of N-acetyl-l-cysteine on damage of porcine oocyte exposed to zearalenone in vitro. *Toxicol Appl Pharmacol* **2015,** *289* (2), 341-8.
8. Qin, X.; Cao, M.; Lai, F.; Yang, F.; Ge, W.; Zhang, X.; Cheng, S.; Sun, X.; Qin, G.; Shen, W.; Li, L., Oxidative stress induced by zearalenone in porcine granulosa cells and its rescue by curcumin in vitro. *PloS one* **2015,** *10* (6), e0127551.
9. Liu, K. H.; Sun, X. F.; Feng, Y. Z.; Cheng, S. F.; Li, B.; Li, Y. P.; Shen, W.; Li, L., The impact of Zearalenone on the meiotic progression and primordial follicle assembly during early oogenesis. *Toxicol Appl Pharmacol* **2017,** *329*, 9-17.
10. Zhang, G. L.; Sun, X. F.; Feng, Y. Z.; Li, B.; Li, Y. P.; Yang, F.; Nyachoti, C. M.; Shen, W.; Sun, S. D.; Li, L., Zearalenone exposure impairs ovarian primordial follicle formation via down-regulation of Lhx8 expression in vitro. *Toxicol Appl Pharmacol* **2017,** *317*, 33-40.
11. Matsuda, F.; Inoue, N.; Manabe, N.; Ohkura, S., Follicular growth and atresia in mammalian ovaries: regulation by survival and death of granulosa cells. *J Reprod Dev* **2012,** *58* (1), 44-50.
12. Lai, F. N.; Liu, J. C.; Li, L.; Ma, J. Y.; Liu, X. L.; Liu, Y. P.; Zhang, X. F.; Chen, H.; De Felici, M.; Dyce, P. W.; Shen, W., Di (2-ethylhexyl) phthalate impairs steroidogenesis in ovarian follicular cells of prepuberal mice. *Arch Toxicol* **2017,** *91* (3), 1279-1292.
13. Zhang, R. Q.; Sun, X. F.; Wu, R. Y.; Cheng, S. F.; Zhang, G. L.; Zhai, Q. Y.; Liu, X. L.; Zhao, Y.; Shen, W.; Li, L., Zearalenone exposure elevated the expression of tumorigenesis genes in mouse ovarian granulosa cells. *Toxicol Appl Pharmacol* **2018,** *356*, 191-203.
14. Liu, X. L.; Wu, R. Y.; Sun, X. F.; Cheng, S. F.; Zhang, R. Q.; Zhang, T. Y.; Zhang, X. F.; Zhao, Y.; Shen, W.; Li, L., Mycotoxin zearalenone exposure impairs genomic stability of swine follicular granulosa cells in vitro. *Int J Biol Sci* **2018,** *14* (3), 294-305.
15. Baley, J.; Li, J., MicroRNAs and ovarian function. *J Ovarian Res* **2012,** *5*, 8.
16. Zhan, L.; Li, J.; Wei, B., Long non-coding RNAs in ovarian cancer. *J Exp Clin Cancer Res* **2018,** *37* (1), 120.
17. Silva, J. M.; Boczek, N. J.; Berres, M. W.; Ma, X.; Smith, D. I., LSINCT5 is over expressed in breast and ovarian cancer and affects cellular proliferation. *RNA Biol* **2011,** *8* (3), 496-505.
18. Lyu, Y.; Lou, J.; Yang, Y.; Feng, J.; Hao, Y.; Huang, S.; Yin, L.; Xu, J.; Huang, D.; Ma, B.; Zou, D.; Wang, Y.;

Zhang, Y.; Zhang, B.; Chen, P.; Yu, K.; Lam, E. W.; Wang, X.; Liu, Q.; Yan, J.; Jin, B., Dysfunction of the WT1-MEG3 signaling promotes AML leukemogenesis via p53-dependent and -independent pathways. *Leukemia* **2017,** *31* (12), 2543-2551.

19. Rossi, M. N.; Antonangeli, F., LncRNAs: New Players in Apoptosis Control. *Int J Cell Biol* **2014,** *2014*, 473857.

20. Pickard, M. R.; Mourtada-Maarabouni, M.; Williams, G. T., Long non-coding RNA GAS5 regulates apoptosis in prostate cancer cell lines. *Biochim Biophys Acta* **2013,** *1832* (10), 1613-23.

21. Wang, O.; Yang, F.; Liu, Y.; Lv, L.; Ma, R.; Chen, C.; Wang, J.; Tan, Q.; Cheng, Y.; Xia, E.; Chen, Y.; Zhang, X., C-MYC-induced upregulation of lncRNA SNHG12 regulates cell proliferation, apoptosis and migration in triple-negative breast cancer. *Am J Transl Res* **2017,** *9* (2), 533-545.

22. Wang, K.; Long, B.; Zhou, L. Y.; Liu, F.; Zhou, Q. Y.; Liu, C. Y.; Fan, Y. Y.; Li, P. F., CARL lncRNA inhibits anoxia-induced mitochondrial fission and apoptosis in cardiomyocytes by impairing miR-539-dependent PHB2 downregulation. *Nature communications* **2014,** *5*, 3596.

23. O'Shea, J. J.; Gadina, M.; Schreiber, R. D., Cytokine signaling in 2002: new surprises in the Jak/Stat pathway. *Cell* **2002,** *109 Suppl*, S121-31.

24. Schroder, K.; Hertzog, P. J.; Ravasi, T.; Hume, D. A., Interferon-gamma: an overview of signals, mechanisms and functions. *J Leukoc Biol* **2004,** *75* (2), 163-89.

25. Catlett-Falcone, R.; Landowski, T. H.; Oshiro, M. M.; Turkson, J.; Levitzki, A.; Savino, R.; Ciliberto, G.; Moscinski, L.; Fernandez-Luna, J. L.; Nunez, G.; Dalton, W. S.; Jove, R., Constitutive activation of Stat3 signaling confers resistance to apoptosis in human U266 myeloma cells. *Immunity* **1999,** *10* (1), 105-15.

26. Chen, S.; Zhou, Y.; Chen, Y.; Gu, J., fastp: an ultra-fast all-in-one FASTQ preprocessor. *Bioinformatics* **2018,** *34* (17), i884-i890.

27. Pertea, M.; Pertea, G. M.; Antonescu, C. M.; Chang, T. C.; Mendell, J. T.; Salzberg, S. L., StringTie enables improved reconstruction of a transcriptome from RNA-seq reads. *Nat Biotechnol* **2015,** *33* (3), 290-5.

28. Sun, L.; Luo, H.; Bu, D.; Zhao, G.; Yu, K.; Zhang, C.; Liu, Y.; Chen, R.; Zhao, Y., Utilizing sequence intrinsic composition to classify protein-coding and long non-coding transcripts. *Nucleic Acids Res* **2013,** *41* (17), e166.

29. Kang, Y. J.; Yang, D. C.; Kong, L.; Hou, M.; Meng, Y. Q.; Wei, L.; Gao, G., CPC2: a fast and accurate coding potential calculator based on sequence intrinsic features. *Nucleic Acids Res* **2017,** *45* (W1), W12-W16.

30. Li, W.; Cowley, A.; Uludag, M.; Gur, T.; McWilliam, H.; Squizzato, S.; Park, Y. M.; Buso, N.; Lopez, R., The EMBL-EBI bioinformatics web and programmatic tools framework. *Nucleic Acids Res* **2015,** *43* (W1), W580-4.

31. Love, M. I.; Huber, W.; Anders, S., Moderated estimation of fold change and dispersion for RNA-seq data with DESeq2. *Genome Biol* **2014,** *15* (12), 550.

32. Ponjavic, J.; Oliver, P. L.; Lunter, G.; Ponting, C. P., Genomic and transcriptional co-localization of protein-coding and long non-coding RNA pairs in the developing brain. *PLoS Genet* **2009,** *5* (8), e1000617.

33. Orom, U. A.; Derrien, T.; Beringer, M.; Gumireddy, K.; Gardini, A.; Bussotti, G.; Lai, F.; Zytnicki, M.; Notredame, C.; Huang, Q.; Guigo, R.; Shiekhattar, R., Long noncoding RNAs with enhancer-like function in human cells. *Cell* **2010,** *143* (1), 46-58.

34. Wucher, V.; Legeai, F.; Hedan, B.; Rizk, G.; Lagoutte, L.; Leeb, T.; Jagannathan, V.; Cadieu, E.; David, A.; Lohi, H.; Cirera, S.; Fredholm, M.; Botherel, N.; Leegwater, P. A. J.; Le Beguec, C.; Fieten, H.; Johnson, J.; Alfoldi, J.; Andre, C.; Lindblad-Toh, K.; Hitte, C.; Derrien, T., FEELnc: a tool for long non-coding RNA annotation and its application to the dog transcriptome. *Nucleic Acids Res* **2017,** *45* (8), e57.

35. Zhan, S.; Dong, Y.; Zhao, W.; Guo, J.; Zhong, T.; Wang, L.; Li, L.; Zhang, H., Genome-wide identification

and characterization of long non-coding RNAs in developmental skeletal muscle of fetal goat. *BMC Genomics* **2016,** *17*, 666.
36. Yu, G.; Wang, L. G.; Han, Y.; He, Q. Y., clusterProfiler: an R package for comparing biological themes among gene clusters. *OMICS* **2012,** *16* (5), 284-7.
37. Bindea, G.; Mlecnik, B.; Hackl, H.; Charoentong, P.; Tosolini, M.; Kirilovsky, A.; Fridman, W. H.; Pages, F.; Trajanoski, Z.; Galon, J., ClueGO: a Cytoscape plug-in to decipher functionally grouped gene ontology and pathway annotation networks. *Bioinformatics* **2009,** *25* (8), 1091-3.
38. Ge, W.; Zhao, Y.; Lai, F. N.; Liu, J. C.; Sun, Y. C.; Wang, J. J.; Cheng, S. F.; Zhang, X. F.; Sun, L. L.; Li, L.; Dyce, P. W.; Shen, W., Cutaneous applied nano-ZnO reduce the ability of hair follicle stem cells to differentiate. *Nanotoxicology* **2017,** *11* (4), 465-474.
39. Chao, H. H.; Zhang, X. F.; Chen, B.; Pan, B.; Zhang, L. J.; Li, L.; Sun, X. F.; Shi, Q. H.; Shen, W., Bisphenol A exposure modifies methylation of imprinted genes in mouse oocytes via the estrogen receptor signaling pathway. *Histochem Cell Biol* **2012,** *137* (2), 249-59.
40. Zhang, P.; Chao, H.; Sun, X.; Li, L.; Shi, Q.; Shen, W., Murine folliculogenesis in vitro is stage-specifically regulated by insulin via the Akt signaling pathway. *Histochem Cell Biol* **2010,** *134* (1), 75-82.
41. Bakshi, R. P.; Galande, S.; Muniyappa, K., Functional and regulatory characteristics of eukaryotic type II DNA topoisomerase. *Crit Rev Biochem Mol Biol* **2001,** *36* (1), 1-37.
42. Singh, B. N.; Achary, V. M. M.; Panditi, V.; Sopory, S. K.; Reddy, M. K., Dynamics of tobacco DNA topoisomerases II in cell cycle regulation: to manage topological constrains during replication, transcription and mitotic chromosome condensation and segregation. *Plant Mol Biol* **2017,** *94* (6), 595-607.
43. Kozuki, T.; Chikamori, K.; Surleac, M. D.; Micluta, M. A.; Petrescu, A. J.; Norris, E. J.; Elson, P.; Hoeltge, G. A.; Grabowski, D. R.; Porter, A. C. G.; Ganapathi, R. N.; Ganapathi, M. K., Roles of the C-terminal domains of topoisomerase IIalpha and topoisomerase IIbeta in regulation of the decatenation checkpoint. *Nucleic Acids Res* **2017,** *45* (10), 5995-6010.
44. Ran, M.; Chen, B.; Li, Z.; Wu, M.; Liu, X.; He, C.; Zhang, S.; Li, Z., Systematic Identification of Long Noncoding RNAs in Immature and Mature Porcine Testes. *Biol Reprod* **2016,** *94* (4), 77.
45. Pauli, A.; Valen, E.; Lin, M. F.; Garber, M.; Vastenhouw, N. L.; Levin, J. Z.; Fan, L.; Sandelin, A.; Rinn, J. L.; Regev, A.; Schier, A. F., Systematic identification of long noncoding RNAs expressed during zebrafish embryogenesis. *Genome research* **2012,** *22* (3), 577-91.
46. Yu, H.; Pardoll, D.; Jove, R., STATs in cancer inflammation and immunity: a leading role for STAT3. *Nat Rev Cancer* **2009,** *9* (11), 798-809.
47. Yu, H.; Lee, H.; Herrmann, A.; Buettner, R.; Jove, R., Revisiting STAT3 signalling in cancer: new and unexpected biological functions. *Nat Rev Cancer* **2014,** *14* (11), 736-46.

Figure legends

Figure 1. The effects of ZEA exposure on porcine GCs *in vitro* culture and the identification of lncRNAs. (A) Brief porcine GCs *in vitro* culture model and the experimental procedures of this study. (B) Bright field imaging of porcine GCs during different stages *in vitro* culture. Scale bar, 100 μm. (C) Annexin-V/PI staining of porcine GCs during different stages *in vitro*

543 culture. Scale bar, 50 μm. (D) Porcine GCs were cultured in the presence of ZEA (0, 10 μM
544 and 30 μM) for 48 h and cell apoptosis levels were determined using flow cytometry. (E)
545 Bioinformatics pipeline for identifying lncRNAs, and "Material and methods" for details. (F)
546 The Joyplot of the length of lncRNAs and mRNAs. (G) Filtration of the candidate lncRNAs
547 indicated by the Venn diagrams based on our filter pipeline. Coding potential analysis of
548 candidate lncRNAs was performed by using three tools (CNCI, CPC2, Pfamscan).
549
550 **Figure 2.** Overview of the differential expression levels of lncRNAs and mRNAs. (A) The
551 Volcano Plot showed the differential expression levels of lncRNAs in different group, and the
552 Bar Chart showed the results. (B) The Volcano Plot showed the differential expression levels
553 of mRNAs in different group, and the Bar Chart showed the results. (C) The Chord Diagram
554 showed the distribution and expression of each lncRNA and mRNA in chromosome.
555
556 **Figure 3.** Overview of the function of DELs. (A) The co-expression mRNAs related to DELs.
557 (B) The results of biological process GO terms of DELs in the Ctrl *vs.* 10 μM group by ClueGO.
558 (C) The results of biological process GO terms of DELs in the Ctrl *vs.* 30 μM group by ClueGO.
559 (D) The results of biological process GO terms of DELs in the Ctrl *vs.* 10 μM group by
560 clusterProfiler. (E) The results of biological process GO terms of DELs in the Ctrl *vs.* 30 μM
561 group by clusterProfiler.
562
563 **Figure 4.** Further analysis of DELs in porcine GCs after ZEA exposure. (A) The Venn diagram
564 showed DELs that it was the intersection between the differentially expressed lncRNA in Ctrl

565 *vs.* 10 μM group and Ctrl *vs.* 30 μM group. (B, C) The Chord Diagram and Heatmap showed
566 the expression model of lncRNAs. (D) The Bar Chart showed the co-expression genes related
567 to lncRNAs. (E) The Bar Chart showed the top 20 biological process GO terms according to
568 *pvalues* by clusterProfiler (Up was the Ctrl *vs.* 10 μM group, down was the Ctrl *vs.* 30 μM
569 group). (F) The Network cahrt showed the Biological process GO terms according to *pvalues*
570 by ClueGO (Lift was the Ctrl *vs.* 10 μM group, right was the Ctrl *vs.* 30 μM group).
571
572 **Figure 5.** Identification of the core lncRNA cluster. (A) The Venn diagram showed DELs that
573 we believed it was the core lncRNA cluster. (B) The Bar Chart showed the co-expression genes
574 related to lncRNAs. (C, E) The Chord Diagram and Heatmap showed the expression model of
575 lncRNAs. (D) The Venn diagram showed the shared GO terms between different groups. (F)
576 The Bar Chart showed the results of co-location analysis (10 kb-100 kb) and co-expression
577 analysis ($|r| > 0.9$ & *pvalue* < 0.05) of core lncRNAs. * means co-location genes, ** means co-
578 location and co-expression genes. (G) The Bar Chart showed the top 20 biological process GO
579 terms according to *pvalues* in the Ctrl *vs.* 10 μM group by clusterProfiler. (H) The Bar Chart
580 showed the top 20 biological process GO terms according to *pvalues* in the Ctrl *vs.* 30 μM
581 group by clusterProfiler. (I) The Network Polt showed the Biological process GO terms
582 produced by ClueGO in the Ctrl *vs.* 10 μM group. (J) The Network Polt showed the Biological
583 process GO terms produced by ClueGO in the Ctrl *vs.* 30 μM group.
584
585 **Figure 6.** The verification of bioinformatic analysis. (A) Immunostaining of STAT3 (Red) in
586 porcine GCs exposed to 0 (Ctrl), 10 or 30 μM ZEA for 48 h, Hoechst 33342 (Blue) was used

for nuclei staining. (B) Immunostaining of JAK2 (Green) in porcine GCs exposed to 0 (Ctrl), 10 or 30 μM ZEA for 48 h, Hoechst 33342 (Blue) was used for nuclei staining. (C) The analysis of the mean intensity of STAT3. (D) The analysis of the mean intensity of JAK2. (E-G) Analysis of the expression level of JAK2-STAT3 signaling pathway related protein by WB in porcine GCs after 0 (Ctrl), 10 and 30 μM ZEA exposure for 48 h. GAPDH was used as loading control. The data are demonstrated as the means ± SEM ($n \geq 3$), * meant *pvalue* < 0.05, ** meant *pvalue* < 0.01, *** meant *pvalue* < 0.001.

Figure 7. Prediction of the key lncRNA related to regulating JAK-STAT signaling pathway. (A) Left: The co-expression analysis of MSTRG.26353 and MSTRG.26355. Middle: The Tree Diagram showed the results of hierarchical cluster analysis of core lncRNAs. Right: The co-expression analysis of MSTRG.22680 and MSTRG.23882. (B) The results of GO enrichment terms of MSTRG.22680 and MSTRG.23882.

Supplementary figure legends

Figure S1. Overview of RNA-seq. (A) The data output and related information in this study. (B) The transcripts of lncRNAs that we finally determined. (C) The Euclidean distances Analysis of samples. (D) The Principal Components Analysis of samples.

Figure S2. KEGG analysis support Figure 4. (A) The KEGG analysis of co-expression mRNAs in the Ctrl *vs.* 10 μM group (Up was produced by clusterProfiler, down was produced

609 by ClueGo). (B) The KEGG analysis of co-expression mRNAs in the Ctrl *vs.*30 μM group (Up
610 is produced by clusterProfiler, down is produced by ClueGo).
611
612 **Figure S3.** Expression and function prediction of lncRNAs that it was the intersection between
613 the differentially expressed lncRNA in the Ctrl *vs.* 10 μM group and the 10 μM *vs.* 30 μM
614 group. (A) The Venn diagram showed DELs that it was the intersection between the
615 differentially expressed lncRNA the Ctrl *vs.* 10 μM group and the 10 μM *vs.* 30 μM group. (B,
616 C) The Chord Diagram and Heatmap showed the expression model of lncRNAs. (D) The Bar
617 Chart showed the co-expression genes related to lncRNAs. (E) The Bar Chart showed the top
618 20 biological process GO terms according to *pvalues* in the Ctrl *vs.* 10 μM group produced by
619 clusterProfiler. (F) The Network Polt showed the Biological process GO terms produced by
620 ClueGO in the Ctrl *vs.* 10 μM group. (G) The Bar Chart showed the KEGG terms produced by
621 clusterProfiler in the Ctrl *vs.* 10 μM group. (H) The Bar Chart showed the KEGG terms
622 produced by ClueGO in the Ctrl *vs.* 10 μM group.
623
624 **Figure S4.** Expression and function prediction of lncRNAs that it was the intersection between
625 the differentially expressed lncRNA in the Ctrl *vs.* 30 μM group and the 10 μM *vs.* 30 μM
626 group. (A) The Venn diagram showed DELs that it was the intersection between the
627 differentially expressed lncRNA in the Ctrl *vs.* 30 μM group and the 10 μM *vs.* 30 μM group.
628 (B, C) The Chord Diagram and Heatmap showed the expression model of lncRNAs. (D) The
629 Bar Chart showed the co-expression genes related to lncRNAs. (E) The Bar Chart showed the
630 top 20 biological process GO terms according to *pvalues* in the Ctrl *vs.* 30 μM group by

clusterProfiler. (F) The Network Polt showed the Biological process GO terms produced by ClueGO in the Ctrl *vs.* 30 μM group. (G) The Bar Chart showed the KEGG terms produced by clusterProfiler in the Ctrl *vs.* 30 μM group. (H) The Bar Chart showed the KEGG terms produced by ClueGO in the Ctrl *vs.* 30 μM group.

Figure S5. KEGG signaling pathway enrichment analysis support Figure 5. (A) The KEGG analysis of co-expression mRNAs in the Ctrl *vs.* 10 μM group (Lift is produced by clusterProfiler, right is produced by ClueGo). (B) The KEGG analysis of co-expression mRNAs in the Ctrl *vs.*30 μM group (Left is produced by clusterProfiler, right is produced by ClueGo).

Supplementary tables

Table S1. Primary antibody of IF.

Table S2. Primary antibody of WB.

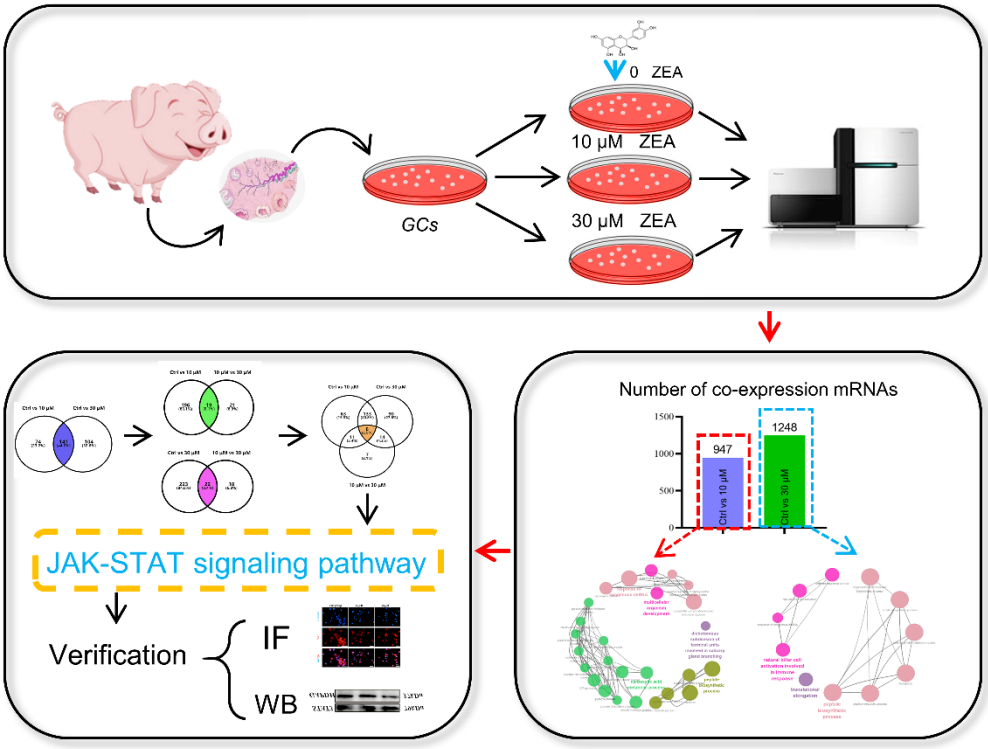
0 ZEA
10 μM ZEA
30 μM ZEA
GCs
Number of co-expression mRNAs
1500
1000
500
0
947
1248
Ctrl vs 10 μM
Ctrl vs 30 μM
JAK-STAT signaling pathway
Verification
IF
WB

647

Figure 1

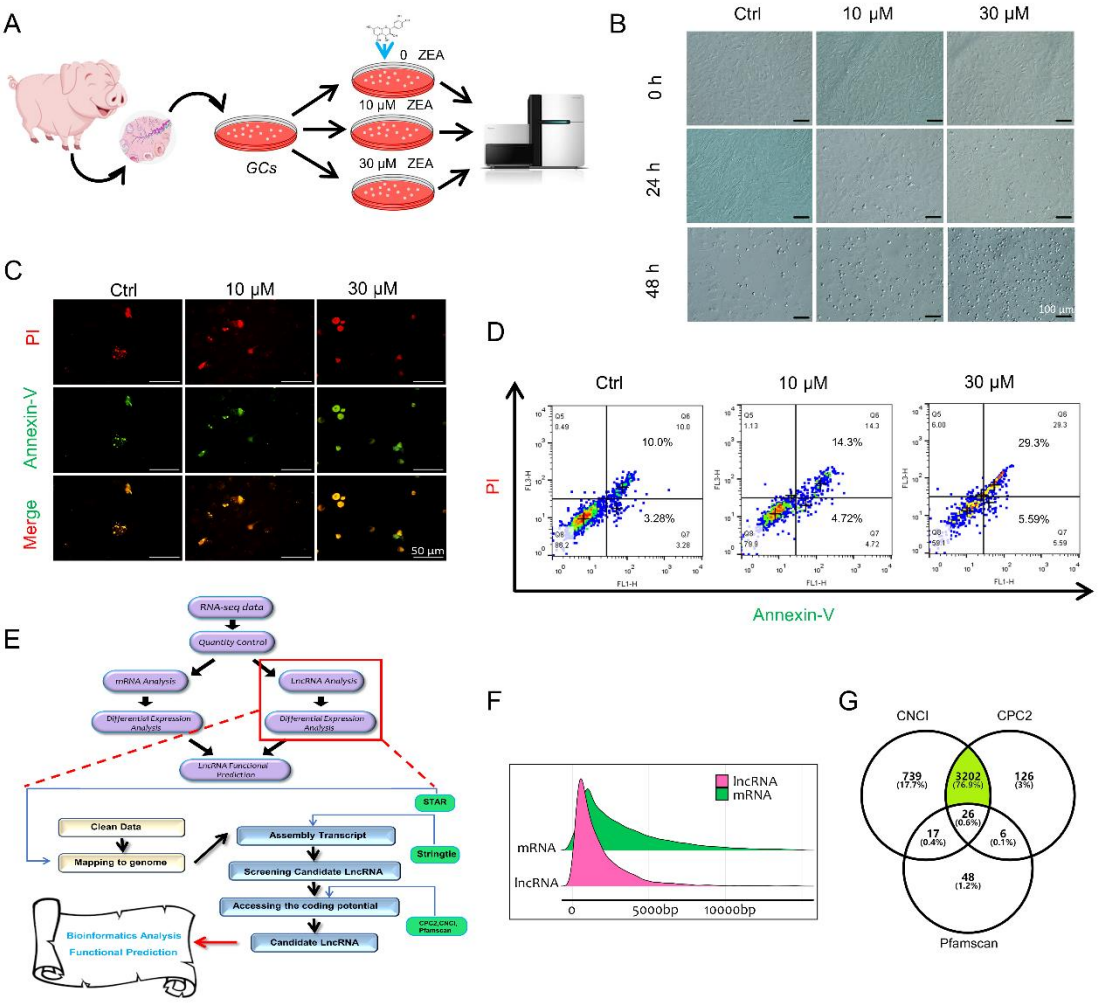
A
0 ZEA
10 μM ZEA
30 μM ZEA
GCs
B
Ctrl
10 μM
30 μM
0 h
24 h
48 h
C
Ctrl
10 μM
30 μM
PI
Annexin-V
Merge
D
Ctrl
10 μM
30 μM
PI
10.0%
3.28%
14.3%
4.72%
29.3%
5.59%
Annexin-V
E
RNA-seq data
Quantity Control
mRNA Analysis
LncRNA Analysis
Differential Expression Analysis
Differential Expression Analysis
LncRNA Functional Prediction
STAR
Clean Data
Mapping to genome
Assembly Transcript
Stringtie
Screening Candidate LncRNA
Accessing the coding potential
CPC2,CNCI, Pfamscan
Candidate LncRNA
Bioinformatics Analysis
Functional Prediction
F
lncRNA
mRNA
mRNA
lncRNA
0
5000bp
10000bp
G
CNCI
CPC2
739
(17.7%)
3202
(76.9%)
126
(3%)
26
(0.6%)
17
(0.4%)
6
(0.1%)
48
(1.2%)
Pfamscan

648

Figure 2

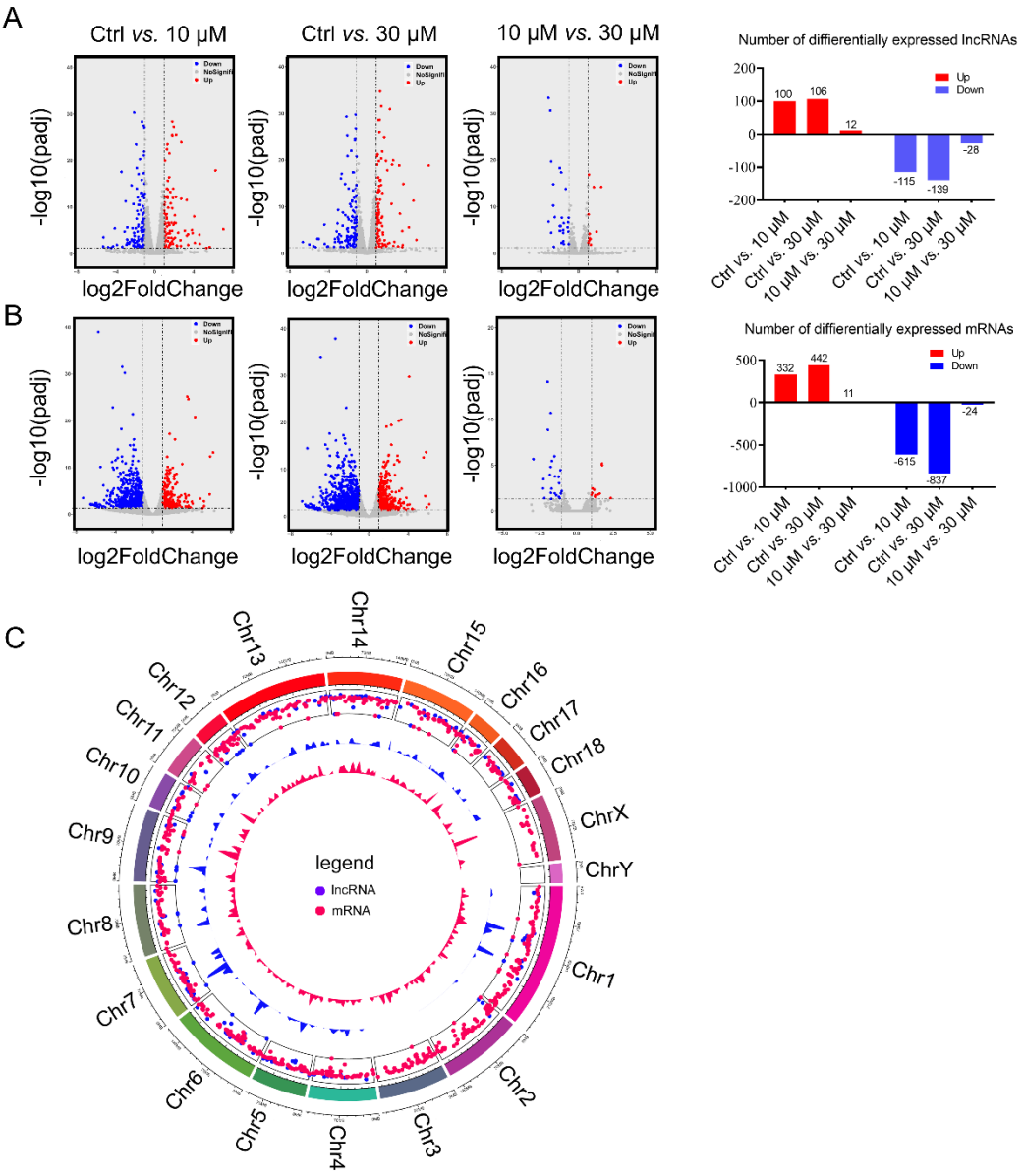
A
Ctrl vs. 10 μM
Ctrl vs. 30 μM
10 μM vs. 30 μM
-log10(padj)
log2FoldChange
Number of differentially expressed lncRNAs
Up
Down
100
106
12
-115
-139
-28
Ctrl vs. 10 μM
Ctrl vs. 30 μM
10 μM vs. 30 μM
B
Number of differentially expressed mRNAs
332
442
11
-615
-837
-24
C
Chr1
Chr2
Chr3
Chr4
Chr5
Chr6
Chr7
Chr8
Chr9
Chr10
Chr11
Chr12
Chr13
Chr14
Chr15
Chr16
Chr17
Chr18
ChrX
ChrY
legend
lncRNA
mRNA

649

Figure 3

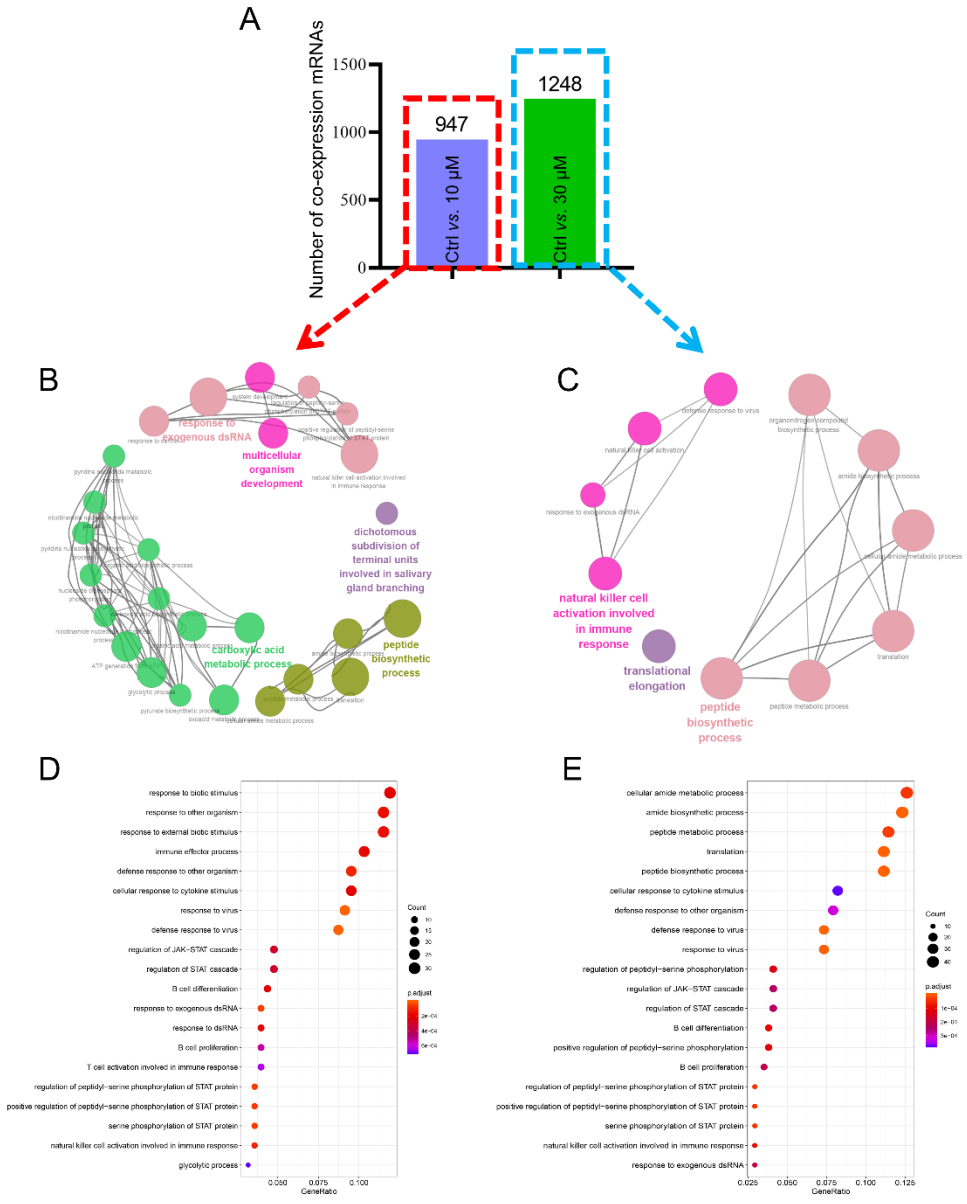
A
Number of co-expression mRNAs
1500
1000
500
0
947
1248
Ctrl vs. 10 μM
Ctrl vs. 30 μM
B
response to exogenous dsRNA
multicellular organism development
dichotomous subdivision of terminal units involved in salivary gland branching
carboxylic acid metabolic process
peptide biosynthetic process
C
natural killer cell activation involved in immune response
translational elongation
peptide biosynthetic process
D
response to biotic stimulus
response to other organism
response to external biotic stimulus
immune effector process
defense response to other organism
cellular response to cytokine stimulus
response to virus
defense response to virus
regulation of JAK-STAT cascade
regulation of STAT cascade
B cell differentiation
response to exogenous dsRNA
response to dsRNA
B cell proliferation
T cell activation involved in immune response
regulation of peptidyl-serine phosphorylation of STAT protein
positive regulation of peptidyl-serine phosphorylation of STAT protein
serine phosphorylation of STAT protein
natural killer cell activation involved in immune response
glycolytic process
GeneRatio
Count
p.adjust
E
cellular amide metabolic process
amide biosynthetic process
peptide metabolic process
translation
peptide biosynthetic process
cellular response to cytokine stimulus
defense response to other organism
defense response to virus
response to virus
regulation of peptidyl-serine phosphorylation
regulation of JAK-STAT cascade
regulation of STAT cascade
B cell differentiation
positive regulation of peptidyl-serine phosphorylation
B cell proliferation
regulation of peptidyl-serine phosphorylation of STAT protein
positive regulation of peptidyl-serine phosphorylation of STAT protein
serine phosphorylation of STAT protein
natural killer cell activation involved in immune response
response to exogenous dsRNA
GeneRatio
Count
p.adjust

650

Figure 4

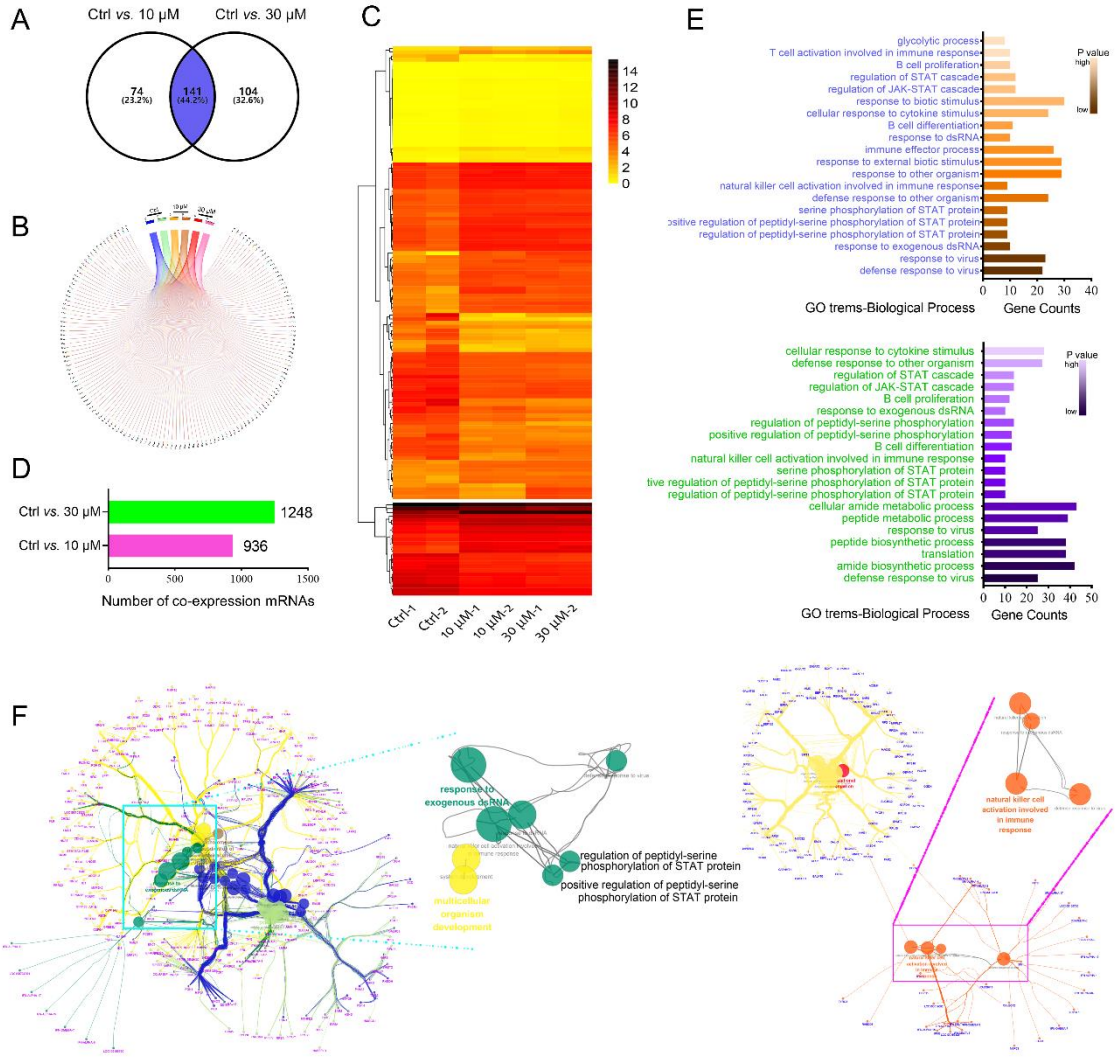
A
Ctrl vs. 10 μM
Ctrl vs. 30 μM
74 (23.2%)
141 (44.2%)
104 (32.6%)
B
C
14
12
10
8
6
4
2
0
Ctrl-1
Ctrl-2
10 μM-1
10 μM-2
30 μM-1
30 μM-2
D
Ctrl vs. 30 μM
1248
Ctrl vs. 10 μM
936
0
500
1000
1500
Number of co-expression mRNAs
E
glycolytic process
T cell activation involved in immune response
B cell proliferation
regulation of STAT cascade
regulation of JAK-STAT cascade
response to biotic stimulus
cellular response to cytokine stimulus
B cell differentiation
response to dsRNA
immune effector process
response to external biotic stimulus
response to other organism
natural killer cell activation involved in immune response
defense response to other organism
serine phosphorylation of STAT protein
ositive regulation of peptidyl-serine phosphorylation of STAT protein
regulation of peptidyl-serine phosphorylation of STAT protein
response to exogenous dsRNA
response to virus
defense response to virus
P value
high
low
0 10 20 30 40
GO trems-Biological Process
Gene Counts
cellular response to cytokine stimulus
defense response to other organism
regulation of STAT cascade
regulation of JAK-STAT cascade
B cell proliferation
response to exogenous dsRNA
regulation of peptidyl-serine phosphorylation
positive regulation of peptidyl-serine phosphorylation
B cell differentiation
natural killer cell activation involved in immune response
serine phosphorylation of STAT protein
tive regulation of peptidyl-serine phosphorylation of STAT protein
regulation of peptidyl-serine phosphorylation of STAT protein
cellular amide metabolic process
peptide metabolic process
response to virus
peptide biosynthetic process
translation
amide biosynthetic process
defense response to virus
P value
high
low
0 10 20 30 40 50
GO trems-Biological Process
Gene Counts
F
response to exogenous dsRNA
multicellular organism development
regulation of peptidyl-serine phosphorylation of STAT protein
positive regulation of peptidyl-serine phosphorylation of STAT protein
natural killer cell activation involved in immune response

651

Figure 5

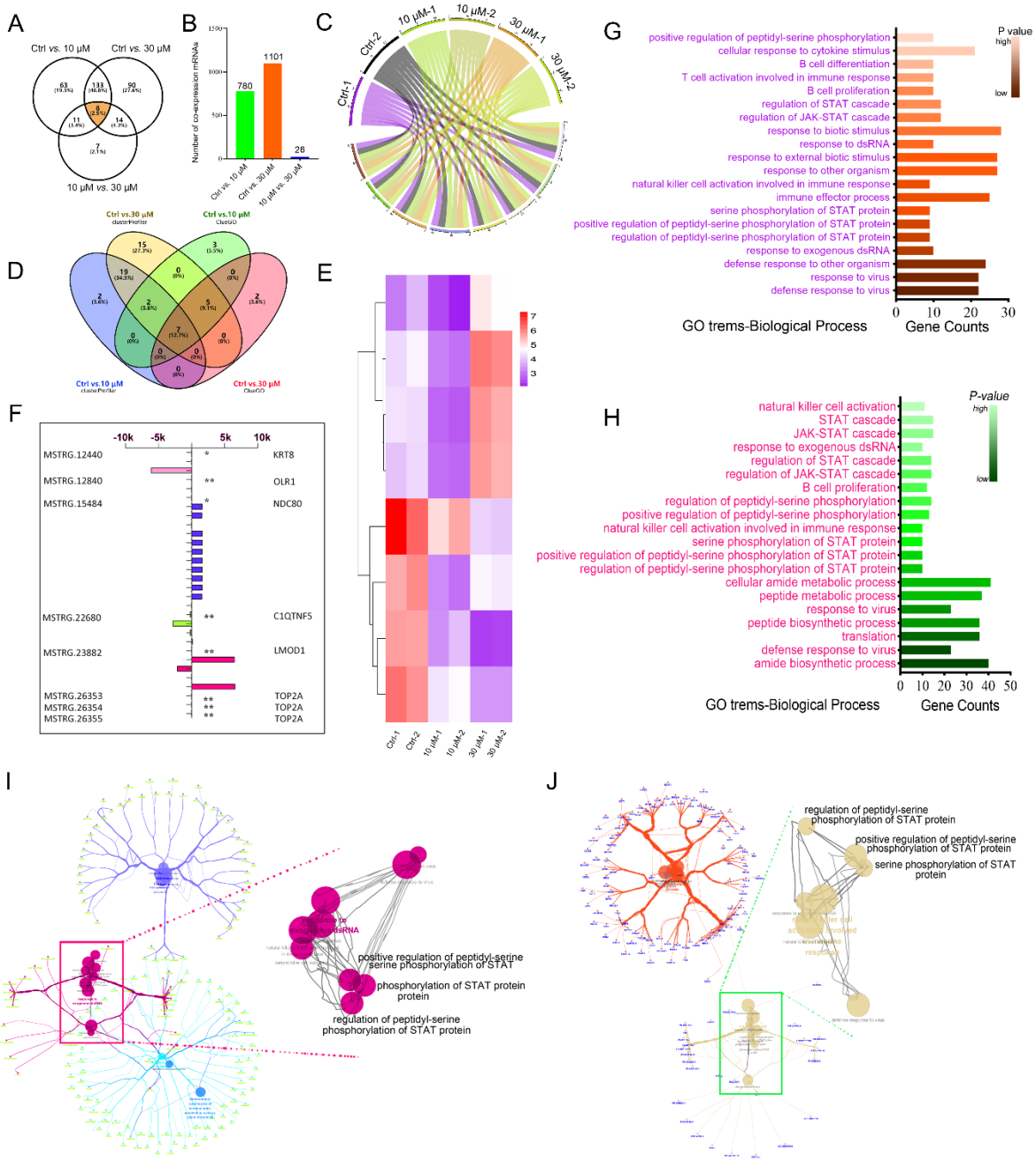
A
Ctrl vs. 10 μM
Ctrl vs. 30 μM
10 μM vs. 30 μM
B
Number of co-expression mRNAs
780
1101
28
C
Ctrl-1
Ctrl-2
10 μM-1
10 μM-2
30 μM-1
30 μM-2
D
E
F
-10k
-5k
5k
10k
MSTRG.12440
KRT8
MSTRG.12840
OLR1
MSTRG.15484
NDC80
MSTRG.22680
C1QTNF5
MSTRG.23882
LMOD1
MSTRG.26353
MSTRG.26354
MSTRG.26355
TOP2A
G
positive regulation of peptidyl-serine phosphorylation
cellular response to cytokine stimulus
B cell differentiation
T cell activation involved in immune response
B cell proliferation
regulation of STAT cascade
regulation of JAK-STAT cascade
response to biotic stimulus
response to dsRNA
response to external biotic stimulus
response to other organism
natural killer cell activation involved in immune response
immune effector process
serine phosphorylation of STAT protein
positive regulation of peptidyl-serine phosphorylation of STAT protein
regulation of peptidyl-serine phosphorylation of STAT protein
response to exogenous dsRNA
defense response to other organism
response to virus
defense response to virus
P value
high
low
GO trems-Biological Process
Gene Counts
H
natural killer cell activation
STAT cascade
JAK-STAT cascade
response to exogenous dsRNA
regulation of STAT cascade
regulation of JAK-STAT cascade
B cell proliferation
regulation of peptidyl-serine phosphorylation
positive regulation of peptidyl-serine phosphorylation
natural killer cell activation involved in immune response
serine phosphorylation of STAT protein
positive regulation of peptidyl-serine phosphorylation of STAT protein
regulation of peptidyl-serine phosphorylation of STAT protein
cellular amide metabolic process
peptide metabolic process
response to virus
peptide biosynthetic process
translation
defense response to virus
amide biosynthetic process
P-value
high
low
GO trems-Biological Process
Gene Counts
I
positive regulation of peptidyl-serine phosphorylation of STAT protein
regulation of peptidyl-serine phosphorylation of STAT protein
J
regulation of peptidyl-serine phosphorylation of STAT protein
positive regulation of peptidyl-serine phosphorylation of STAT protein
serine phosphorylation of STAT protein

652

Figure 6

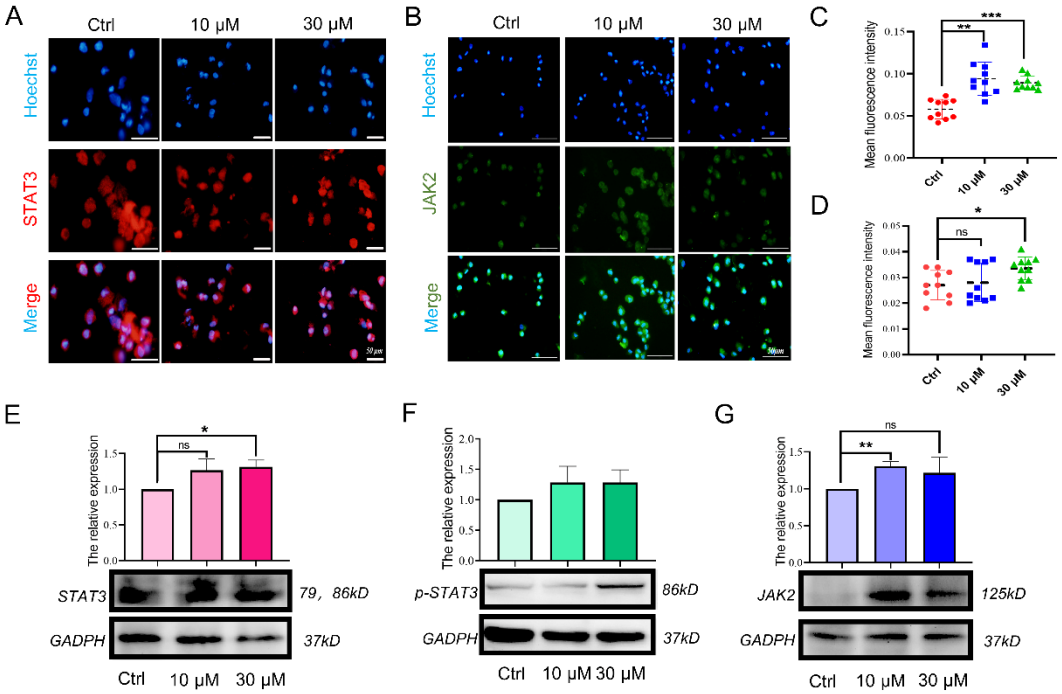
A
Ctrl
10 μM
30 μM
Hoechst
STAT3
Merge
B
Ctrl
10 μM
30 μM
Hoechst
JAK2
Merge
C
Mean fluorescence intensity
**
***
Ctrl
10 μM
30 μM
D
Mean fluorescence intensity
ns
*
Ctrl
10 μM
30 μM
E
The relative expression
ns
*
STAT3
79, 86kD
GADPH
37kD
Ctrl
10 μM
30 μM
F
The relative expression
p-STAT3
86kD
GADPH
37kD
Ctrl
10 μM
30 μM
G
The relative expression
ns
**
JAK2
125kD
GADPH
37kD
Ctrl
10 μM
30 μM

653

Figure 7

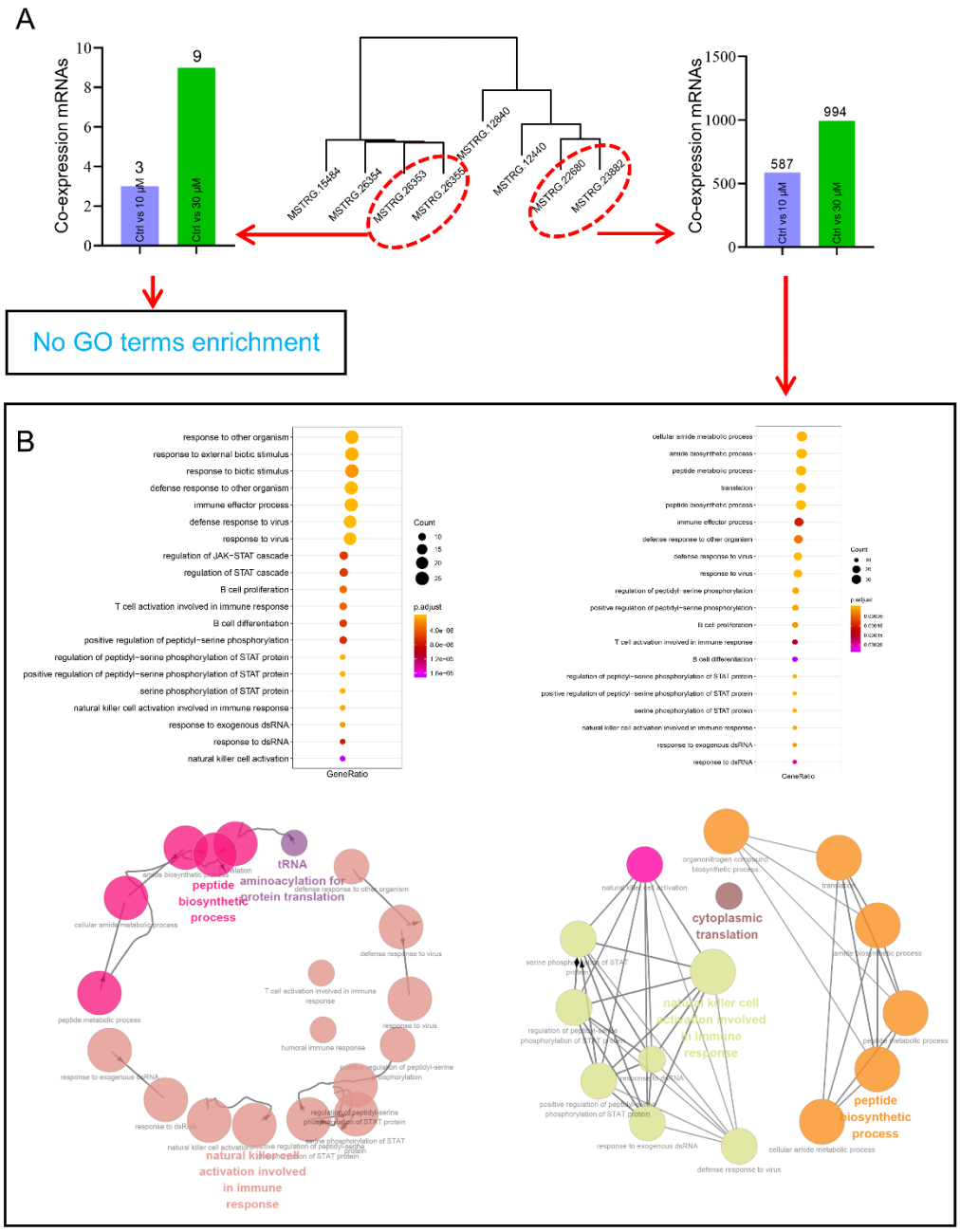
A
Co-expression mRNAs
10
8
6
4
2
0
3
9
Ctrl vs 10 μM
Ctrl vs 30 μM
MSTRG.15484
MSTRG.26354
MSTRG.26353
MSTRG.26354
MSTRG.12840
MSTRG.12440
MSTRG.22680
MSTRG.23882
Co-expression mRNAs
1500
1000
500
0
587
994
Ctrl vs 10 μM
Ctrl vs 30 μM
No GO terms enrichment
B
response to other organism
response to external biotic stimulus
response to biotic stimulus
defense response to other organism
immune effector process
defense response to virus
response to virus
regulation of JAK-STAT cascade
regulation of STAT cascade
B cell proliferation
T cell activation involved in immune response
B cell differentiation
positive regulation of peptidyl−serine phosphorylation
regulation of peptidyl−serine phosphorylation of STAT protein
positive regulation of peptidyl−serine phosphorylation of STAT protein
serine phosphorylation of STAT protein
natural killer cell activation involved in immune response
response to exogenous dsRNA
response to dsRNA
natural killer cell activation
GeneRatio
Count
p.adjust
cellular amide metabolic process
amide biosynthetic process
peptide metabolic process
translation
peptide biosynthetic process
immune effector process
defense response to other organism
defense response to virus
response to virus
regulation of peptidyl−serine phosphorylation
positive regulation of peptidyl−serine phosphorylation
B cell proliferation
T cell activation involved in immune response
B cell differentiation
regulation of peptidyl−serine phosphorylation of STAT protein
positive regulation of peptidyl−serine phosphorylation of STAT protein
serine phosphorylation of STAT protein
natural killer cell activation involved in immune response
response to exogenous dsRNA
response to dsRNA
GeneRatio
tRNA aminoacylation for protein translation
peptide biosynthetic process
cellular amide metabolic process
peptide metabolic process
response to dsRNA
response to exogenous dsRNA
T cell activation involved in immune response
humoral immune response
defense response to virus
response to virus
natural killer cell activation involved in immune response
cytoplasmic translation
translation
peptide biosynthetic process
peptide metabolic process
cellular amide metabolic process
response to exogenous dsRNA
defense response to virus

654

Figure S1

A

Sample	Raw reads	Clean reads	Q20(%)	Q30(%)	GC contemt (%)
Ctrl-1	10677946	10559016	93.71	87.63	47.20
Ctrl-2	9792352	9668258	94.10	88.00	49.92
10 μM-1	10890598	10813977	94.56	88.92	49.52
10 μM-2	12625870	12532210	95.68	91.33	49.04
30 μM-1	11087387	11014287	95.94	91.81	49.37
30 μM-2	9090533	8999512	94.29	88.28	48.88

B

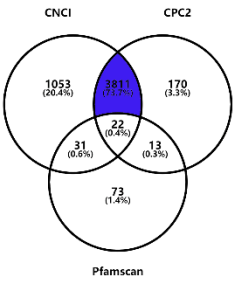

C

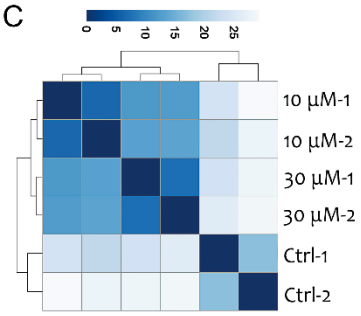

D

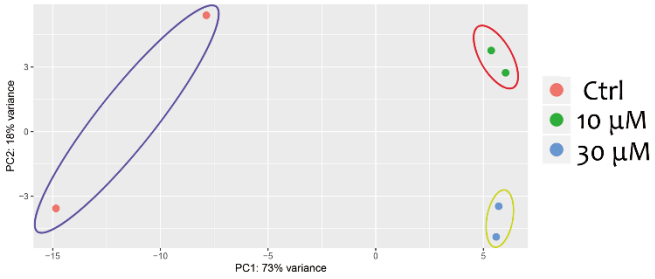

655

656

Figure S2

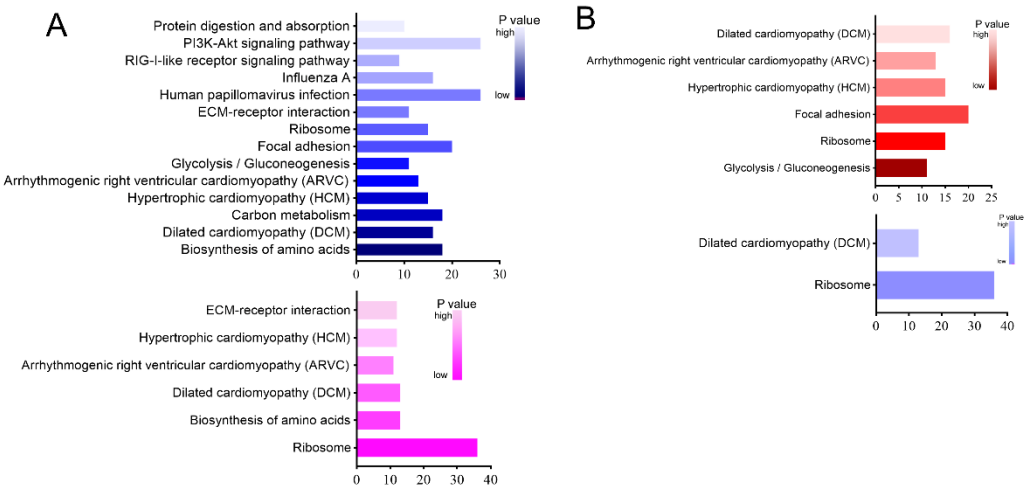

657

Figure S3

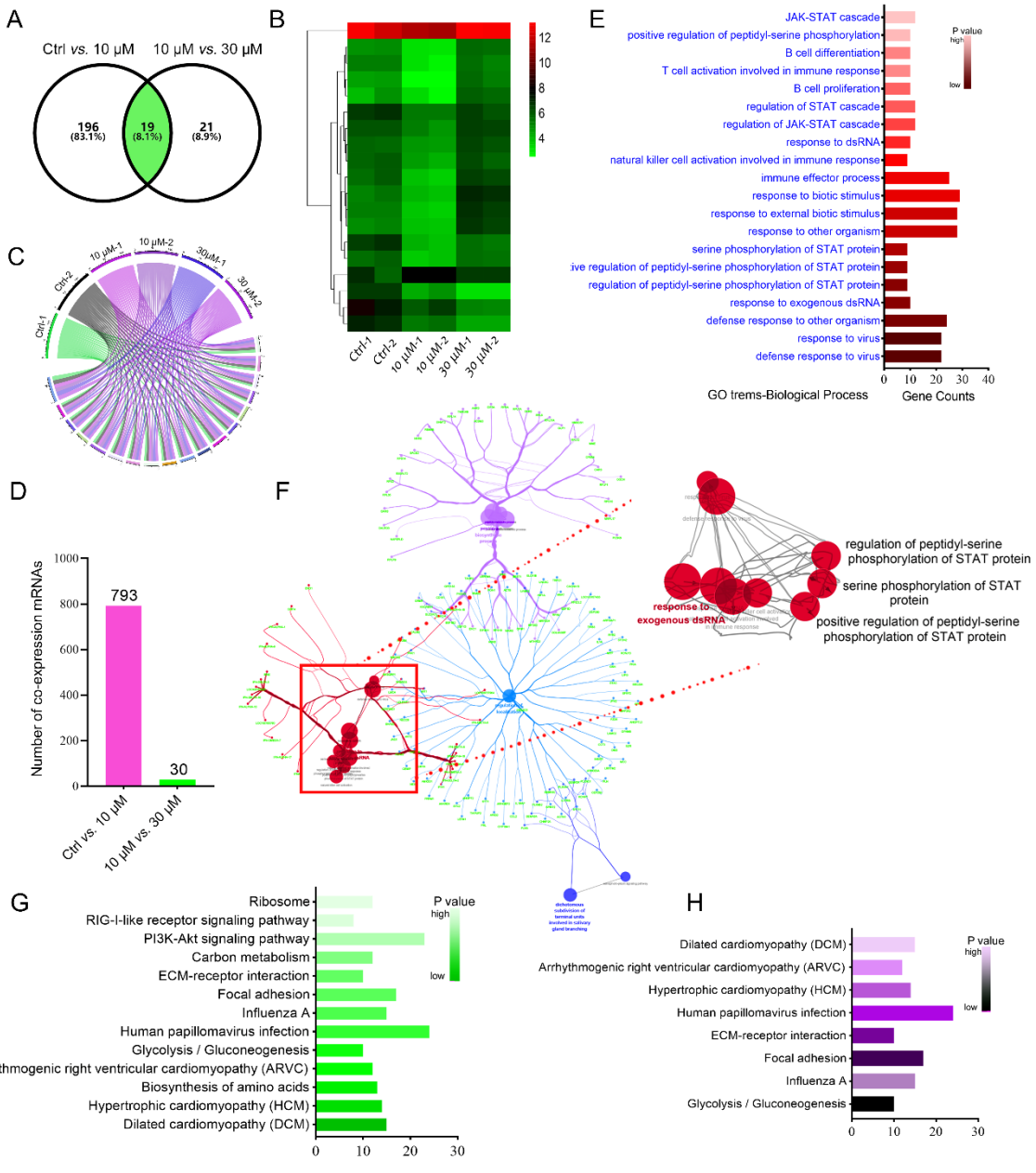

658

Figure S4

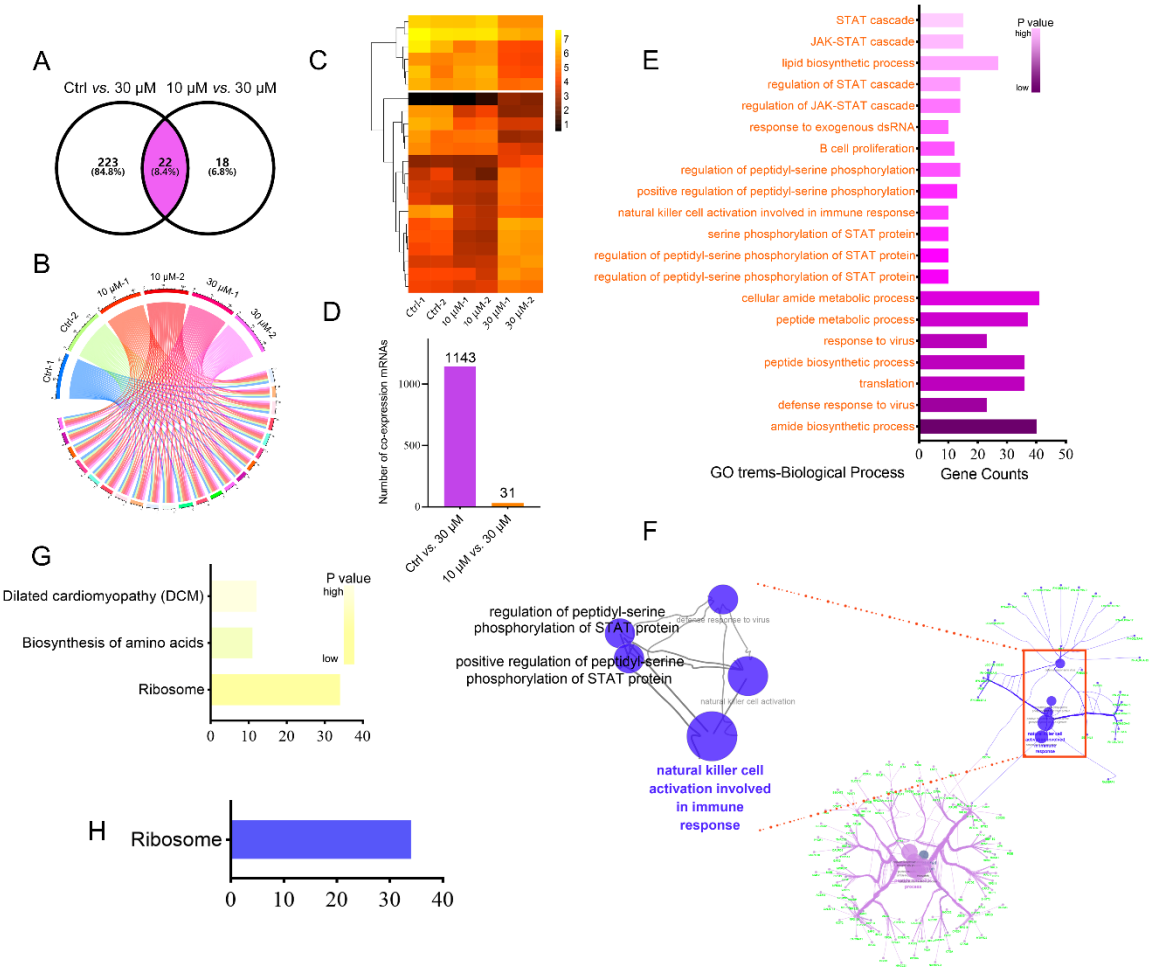

659
660

Figure S5

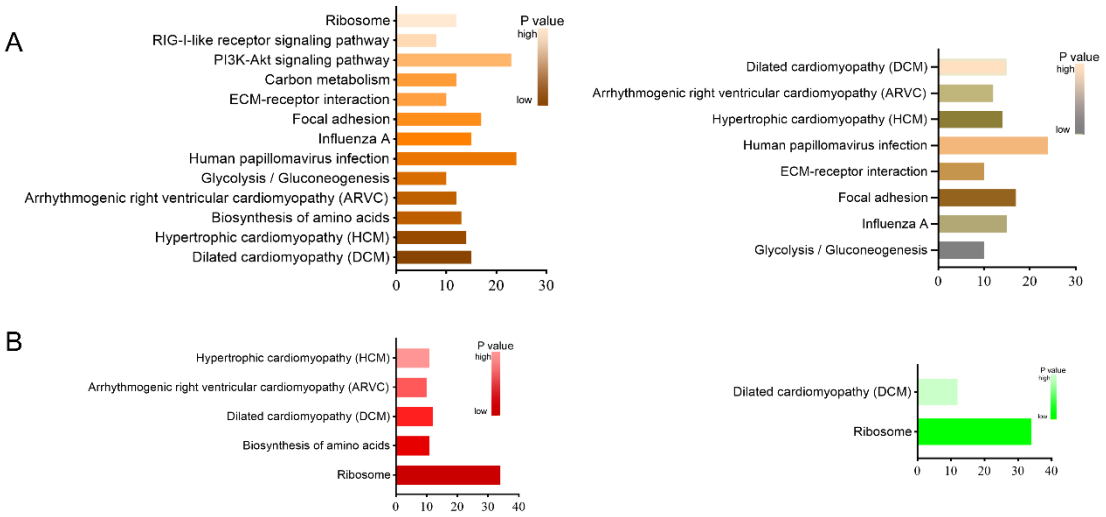

661

662

663 **Table S1.** Primary antibody of IF

Primary antibody	Art.No.	Manufacturers
STAT3	#9139	Cell Signal Technology, US
JAK2	#3230	Cell Signal Technology, US

664

665 **Table S2.** Primary antibody of WB

Primary antibody	Art.No.	Manufacturers
STAT3	#9139	Cell Signal Technology, US
p-STAT3	#9134	Cell Signal Technology, US
JAK2	#3230	Cell Signal Technology, US

666

Firstly, we would like to thank the editor very much for your comments.

1. Title page: Please use symbols (#*&...) to designate each author's affiliation.

Response: Thanks for your suggestion. We adopt your suggestion and used symbols (&, #, +, *) to designate each author's affiliation.

2. Please incorporate all figures, tables and TOC graphic to the end of manuscript.

Response: Thanks for your suggestion. We incorporated TOC, all figures and tables graphic to the end of manuscript.

3. Please make sure to remove any track changes, highlights, comments or font colors in your manuscript file. And submit one clean copy of manuscript.

Response: Thanks for your suggestion. All track changes, highlights, comments or font colors in manuscript file were removed. And we will submit a clean copy of manuscript.

Once again, we would like to thank the editor for the helpful comments, and hope our responses will meet your expectations. We are looking forward to hearing from you for publication of this manuscript.

Zearalenone Exposure Induces the Apoptosis of Porcine Granulosa Cells and Changes Long Noncoding RNA Expression to Promote Anti-Apoptosis by Activating the JAK2-STAT3 Pathway

Fa-Li Zhang [1&], Na Li [2#], Han Wang [1&], Jin-Mei Ma [3+], Wei Shen [1&], Lan Li [1&,*]

[1&] *College of Life Sciences, Qingdao Agricultural University, Qingdao 266109, China;*

[2#] *College of Animal Science and Technology, Qingdao Agricultural University, Qingdao 266109, China;*

[3+] *Animal Husbandry and Veterinary Station of Penglai City, Yantai 265600, China*

*** Correspondence and reprint requests to:**

Dr. Lan Li, E-mail: lli@qau.edu.cn; lilan9600@126.com

ABSTRACT

Zearalenone (ZEA), a pathogenic toxin produced by *Fusarium*, is widely detected in moldy feed materials. Previous studies have reported that ZEA exerts a harmful influence to animal reproductive systems, however, its effects on the changes of long noncoding RNAs (lncRNAs) remain unclear. Here, tackling this question, we performed RNA-seq on porcine granulosa cells (GCs) after being exposed to 10 μM and 30 μM ZEA *in vitro*. The results showed that ZEA exposure observably changed the expression of lncRNAs in porcine GCs and increased the rate of apoptosis. Furthermore, Gene Ontology analysis showed that ZEA exposure induced variation of the JAK2-STAT3 signaling pathway in porcine GCs. To verify our bioinformatics analysis, western blotting and immunofluorescence analysis were performed and the results demonstrated that porcine GCs after ZEA exposure increased the expression of key proteins in the JAK2-STAT3 signaling pathway. Further bioinformatics analysis found that MSTRG.22680 and MSTRG.23882 played a pivotal role in activating the JAK2-STAT3 signaling pathway. To summarize, our results throw light on the fact that ZEA exposure dramatically increases the apoptosis of porcine GCs and alters the expression of lncRNAs that play an anti-apoptotic role in porcine GCs via activating the JAK2-STAT3 signaling pathway.

Key words: Zearalenone; porcine granulosa cells; apoptosis; lncRNA; JAK2-STAT3 signaling pathway

Introduction

Zearalenone (ZEA), produced by *Fusarium*[1], tends to lead to reproductive toxicity and can be easily detected in contaminated livestock feeds[2]. It was reported that ZEA contamination was as high as 800-1,000 mg/kg in some feed materials in some regions[3]. Moreover, numerous studies reported that ZEA had a structure similar to 17β-estradiol (E2), and ZEA and estrogen combined competitively with estrogen receptors (ERs)[4], which led to ZEA exerting estrogenic effects when animals were exposed to it[5]. ZEA has been shown to perform a bad effect on the reproductive system of exposed animals, mainly influencing the ovary, uterus and so on, in which ERs tend to show high levels of expression[6]. Notably, the findings of a previous research revealed that ZEA exposure affected follicular development and oocyte maturation[7], and studies else indicated that ZEA induced oxidative stress in porcine granulosa cells (GCs)[8] and affected the progression of meiosis in mouse oocytes[9]. In addition, ZEA exposure down-regulated the expression of LIM Homeobox 8 (*Lhx8)*, in turn, impaired ovarian primordial follicle formation in mice[10]. Thus, ZEA exposure exerts negative effects on animal production systems, the research of the mechanism of ZEA exposure is necessary to alleviate the loss resulting from ZEA exposure, unfortunately, so far, it remains an unanswered question.

How does ZEA affect animal reproductive systems? There are the two primary events, such as follicular growth and atresia. During folliculogenesis, atresia largely results from the apoptosis of granulosa cells (GCs)[11]. GCs were indispensable for folliculogenesis and the studies demonstrated that GCs affected follicular development via releasing signal molecules that were essential for follicular development and maturation[12]. In addition, recent work has shown that ZEA exposure induces apoptosis of the GCs in several species[13-14]. Though we have

done many works to reveal the potential effects caused by ZEA exposure[8-9, 13-14], the exact molecular mechanism underlying ZEA induced cytotoxicity remains unclear. In fact, most studies focused on the dynamical changes at the mRNA level, while limited studies are available that investigated the mechanism of how ZEA exposure affects cellular apoptosis by the changes of long non-coding RNAs (lncRNAs).

LncRNAs are referred to cellular RNAs molecules, which length is longer than 200 bp and cannot be translated into proteins[15]. LncRNAs studies on the ovary have mainly been focused on their effects on ovarian cancers. Many lncRNAs have been shown to play the vital roles in promoting cellular proliferation and inhibiting cellular apoptosis in ovarian cancers including PVT1, LSINCT5, MEG3 and others[16-18]. A growing number of studies have illustrated that lncRNAs perform an important function in multiple biologic processes, such as apoptosis[19,20-21]. Additionally, one of the mechanisms by which lncRNAs regulate cellular apoptosis is the silencing of microRNA[22]. Currently, lncRNAs are emerging as new participants in gene regulation but the mechanism of how lncRNAs work to regulate growth and apoptosis in GCs remains to be fully described.

The JAK-STAT signaling pathway is relevant to many important biological processes including cellular proliferation, differentiation, apoptosis and immune regulation[23]. Compared with other signaling pathways, JAK-STAT signaling pathway is relatively simple and consists of three components, namely, tyrosine kinase associated receptor, Janus kinase (JAK) and the signal transducer and activator of transcription (STAT)[24]. One of the branches is the JAK2-STAT3 signaling pathway, which main function of it is anti-apoptosis[25]. It's worth noting that STAT3 is an anti-apoptosis transcription factor[25].

Distinct from previous reports, the aim here is to better uncover the in-depth mechanism of lncRNAs in porcine GCs after ZEA exposure. The function of lncRNAs about apoptosis of porcine GCs after ZEA exposure was preliminarily explored in this research. The findings of our research will provide a theoretical basis for the mitigation of the harmful effects of ZEA in animal husbandry.

Materials and Methods

Porcine granulosa cell culture and experimental design

Porcine ovaries were collected into saline supplemented with 1 % penicillin-streptomycin from Qingdao Wanfu Group Co., Ltd. (Qingdao, Shandong, China) and taken it back to the laboratory within 2 h. Briefly, follicular fluid in 3 to 5 mm follicles was collected by a 10 ml syringe, then the GCs were isolated and cultured in DMEM high glucose medium (HyClone, SH30022.01, Beijing, China). 10 % fetal bovine serum (FBS, Gibco, 10099-141, Australia), 1 % penicillin-streptomycin (HyClone, SV30010, Beijing, China) and 0.2 % gentamicin (BBI, EB30KA0357, Shanghai, China) were added to medium, then the GCs were cultured at 37 °C in a 5 % CO_2 atmosphere.

When primary GCs grew to about 50 % - 70 % confluency, they were treated with 10 μM or 30 μM ZEA (Sigma-Aldrich, Z2125, MO, USA), Dimethyl sulfoxide (DMSO) was adopted to dissolve ZEA and it was stored at -20 °C, meanwhile the control (Ctrl) group was treated with vehicle only. Concentrations used in this study were based on our previous finding that 10 and 30 μM of ZEA had dramatic adverse effects on porcine GCs[14]. All the animal treatment procedures in this paper have been approved by the Ethics Committee of Qingdao Agricultural

University.

Sequencing and quality control

Briefly, about total 4 μg RNA was isolated per sample and the sequencing libraries were generated according to standard protocol, then the libraries were sequenced using the Hiseq4000 platform at Novogene Co., Ltd. (Beijing, China).

FastQC (version v0.11.8) was adopted to assess the quality of the raw data. Moreover, Fastp (version v0.19.5) was used to remove low quality data, adapter and poly-N sequences. Clean data were collected, and then the basic information, including the value of GC content, Q20 and Q30, of it was calculated[26]. All analysis of downstream steps was done using the filtered clean data.

Transcriptome assembly

We downloaded porcine reference genome and gene model annotation files from the NCBI database (version Sscrofa11.1). STAR (version STAR_2.7.0b) was selected to build the index of reference genome, subsequently we utilized STAR to put paired-end clean reads aligned to the reference genome. Moreover, we utilized Stringtie (version 1.3.4d) to assemble the transcriptome of each library[27]. Stringtie run with "-rf", "FPKM=0.5", "TPM=0.5" and other options were set as default.

Filtering pipeline in order to identify lncRNAs

We selected candidate lncRNAs using the following filtering pipeline: 1) The transcripts,

annotated as “i”, “x”, “u”, “o” or “e” by the bio-software gffcompare (version v0.10.6), were left for the moreover filter. 2) The transcripts of single-exon, length ≤ 200, FPKM (Fragments Per Kilobase per Million reads) < 0.5 and TPM (Transcripts Per Kilobase Million) < 0.5 were filtered by Stringtie when merging the file of transcripts. 3) The remaining transcripts which passed above filtered steps, were assessed their coding potential by the Coding Potential Calculator 2 (CPC2), Coding-Non-Coding-Index (CNCI) and Pfamscan, and the threshold of these softwares were that score < 0 and tag as ‘noncoding’, score < 0 and tag as ‘noncoding’, tag as ‘noncoding’, respectively[28-30]. 4) The left behind was perceived as the transcriptome of lncRNA. The HTSeq software was adopted to count reads of lncRNAs for providing input for later analysis. Parameters were ‘-s yes’ and default of others.

Expression analysis

The expression of mRNA and lncRNA was confirmed with FPKM calculated by a custom script and in this study all expression of mRNA and LncRNA was used in this data. The DESeq2 software package was used to determine differentially expressed mRNAs (DEMs) and differentially expressed lncRNAs (DELs). We used the *padj* < 0.05 and | log2FoldChange | >1 as threshold to determine the differently expressed lncRNAs or mRNAs[31]. The trend of expression level and trend of lncRNAs were observed by the Chord Diagram and Heatmap.

Co-location analysis

Cis-role of lncRNA is aimed at adjacent genes[32-33]. The FEELnc (version v0.1.1) was used to search for all coding genes which located at 10 kb – 100 kb upstream or downstream of all the

confirmed lncRNAs[34]. We only made co-location analysis of the core lncRNAs. The core lncRNA that we used a step - by - step reduction scheme to determine. Briefly, we obtained the intersection of different difference groups, finally we gained the core lncRNAs.

Co-expression analysis

It was reported that the *trans*-role of lncRNAs was related to their co-expressed genes[35]. The DEMs and DELs were identified by co-expression analysis. In order to investigate the function of DELs, we calculated Pearson's correlation coefficients (r) between DELs and DEMs using R package named Hmisc (version 4.2-0, http://biostat.mc.vanderbilt.edu/Hmisc). We selected relational pair with $| r | > 0.9$ and $pvalue < 0.05$ as the co-expressed genes of lncRNAs.

Gene Ontology (GO) and Kyoto Encyclopedia of Genes and Genomes (KEGG) signaling pathway enrich analysis

The co-location and co-expression genes were performed function enrich analysis, including GO terms and KEGG signaling pathway analysis, by clusterProfiler (R package, version 3.8.1, R version 3.5.1) and ClueGo (a plugin of Cytospace, version v2.5.4, Cytospace version v3.7.1)[36-37]. GO terms with $pvalue < 0.01$ and KEGG pathways with $pvalue < 0.05$ were considered as significantly enriched.

Flow cytometry analysis of apoptosis

After porcine GCs exposed 10 μM or 30 μM ZEA for 48 h, the flow cytometry was utilized to detect the level of apoptosis of it. Briefly, GCs were collected and we utilized PBS to wash it

at least three times. Then, according to the manufacturer's instructions the Annexin V-FITC/PI kit (Tran, Fa101, Beijing, China) was added to samples. Notably, the PI has adhesion, so before flow cytometry, the GCs were filtered using 150 mesh sieves and washed clean as much as possible. Subsequently, the FACSCalibur flow cytometer detected these samples.

Immunofluorescence

Immunofluorescence analysis (IF) was performed by a standard method with minor modifications[38]. Briefly, immunofluorescence was performed with the following steps: 1) We collected the adherent GCs, which were digested with trypsin for 3 minutes at 37 °C. 2) GCs were put into 4 % paraformaldehyde at 4 °C for at least 45 minutes. 3) About 30 μl cell suspensions were smeared on slide glass. The smears were permeabilized for 10 minutes in PBST (PBS added 0.5 % Triton X-100) then blocked for 45 minutes in PBST supplemented with 10 % goat serum (BOSTER, AR0009, Wuhan, China). 4) Slides were then incubated with primary antibodies (Table S1) at 4 °C overnight. 5) Then the secondary antibodies were added and incubated for at least 45 minutes at 37 °C. 6) We used Hoechst33342 to perform nuclei staining for 5 minutes and the slides were finally mounted with Antifade Mounting Medium. The fluorescence imaging system (Olympus BX51, Tokyo, Japan) was used to take photos and performed subsequent analysis.

Western blotting

Western blotting (WB) analysis was performed by a standard method with minor modifications and was used to detect the expression of proteins [39-40]. Briefly, the SDS-PAGE separated the

total proteins and then shifted it to PVDF membranes. Subsequently, blocked the PVDF membranes carrying protein in TBST (Tris-buffered saline with Tween-20) buffer added 5 % bovine serum albumin (BSA, Solarbio, A8020, Beijing, China) at 4 °C for at least 2 h, the PVDF membranes were then incubated in TBST buffer added 10 % BSA with primary antibody (Table S2) for at least 7 h at 4 °C. The next step is that the PVDF membranes were incubated in TBST buffer with secondary antibodies for 2 h. Finally, we adopted AlphaView SA software to determine the levels of expression of proteins.

Statistical analysis

All experiments were subjected to at least three independent replicates, except for Flow cytometry analysis of apoptosis, because we only wanted to verify the repeatability of previous studies. We adopted mean ± SEM (Standard Error of Mean) to show data, used one-way ANOVA with Duncan's multiple range test to determine differences among samples and further rechecked the results by Student's t test via Graphpad Prism 8.0 software.

Results

Overview of RNA sequencing and lncRNAs identification in porcine GCs exposed to ZEA *in vitro*

Previous research has indicated that ZEA exposure causes toxic effects on animal ovarian cells [13-14], but the effect on lncRNA expression in porcine GCs has not been described. To investigate the lncRNA expression dynamics following ZEA exposure, the porcine GCs were cultured *in vitro* and exposed to different concentration ZEA, including 10 μM and 30 μM, respectively

(Fig. 1A).

As culture proceeded, cellular apoptosis increased from 24 h and 48 h groups (Fig. 1B). Annexin-V fluorescence analysis showed that after ZEA exposure for 48 h, in terms of the experimental group, the percentage of positive GCs was dramatically increased with ZEA concentration (Fig. 1C). Early apoptotic cells were slightly elevated in the Ctrl (3.28 %), 10 μM (4.72 %) and 30 μM (5.59 %) groups, respectively. A larger change was seen in the late apoptotic cells where the 30 μM ZEA exposed group (29.3 %) was significantly higher when comparing to the Ctrl (10.0 %) and the 10 μM (14.3 %) groups (Fig. 1D).

To further study the toxic effect of ZEA exposure on porcine GCs, we performed an RNA-seq study. A brief diagrammatic drawing of the porcine GCs *in vitro* culture model and experimental procedures of this study are in Fig. 1A. With the RNA-seq 64,164,686 raw reads were generated in all 6 libraries, and after quality control we gained 63,587,260 clean reads (Fig. S1A). We adopted a highly strict filtering pipeline to identify the lncRNAs, which could remove transcripts without the characteristics of lncRNA (Fig. 1E). We compared the length of mRNA and lncRNA and revealed that mRNA was located on 0 to 10,000 bp, while the lncRNA was located on 200 to 5,000 bp (Fig. 1F). This pipeline produced 3,202 lncRNA genes with 3,811 lncRNA transcripts relevant to this (Figs. 1G and S1B). To verify the stability of samples, we made the correlation analysis based on Euclidean distances and the principal components analysis (Figs. S1C and S1D).

Identification of differential expression of lncRNAs and mRNAs

To further explore the effect of ZEA on the differential expression of lncRNAs and mRNAs in

porcine GCs, DESeq2 was utilized. For lncRNAs, there were 100, 106 and 12 up-regulated lncRNAs in the Ctrl *vs.* 10 μM group, the Ctrl *vs.* 30 μM group and the 10 μM *vs.* 30 μM group, respectively; conversely, the down-regulated lncRNAs were 115, 139 and 28, respectively (Fig. 2A). For mRNAs, the up-regulated expression was 332, 442 and 11 in the different groups, respectively. Meanwhile, the down-regulated expression was 615, 837 and 24 in the different groups, respectively (Fig. 2B).

Furthermore, Chord Diagram was utilized to show the distribution and expression of each lncRNA and mRNA per chromosome (Fig. 2C). Interestingly, overall the number of DELs was less than DEMs. In chromosome 2, chromosome 3 and chromosome X, the DEMs were much more than the DELs. In chromosome 7, there was an expressional peak of lncRNAs, and in chromosome X, there was an expressional peak of mRNAs, which may be related to their respective functions.

Function overview of DELs

It has been reported that the *trans*-role of lncRNAs is related to their co-expressed genes[35]. To investigate the function of DELs, in the different treatment groups, we calculated the Pearson's correlation coefficients between DELs and DEMs using Hmisc. The results showed that 947 co-expressed mRNAs (CEMs) related to lncRNAs were differentially expressed in the Ctrl *vs.* 10 μM group, and 1,248 CEMs related to lncRNAs were differentially expressed in the Ctrl *vs.* 30 μM group (Fig. 3A).

Subsequently, we performed the GO enrich analysis of these CEMs. In the Ctrl *vs.* 10 μM group (Figs. 3B and 3D), we found that the CEMs carried 70 biological process GO terms and

we showed the top 20 according to *pvalues*. Furthermore, ClueGo, showed 26 biological process GO terms. We found that the top 3 GO terms according to *pvalues* were GO:0051607 (defense response to virus), GO:0009615 (response to virus) and GO:0043330 (response to exogenous dsRNA), using clusterProfiler. Moreover, ClueGo also showed the biological process GO term, GO:0043330. In the Ctrl *vs.* the 30 μM group (Figs. 3C and 3E) we found that the CEMs carried 54 biological process GO terms and we showed the top 20 according to *pvalues*. ClueGo, showed 11 biological process GO terms. We found that the top 3 GO terms according to *pvalues* were GO:0051607, GO:0043604 (amide biosynthetic process), and GO:0006412 (translation). Moreover, ClueGo also showed the biological process GO term, GO:0051607.

In addition, some biological process GO terms related to the JAK-STAT signaling pathway were enriched, including GO:0033139 (regulation of peptidyl-serine phosphorylation of STAT protein), GO:0033141 (positive regulation of peptidyl-serine phosphorylation of STAT protein) and GO:0042501 (serine phosphorylation of STAT protein), which suggested that the JAK-STAT signaling pathway plays crucial roles in porcine GCs after ZEA exposure.

Further analysis of DELs

Further exploration of the function of different clustered lncRNAs was performed. We explored the function of lncRNAs, including the intersection between the differentially expressed lncRNA in the Ctrl *vs.* 10 μM group and the Ctrl *vs.* 30 μM group (Fig. 4A).

We found the Chord Diagram and Heatmap showed dynamic expression patterns (Figs. 4B-4C). Subsequently, GO and KEGG signaling pathway enrichment analysis of CEMs were

283 performed in the Ctrl *vs.* 10 μM group. We found 936 CEMs and in the Ctrl *vs.* 30 μM group
284 co-expression of mRNAs was 1,248 (Fig. 4D). Similarly, we utilized the two software
285 platforms, clusterProfiler and ClueGO, to perform GO and KEGG signaling pathway
286 enrichment analysis. We identified GO terms related to the JAK-STAT signaling pathway,
287 including GO:0033141 and GO:0033139 (Figs. 4E and 4F). KEGG signaling pathway
288 enrichment analysis showed that many terms related to disease, such as ssc05414 (dilated
289 cardiomyopathy (DCM)) were enriched (Figs. S2A and S2B).
290 Next, we performed the same analysis for the following lncRNAs, including the
291 intersection between the DELs in the Ctrl *vs.* 10 μM group and the 10 μM *vs.* 30 μM group
292 (Figs. S3) and the intersection between the DELs in the Ctrl *vs.* 30 μM group and the 10 μM
293 *vs.* 30 μM group (Figs. S4).
294
295 **Identification of the core lncRNA cluster**
296 In order to identify the core lncRNA cluster, we believed that the intersections between the
297 differentially expressed lncRNA in the Ctrl *vs.* 10 μM group, the Ctrl *vs.* 30 μM group and the
298 10 μM *vs.* 30 μM group would identify the core lncRNA cluster. To identify the function of
299 this cluster of lncRNAs (Fig. 5A), the Chord Diagram and Heatmap showed dramatically
300 dynamic expression patterns in this cluster (Figs. 5C and 5E). *Cis*-regulation analysis and
301 *trans*-regulation analysis were performed.
302 On the one hand, lncRNA could serve as trans-regulatory elements and control the
303 expression of adjacent genes, here we detected 780, 1,101 and 26 CEMs in the Ctrl *vs.* 10 μM
304 group, the Ctrl *vs.* 30 μM group and the 10 μM *vs.* 30 μM group, respectively (Fig. 5B). Two

methods, GO and KEGG signaling pathway enrichment analysis, were used to predict the function of the lncRNAs.

In the Ctrl *vs.* 10 μM groups we found that the CEMs carried 30 biological process GO terms while ClueGo showed 17 biological process GO terms (Figs. 5G and 5I). In these GO terms, many were related to the JAK2-STAT3 signaling pathway, including GO:0033139, GO:0033141, GO:0042501 and so on. For KEGG signaling pathway terms in this group, the results indicated that many terms were related to disease, such as ssc05414 (Fig. S5A). In the Ctrl *vs.* 30 μM group, we found that the CEMs carried 48 biological process GO terms while ClueGO showed 14 Biological process GO terms (Figs. 5H and 5J). Many of the GO terms were related to the JAK-STAT signaling pathway by further analysis, including GO:0033139, GO:0046425 (regulation of JAK-STAT cascade), GO:1904892 (regulation of STAT cascade), and so on. We analyzed all biological process GO terms and the Venn diagram showed a relationship between the different group, including 7 shared terms (Fig. 5D)**.** We analyzed the 7 shared terms and found that some terms were related to the JAK-STAT signaling pathway, including GO:0033139, GO:0033141 and GO:0042501, this GO terms hinted that it was related to regulation STAT protein.

The results of KEGG signaling pathway analysis in this group showed that this part of lncRNA (Fig. 5A) may be related to disease, such as ssc05414 (Fig. S5B). One the other hand, we searched for all coding genes, which were located at 10 kb-100 kb upstream and downstream of this part of lncRNAs (Fig. 5A). The results showed that MSTRG.26353, MSTRG.26354 and MSTRG.26355 were next to *TOP2A* (Fig. 5F). It had been reported that *TOP2A* was related to cell cycle, cell survival and so on[41-43].

Based on the above analysis, we chose to verify the core proteins of the JAK-STAT signaling pathway by WB and IF analysis, such as JAK2 and STAT3. The results of IF analysis showed that porcine GCs significantly up-regulated the expression of STAT3 after ZEA exposure (Figs. 6A and 6C). Porcine GCs also up-regulated the expression of JAK2 after ZEA exposure, however it was not as obvious as STAT3 (Figs. 6B and 6D). The results of WB analysis showed that porcine GCs up-regulated the expression of JAK2 and STAT3 after ZEA exposure, meanwhile the functional STAT3 protein, p-STAT3, was also up-regulated though not significantly (Figs. 6E-6G).

Prediction of the key lncRNA of regulating JAK-STAT signaling pathway

In order to find which lncRNA played a core role in regulating the JAK-STAT signaling pathway, we performed hierarchical cluster analysis. The results showed that for the left branch, the correlation between MSTRG.26353 and MSTRG.26355 was strongest, and for the right, the correlation between MSTRG.22680 and MSTRG.23882 was strongest (Fig. 7A). We hypothesize that either MSTRG.26353 and MSTRG.26355 or MSTRG.22680 and MSTRG.23882 played pivotal role in regulating JAK-STAT signaling pathway.

We then performed co-expression analysis of MSTRG.26353 and MSTRG.26355 or MSTRG.22680 and MSTRG.23882. The results showed that in the Ctrl *vs.* 10 μM groups MSTRG.26353 and MSTRG.26355 carried 3 CEMs, and in the Ctrl *vs.* 30 μM group it carried 9 (Fig. 7A). For MSTRG.22680 and MSTRG.23882, it carried 587 CEMs in the Ctrl *vs.* 10 μM groups and 994 in the Ctrl *vs.* 30 μM groups (Fig. 7A). We performed GO enrichment analysis for co-expression. There were no GO terms enriched in the CEMs of MSTRG.26353

and MSTRG.26355. However, these CEMs of MSTRG.22680 and MSTRG.23882 showed GO terms related to the JAK2-STAT3 signaling pathway (Fig. 7B), which indicated that MSTRG.22680 and MSTRG.23882 may play a vital role in regulating JAK2-STAT3 signaling pathway.

Discussion

ZEA, a harmful toxin commonly found in contaminated feedstuffs, played negative influences in the development of GCs. Consistent to previous studies[10, 13-14], we also found that ZEA exposure was able to induce the apoptosis of porcine GCs. Based on this, the study of porcine GCs after ZEA exposure carries a certain significance, which may provide the theoretical basis to reduce the loss resulting from ZEA exposure to the animal industry.

Recently, studies of ZEA exposure have been mainly focused on mRNAs rather than on lncRNAs[10, 14]. In this paper, for the first time we focused on the changes of lncRNA in porcine GCs after ZEA exposure. To obtain a better comprehension of regulation of lncRNAs in porcine GCs after ZEA exposure, we adopted RNA-seq technology in this research. Moreover, RNA-seq also revealed that porcine GCs after ZEA exposure had altered lncRNAs and mRNAs expression. Notably, the potential coding capability was the key to distinguish the non-coding and protein-coding genes. In this research, we performed a highly rigorous filtering workflow to maximize the identification of positive candidate lncRNAs. We selected Stringtie to perform transcriptome assembly and identified 3202 candidate lncRNAs[27]. In agreement with similar studies, the candidate lncRNAs had these basic characteristics, compared with the protein-coding genes, they had fewer exon numbers and their transcript lengths were shorter[44-45]. Our

data showed that the expression of lncRNA was dramatically changed. In general, there were more up-regulated lncRNAs in porcine GCs after ZEA exposure, which indicated that porcine GCs after ZEA exposure caused changes in genomic expression[14].

In order to better understand the functional mechanism of lncRNAs, we took the function of the DELs after exposure to ZEA into consideration. The GO terms of CEMs were related to the JAK-STAT signaling pathway. Moreover, through further analysis of the GO terms we specifically identified the JAK2-STAT3 signaling pathway, which was a branch of JAK-STAT signaling pathway, playing a major role. Interestingly, JAK2-STAT3 signaling pathway is related to anti-apoptosis mechanism[25]. The above analysis seems to be at odds with previous studies[14], but may be interpreted that it is a self-protection mechanism. In order to explore this, we analyzed the intersection of differentially expressed lncRANs in different groups. We found that some lncRNAs were indeed related to the regulation of the JAK2-STAT3 signaling pathway. In addition, we determined the core lncRNA cluster showing that its function was related to regulating the JAK2-STAT3 signaling pathway. Many studies illustrated that the JAK2-STAT3 signaling pathway exerts a vital role in regulating apoptosis since STAT3 has anti-apoptosis abilities[46-47]. After ZEA exposure, the expression of related proteins was up-regulated. GCs will regulate lncRNAs to activate the JAK2-STAT3 signaling pathway when their survival is threatened as an instinctive form of self-preservation. For the core lncRNA cluster, MSTRG.22680 and MSTRG.23882 played a key role in activating the JAK2-STAT3 signaling pathway, which provides guidance for subsequent studies.

In summary, our findings suggest that ZEA exposure dramatically increases the porcine GCs apoptosis and the change of lncRNAs expression promotes GCs anti-apoptosis via

activating the JAK2-STAT3 signaling pathway.

Abbreviations used

ZEA, Zearalenone; GCs, granulosa cells; JAK, Janus kinase; STAT, signal transducer and activator of transcription; RNA-seq, ribonucleic acid sequencing; FPKM, fragments per kilobase per million reads; TPM, transcripts per kilobase million; CPC2, coding potential calculator 2; CNCI, coding-non-coding-index; DMEM, Dulbecco's modified Eagle's medium; FBS, fetal bovine serum; BSA, bovine serum albumin; GO, gene ontology; KEGG, kyoto encyclopedia of genes and genomes; WB, western blotting; IF, immunofluorescence; SEM, standard error of mean; DELs, differentially expressed lncRNAs; DEMs, differentially expressed mRNAs; CEMs, co-expressed mRNAs.

Conflicts of interest

None.

Acknowledgements

This work was supported by National Natural Science Foundation of China (31572225), National Key Research and Development Program of China (2016YFD0501207) and Taishan Scholar Construction Foundation of Shandong Province. The authors would also like to thank Dr. Paul W. Dyce at the University of Auburn and Dr. Shen Yin at Qingdao Agricultural University for their careful edits to the manuscript.

References

1. Caldwell, R. W.; Tuite, J.; Stob, M.; Baldwin, R., Zearalenone production by Fusarium species. *Appl Microbiol* **1970,** *20* (1), 31-4.
2. Kuiper-Goodman, T.; Scott, P. M.; Watanabe, H., Risk assessment of the mycotoxin zearalenone. *Regul Toxicol Pharmacol* **1987,** *7* (3), 253-306.
3. Muller, H. M.; Reimann, J.; Schumacher, U.; Schwadorf, K., Fusarium toxins in wheat harvested during six years in an area of southwest Germany. *Nat Toxins* **1997,** *5* (1), 24-30.
4. Pang, J.; Zhou, Q.; Sun, X.; Li, L.; Zhou, B.; Zeng, F.; Zhao, Y.; Shen, W.; Sun, Z., Effect of low-dose zearalenone exposure on reproductive capacity of male mice. *Toxicol Appl Pharmacol* **2017,** *333*, 60-67.
5. Yang, D.; Jiang, X.; Sun, J.; Li, X.; Li, X.; Jiao, R.; Peng, Z.; Li, Y.; Bai, W., Toxic effects of zearalenone on gametogenesis and embryonic development: A molecular point of review. *Food Chem Toxicol* **2018,** *119*, 24-30.
6. Kuiper, G. G.; Lemmen, J. G.; Carlsson, B.; Corton, J. C.; Safe, S. H.; van der Saag, P. T.; van der Burg, B.; Gustafsson, J. A., Interaction of estrogenic chemicals and phytoestrogens with estrogen receptor beta. *Endocrinology* **1998,** *139* (10), 4252-63.
7. Lai, F. N.; Ma, J. Y.; Liu, J. C.; Wang, J. J.; Cheng, S. F.; Sun, X. F.; Li, L.; Li, B.; Nyachoti, C. M.; Shen, W., The influence of N-acetyl-l-cysteine on damage of porcine oocyte exposed to zearalenone in vitro. *Toxicol Appl Pharmacol* **2015,** *289* (2), 341-8.
8. Qin, X.; Cao, M.; Lai, F.; Yang, F.; Ge, W.; Zhang, X.; Cheng, S.; Sun, X.; Qin, G.; Shen, W.; Li, L., Oxidative stress induced by zearalenone in porcine granulosa cells and its rescue by curcumin in vitro. *PloS one* **2015,** *10* (6), e0127551.
9. Liu, K. H.; Sun, X. F.; Feng, Y. Z.; Cheng, S. F.; Li, B.; Li, Y. P.; Shen, W.; Li, L., The impact of Zearalenone on the meiotic progression and primordial follicle assembly during early oogenesis. *Toxicol Appl Pharmacol* **2017,** *329*, 9-17.
10. Zhang, G. L.; Sun, X. F.; Feng, Y. Z.; Li, B.; Li, Y. P.; Yang, F.; Nyachoti, C. M.; Shen, W.; Sun, S. D.; Li, L., Zearalenone exposure impairs ovarian primordial follicle formation via down-regulation of Lhx8 expression in vitro. *Toxicol Appl Pharmacol* **2017,** *317*, 33-40.
11. Matsuda, F.; Inoue, N.; Manabe, N.; Ohkura, S., Follicular growth and atresia in mammalian ovaries: regulation by survival and death of granulosa cells. *J Reprod Dev* **2012,** *58* (1), 44-50.
12. Lai, F. N.; Liu, J. C.; Li, L.; Ma, J. Y.; Liu, X. L.; Liu, Y. P.; Zhang, X. F.; Chen, H.; De Felici, M.; Dyce, P. W.; Shen, W., Di (2-ethylhexyl) phthalate impairs steroidogenesis in ovarian follicular cells of prepuberal mice. *Arch Toxicol* **2017,** *91* (3), 1279-1292.
13. Zhang, R. Q.; Sun, X. F.; Wu, R. Y.; Cheng, S. F.; Zhang, G. L.; Zhai, Q. Y.; Liu, X. L.; Zhao, Y.; Shen, W.; Li, L., Zearalenone exposure elevated the expression of tumorigenesis genes in mouse ovarian granulosa cells. *Toxicol Appl Pharmacol* **2018,** *356*, 191-203.
14. Liu, X. L.; Wu, R. Y.; Sun, X. F.; Cheng, S. F.; Zhang, R. Q.; Zhang, T. Y.; Zhang, X. F.; Zhao, Y.; Shen, W.; Li, L., Mycotoxin zearalenone exposure impairs genomic stability of swine follicular granulosa cells in vitro. *Int J Biol Sci* **2018,** *14* (3), 294-305.
15. Baley, J.; Li, J., MicroRNAs and ovarian function. *J Ovarian Res* **2012,** *5*, 8.
16. Zhan, L.; Li, J.; Wei, B., Long non-coding RNAs in ovarian cancer. *J Exp Clin Cancer Res* **2018,** *37* (1), 120.
17. Silva, J. M.; Boczek, N. J.; Berres, M. W.; Ma, X.; Smith, D. I., LSINCT5 is over expressed in breast and ovarian cancer and affects cellular proliferation. *RNA Biol* **2011,** *8* (3), 496-505.
18. Lyu, Y.; Lou, J.; Yang, Y.; Feng, J.; Hao, Y.; Huang, S.; Yin, L.; Xu, J.; Huang, D.; Ma, B.; Zou, D.; Wang, Y.;

Zhang, Y.; Zhang, B.; Chen, P.; Yu, K.; Lam, E. W.; Wang, X.; Liu, Q.; Yan, J.; Jin, B., Dysfunction of the WT1-MEG3 signaling promotes AML leukemogenesis via p53-dependent and -independent pathways. *Leukemia* **2017,** *31* (12), 2543-2551.

19. Rossi, M. N.; Antonangeli, F., LncRNAs: New Players in Apoptosis Control. *Int J Cell Biol* **2014,** *2014*, 473857.

20. Pickard, M. R.; Mourtada-Maarabouni, M.; Williams, G. T., Long non-coding RNA GAS5 regulates apoptosis in prostate cancer cell lines. *Biochim Biophys Acta* **2013,** *1832* (10), 1613-23.

21. Wang, O.; Yang, F.; Liu, Y.; Lv, L.; Ma, R.; Chen, C.; Wang, J.; Tan, Q.; Cheng, Y.; Xia, E.; Chen, Y.; Zhang, X., C-MYC-induced upregulation of lncRNA SNHG12 regulates cell proliferation, apoptosis and migration in triple-negative breast cancer. *Am J Transl Res* **2017,** *9* (2), 533-545.

22. Wang, K.; Long, B.; Zhou, L. Y.; Liu, F.; Zhou, Q. Y.; Liu, C. Y.; Fan, Y. Y.; Li, P. F., CARL lncRNA inhibits anoxia-induced mitochondrial fission and apoptosis in cardiomyocytes by impairing miR-539-dependent PHB2 downregulation. *Nature communications* **2014,** *5*, 3596.

23. O'Shea, J. J.; Gadina, M.; Schreiber, R. D., Cytokine signaling in 2002: new surprises in the Jak/Stat pathway. *Cell* **2002,** *109 Suppl*, S121-31.

24. Schroder, K.; Hertzog, P. J.; Ravasi, T.; Hume, D. A., Interferon-gamma: an overview of signals, mechanisms and functions. *J Leukoc Biol* **2004,** *75* (2), 163-89.

25. Catlett-Falcone, R.; Landowski, T. H.; Oshiro, M. M.; Turkson, J.; Levitzki, A.; Savino, R.; Ciliberto, G.; Moscinski, L.; Fernandez-Luna, J. L.; Nunez, G.; Dalton, W. S.; Jove, R., Constitutive activation of Stat3 signaling confers resistance to apoptosis in human U266 myeloma cells. *Immunity* **1999,** *10* (1), 105-15.

26. Chen, S.; Zhou, Y.; Chen, Y.; Gu, J., fastp: an ultra-fast all-in-one FASTQ preprocessor. *Bioinformatics* **2018,** *34* (17), i884-i890.

27. Pertea, M.; Pertea, G. M.; Antonescu, C. M.; Chang, T. C.; Mendell, J. T.; Salzberg, S. L., StringTie enables improved reconstruction of a transcriptome from RNA-seq reads. *Nat Biotechnol* **2015,** *33* (3), 290-5.

28. Sun, L.; Luo, H.; Bu, D.; Zhao, G.; Yu, K.; Zhang, C.; Liu, Y.; Chen, R.; Zhao, Y., Utilizing sequence intrinsic composition to classify protein-coding and long non-coding transcripts. *Nucleic Acids Res* **2013,** *41* (17), e166.

29. Kang, Y. J.; Yang, D. C.; Kong, L.; Hou, M.; Meng, Y. Q.; Wei, L.; Gao, G., CPC2: a fast and accurate coding potential calculator based on sequence intrinsic features. *Nucleic Acids Res* **2017,** *45* (W1), W12-W16.

30. Li, W.; Cowley, A.; Uludag, M.; Gur, T.; McWilliam, H.; Squizzato, S.; Park, Y. M.; Buso, N.; Lopez, R., The EMBL-EBI bioinformatics web and programmatic tools framework. *Nucleic Acids Res* **2015,** *43* (W1), W580-4.

31. Love, M. I.; Huber, W.; Anders, S., Moderated estimation of fold change and dispersion for RNA-seq data with DESeq2. *Genome Biol* **2014,** *15* (12), 550.

32. Ponjavic, J.; Oliver, P. L.; Lunter, G.; Ponting, C. P., Genomic and transcriptional co-localization of protein-coding and long non-coding RNA pairs in the developing brain. *PLoS Genet* **2009,** *5* (8), e1000617.

33. Orom, U. A.; Derrien, T.; Beringer, M.; Gumireddy, K.; Gardini, A.; Bussotti, G.; Lai, F.; Zytnicki, M.; Notredame, C.; Huang, Q.; Guigo, R.; Shiekhattar, R., Long noncoding RNAs with enhancer-like function in human cells. *Cell* **2010,** *143* (1), 46-58.

34. Wucher, V.; Legeai, F.; Hedan, B.; Rizk, G.; Lagoutte, L.; Leeb, T.; Jagannathan, V.; Cadieu, E.; David, A.; Lohi, H.; Cirera, S.; Fredholm, M.; Botherel, N.; Leegwater, P. A. J.; Le Beguec, C.; Fieten, H.; Johnson, J.; Alfoldi, J.; Andre, C.; Lindblad-Toh, K.; Hitte, C.; Derrien, T., FEELnc: a tool for long non-coding RNA annotation and its application to the dog transcriptome. *Nucleic Acids Res* **2017,** *45* (8), e57.

35. Zhan, S.; Dong, Y.; Zhao, W.; Guo, J.; Zhong, T.; Wang, L.; Li, L.; Zhang, H., Genome-wide identification

and characterization of long non-coding RNAs in developmental skeletal muscle of fetal goat. *BMC Genomics* **2016,** *17*, 666.
36. Yu, G.; Wang, L. G.; Han, Y.; He, Q. Y., clusterProfiler: an R package for comparing biological themes among gene clusters. *OMICS* **2012,** *16* (5), 284-7.
37. Bindea, G.; Mlecnik, B.; Hackl, H.; Charoentong, P.; Tosolini, M.; Kirilovsky, A.; Fridman, W. H.; Pages, F.; Trajanoski, Z.; Galon, J., ClueGO: a Cytoscape plug-in to decipher functionally grouped gene ontology and pathway annotation networks. *Bioinformatics* **2009,** *25* (8), 1091-3.
38. Ge, W.; Zhao, Y.; Lai, F. N.; Liu, J. C.; Sun, Y. C.; Wang, J. J.; Cheng, S. F.; Zhang, X. F.; Sun, L. L.; Li, L.; Dyce, P. W.; Shen, W., Cutaneous applied nano-ZnO reduce the ability of hair follicle stem cells to differentiate. *Nanotoxicology* **2017,** *11* (4), 465-474.
39. Chao, H. H.; Zhang, X. F.; Chen, B.; Pan, B.; Zhang, L. J.; Li, L.; Sun, X. F.; Shi, Q. H.; Shen, W., Bisphenol A exposure modifies methylation of imprinted genes in mouse oocytes via the estrogen receptor signaling pathway. *Histochem Cell Biol* **2012,** *137* (2), 249-59.
40. Zhang, P.; Chao, H.; Sun, X.; Li, L.; Shi, Q.; Shen, W., Murine folliculogenesis in vitro is stage-specifically regulated by insulin via the Akt signaling pathway. *Histochem Cell Biol* **2010,** *134* (1), 75-82.
41. Bakshi, R. P.; Galande, S.; Muniyappa, K., Functional and regulatory characteristics of eukaryotic type II DNA topoisomerase. *Crit Rev Biochem Mol Biol* **2001,** *36* (1), 1-37.
42. Singh, B. N.; Achary, V. M. M.; Panditi, V.; Sopory, S. K.; Reddy, M. K., Dynamics of tobacco DNA topoisomerases II in cell cycle regulation: to manage topological constrains during replication, transcription and mitotic chromosome condensation and segregation. *Plant Mol Biol* **2017,** *94* (6), 595-607.
43. Kozuki, T.; Chikamori, K.; Surleac, M. D.; Micluta, M. A.; Petrescu, A. J.; Norris, E. J.; Elson, P.; Hoeltge, G. A.; Grabowski, D. R.; Porter, A. C. G.; Ganapathi, R. N.; Ganapathi, M. K., Roles of the C-terminal domains of topoisomerase IIalpha and topoisomerase IIbeta in regulation of the decatenation checkpoint. *Nucleic Acids Res* **2017,** *45* (10), 5995-6010.
44. Ran, M.; Chen, B.; Li, Z.; Wu, M.; Liu, X.; He, C.; Zhang, S.; Li, Z., Systematic Identification of Long Noncoding RNAs in Immature and Mature Porcine Testes. *Biol Reprod* **2016,** *94* (4), 77.
45. Pauli, A.; Valen, E.; Lin, M. F.; Garber, M.; Vastenhouw, N. L.; Levin, J. Z.; Fan, L.; Sandelin, A.; Rinn, J. L.; Regev, A.; Schier, A. F., Systematic identification of long noncoding RNAs expressed during zebrafish embryogenesis. *Genome research* **2012,** *22* (3), 577-91.
46. Yu, H.; Pardoll, D.; Jove, R., STATs in cancer inflammation and immunity: a leading role for STAT3. *Nat Rev Cancer* **2009,** *9* (11), 798-809.
47. Yu, H.; Lee, H.; Herrmann, A.; Buettner, R.; Jove, R., Revisiting STAT3 signalling in cancer: new and unexpected biological functions. *Nat Rev Cancer* **2014,** *14* (11), 736-46.

Figure legends

Figure 1. The effects of ZEA exposure on porcine GCs *in vitro* culture and the identification of lncRNAs. (A) Brief porcine GCs *in vitro* culture model and the experimental procedures of this study. (B) Bright field imaging of porcine GCs during different stages *in vitro* culture. Scale bar, 100 μm. (C) Annexin-V/PI staining of porcine GCs during different stages *in vitro*

543 culture. Scale bar, 50 μm. (D) Porcine GCs were cultured in the presence of ZEA (0, 10 μM
544 and 30 μM) for 48 h and cell apoptosis levels were determined using flow cytometry. (E)
545 Bioinformatics pipeline for identifying lncRNAs, and "Material and methods" for details. (F)
546 The Joyplot of the length of lncRNAs and mRNAs. (G) Filtration of the candidate lncRNAs
547 indicated by the Venn diagrams based on our filter pipeline. Coding potential analysis of
548 candidate lncRNAs was performed by using three tools (CNCI, CPC2, Pfamscan).
549
550 **Figure 2.** Overview of the differential expression levels of lncRNAs and mRNAs. (A) The
551 Volcano Plot showed the differential expression levels of lncRNAs in different group, and the
552 Bar Chart showed the results. (B) The Volcano Plot showed the differential expression levels
553 of mRNAs in different group, and the Bar Chart showed the results. (C) The Chord Diagram
554 showed the distribution and expression of each lncRNA and mRNA in chromosome.
555
556 **Figure 3.** Overview of the function of DELs. (A) The co-expression mRNAs related to DELs.
557 (B) The results of biological process GO terms of DELs in the Ctrl *vs.* 10 μM group by ClueGO.
558 (C) The results of biological process GO terms of DELs in the Ctrl *vs.* 30 μM group by ClueGO.
559 (D) The results of biological process GO terms of DELs in the Ctrl *vs.* 10 μM group by
560 clusterProfiler. (E) The results of biological process GO terms of DELs in the Ctrl *vs.* 30 μM
561 group by clusterProfiler.
562
563 **Figure 4.** Further analysis of DELs in porcine GCs after ZEA exposure. (A) The Venn diagram
564 showed DELs that it was the intersection between the differentially expressed lncRNA in Ctrl

565 *vs.* 10 μM group and Ctrl *vs.* 30 μM group. (B, C) The Chord Diagram and Heatmap showed
566 the expression model of lncRNAs. (D) The Bar Chart showed the co-expression genes related
567 to lncRNAs. (E) The Bar Chart showed the top 20 biological process GO terms according to
568 *pvalues* by clusterProfiler (Up was the Ctrl *vs.* 10 μM group, down was the Ctrl *vs.* 30 μM
569 group). (F) The Network cahrt showed the Biological process GO terms according to *pvalues*
570 by ClueGO (Lift was the Ctrl *vs.* 10 μM group, right was the Ctrl *vs.* 30 μM group).
571
572 **Figure 5.** Identification of the core lncRNA cluster. (A) The Venn diagram showed DELs that
573 we believed it was the core lncRNA cluster. (B) The Bar Chart showed the co-expression genes
574 related to lncRNAs. (C, E) The Chord Diagram and Heatmap showed the expression model of
575 lncRNAs. (D) The Venn diagram showed the shared GO terms between different groups. (F)
576 The Bar Chart showed the results of co-location analysis (10 kb-100 kb) and co-expression
577 analysis ($|r| > 0.9$ & *pvalue* < 0.05) of core lncRNAs. * means co-location genes, ** means co-
578 location and co-expression genes. (G) The Bar Chart showed the top 20 biological process GO
579 terms according to *pvalues* in the Ctrl *vs.* 10 μM group by clusterProfiler. (H) The Bar Chart
580 showed the top 20 biological process GO terms according to *pvalues* in the Ctrl *vs.* 30 μM
581 group by clusterProfiler. (I) The Network Polt showed the Biological process GO terms
582 produced by ClueGO in the Ctrl *vs.* 10 μM group. (J) The Network Polt showed the Biological
583 process GO terms produced by ClueGO in the Ctrl *vs.* 30 μM group.
584
585 **Figure 6.** The verification of bioinformatic analysis. (A) Immunostaining of STAT3 (Red) in
586 porcine GCs exposed to 0 (Ctrl), 10 or 30 μM ZEA for 48 h, Hoechst 33342 (Blue) was used

for nuclei staining. (B) Immunostaining of JAK2 (Green) in porcine GCs exposed to 0 (Ctrl), 10 or 30 μM ZEA for 48 h, Hoechst 33342 (Blue) was used for nuclei staining. (C) The analysis of the mean intensity of STAT3. (D) The analysis of the mean intensity of JAK2. (E-G) Analysis of the expression level of JAK2-STAT3 signaling pathway related protein by WB in porcine GCs after 0 (Ctrl), 10 and 30 μM ZEA exposure for 48 h. GAPDH was used as loading control. The data are demonstrated as the means ± SEM ($n \geq 3$), * meant *pvalue* < 0.05, ** meant *pvalue* < 0.01, *** meant *pvalue* < 0.001.

Figure 7. Prediction of the key lncRNA related to regulating JAK-STAT signaling pathway. (A) Left: The co-expression analysis of MSTRG.26353 and MSTRG.26355. Middle: The Tree Diagram showed the results of hierarchical cluster analysis of core lncRNAs. Right: The co-expression analysis of MSTRG.22680 and MSTRG.23882. (B) The results of GO enrichment terms of MSTRG.22680 and MSTRG.23882.

Supplementary figure legends

Figure S1. Overview of RNA-seq. (A) The data output and related information in this study. (B) The transcripts of lncRNAs that we finally determined. (C) The Euclidean distances Analysis of samples. (D) The Principal Components Analysis of samples.

Figure S2. KEGG analysis support Figure 4. (A) The KEGG analysis of co-expression mRNAs in the Ctrl *vs.* 10 μM group (Up was produced by clusterProfiler, down was produced

609 by ClueGo). (B) The KEGG analysis of co-expression mRNAs in the Ctrl *vs.*30 μM group (Up
610 is produced by clusterProfiler, down is produced by ClueGo).
611
612 **Figure S3.** Expression and function prediction of lncRNAs that it was the intersection between
613 the differentially expressed lncRNA in the Ctrl *vs.* 10 μM group and the 10 μM *vs.* 30 μM
614 group. (A) The Venn diagram showed DELs that it was the intersection between the
615 differentially expressed lncRNA the Ctrl *vs.* 10 μM group and the 10 μM *vs.* 30 μM group. (B,
616 C) The Chord Diagram and Heatmap showed the expression model of lncRNAs. (D) The Bar
617 Chart showed the co-expression genes related to lncRNAs. (E) The Bar Chart showed the top
618 20 biological process GO terms according to *pvalues* in the Ctrl *vs.* 10 μM group produced by
619 clusterProfiler. (F) The Network Polt showed the Biological process GO terms produced by
620 ClueGO in the Ctrl *vs.* 10 μM group. (G) The Bar Chart showed the KEGG terms produced by
621 clusterProfiler in the Ctrl *vs.* 10 μM group. (H) The Bar Chart showed the KEGG terms
622 produced by ClueGO in the Ctrl *vs.* 10 μM group.
623
624 **Figure S4.** Expression and function prediction of lncRNAs that it was the intersection between
625 the differentially expressed lncRNA in the Ctrl *vs.* 30 μM group and the 10 μM *vs.* 30 μM
626 group. (A) The Venn diagram showed DELs that it was the intersection between the
627 differentially expressed lncRNA in the Ctrl *vs.* 30 μM group and the 10 μM *vs.* 30 μM group.
628 (B, C) The Chord Diagram and Heatmap showed the expression model of lncRNAs. (D) The
629 Bar Chart showed the co-expression genes related to lncRNAs. (E) The Bar Chart showed the
630 top 20 biological process GO terms according to *pvalues* in the Ctrl *vs.* 30 μM group by

clusterProfiler. (F) The Network Polt showed the Biological process GO terms produced by ClueGO in the Ctrl *vs.* 30 μM group. (G) The Bar Chart showed the KEGG terms produced by clusterProfiler in the Ctrl *vs.* 30 μM group. (H) The Bar Chart showed the KEGG terms produced by ClueGO in the Ctrl *vs.* 30 μM group.

Figure S5. KEGG signaling pathway enrichment analysis support Figure 5. (A) The KEGG analysis of co-expression mRNAs in the Ctrl *vs.* 10 μM group (Lift is produced by clusterProfiler, right is produced by ClueGo). (B) The KEGG analysis of co-expression mRNAs in the Ctrl *vs.*30 μM group (Left is produced by clusterProfiler, right is produced by ClueGo).

Supplementary tables

Table S1. Primary antibody of IF.

Table S2. Primary antibody of WB.

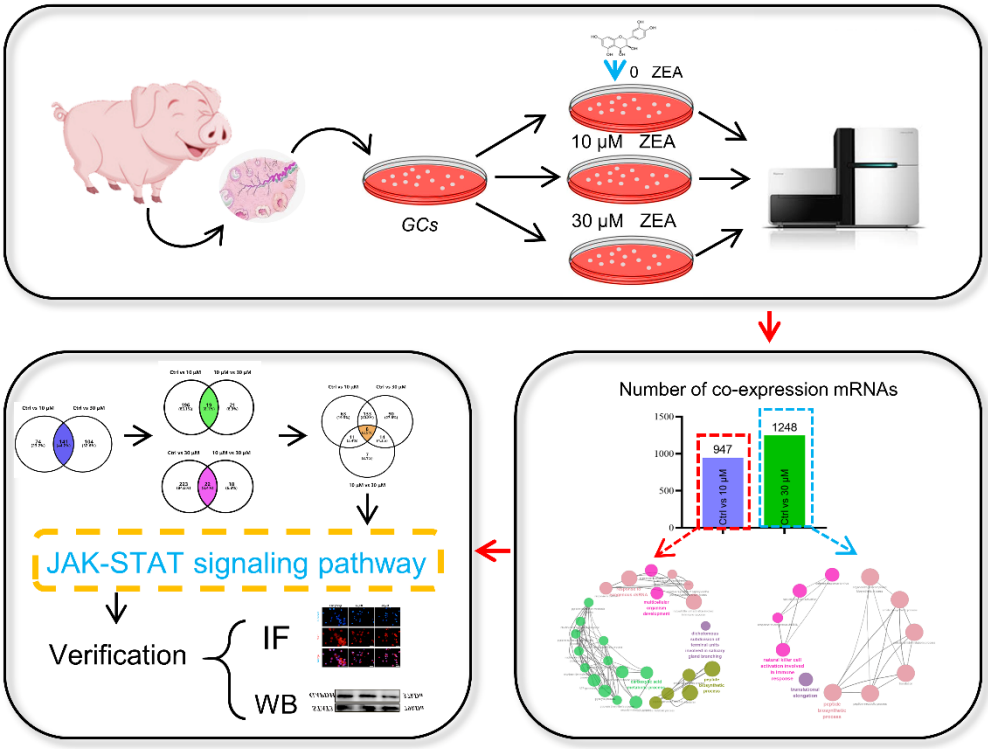
0 ZEA
10 μM ZEA
30 μM ZEA
GCs
Number of co-expression mRNAs
1500
1000
500
0
947
1248
Ctrl vs 10 μM
Ctrl vs 30 μM
JAK-STAT signaling pathway
Verification
IF
WB

647

Figure 1

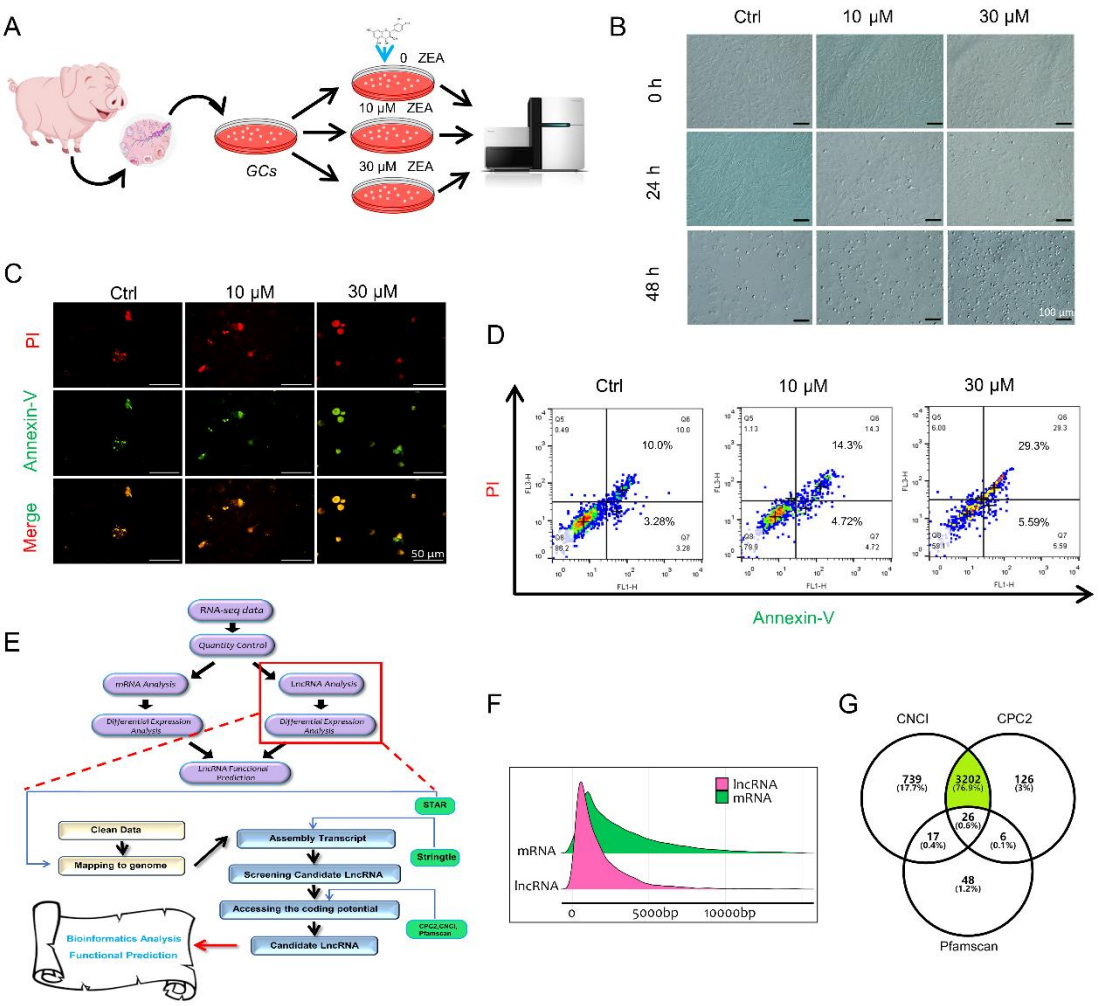
A
0 ZEA
10 μM ZEA
30 μM ZEA
GCs
B
Ctrl
10 μM
30 μM
0 h
24 h
48 h
C
Ctrl
10 μM
30 μM
PI
Annexin-V
Merge
D
Ctrl
10 μM
30 μM
PI
10.0%
3.28%
14.3%
4.72%
29.3%
5.59%
Annexin-V
E
RNA-seq data
Quantity Control
mRNA Analysis
LncRNA Analysis
Clean Data
Mapping to genome
Assembly Transcript
Screening Candidate LncRNA
Accessing the coding potential
Candidate LncRNA
Bioinformatics Analysis
Functional Prediction
STAR
Stringtie
F
lncRNA
mRNA
mRNA
lncRNA
0
5000bp
10000bp
G
CNCI
CPC2
Pfamscan
739
(17.7%)
3202
(76.9%)
126
(3%)
26
(0.6%)
17
(0.4%)
6
(0.1%)
48
(1.2%)

Figure 2

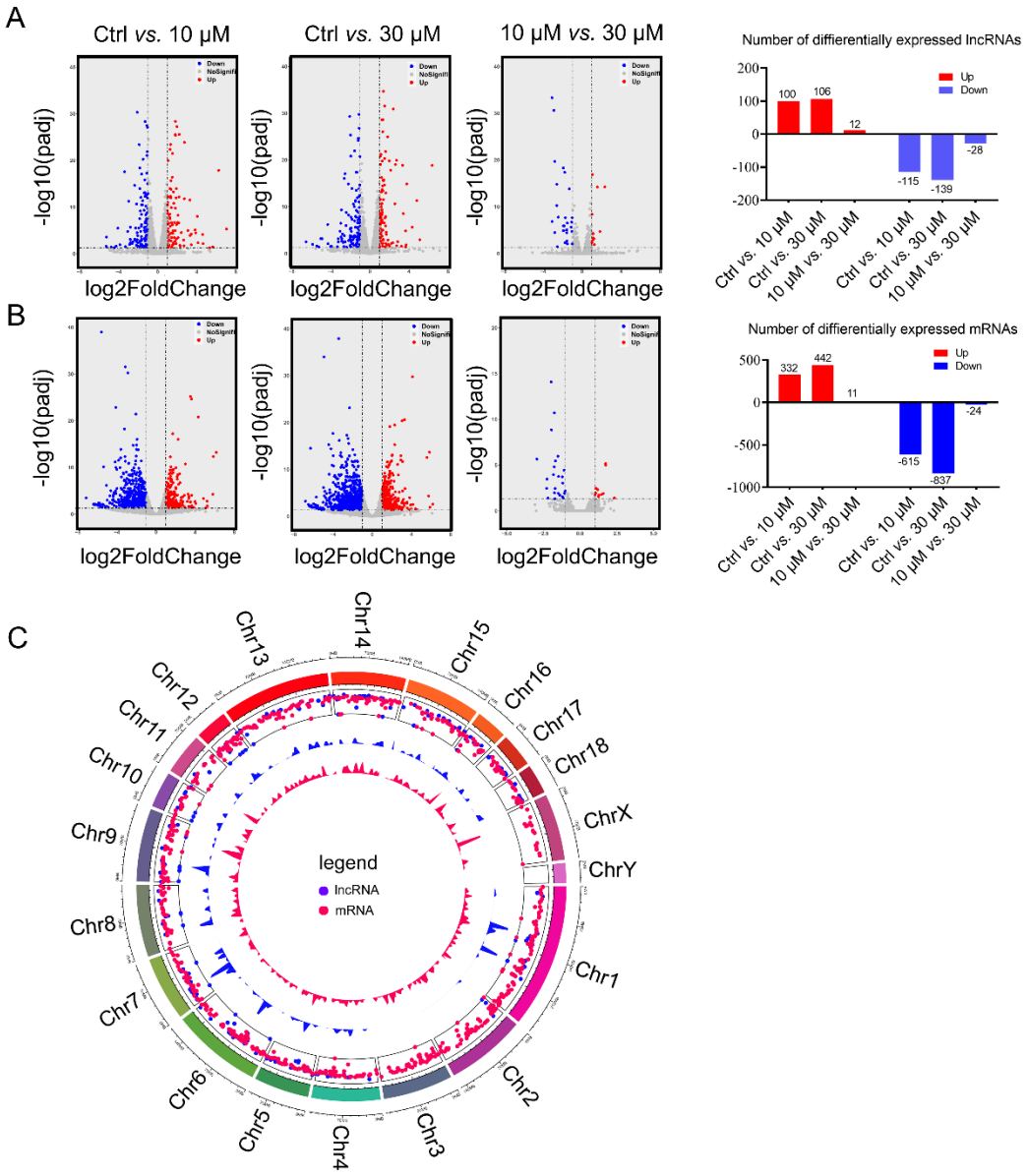
A
Ctrl vs. 10 μM
Ctrl vs. 30 μM
10 μM vs. 30 μM
-log10(padj)
log2FoldChange
B
Number of differentially expressed lncRNAs
Number of differentially expressed mRNAs
Up
Down
Ctrl vs. 10 μM
Ctrl vs. 30 μM
10 μM vs. 30 μM
C
legend
lncRNA
mRNA
Chr1
Chr2
Chr3
Chr4
Chr5
Chr6
Chr7
Chr8
Chr9
Chr10
Chr11
Chr12
Chr13
Chr14
Chr15
Chr16
Chr17
Chr18
ChrX
ChrY

649

Figure 3

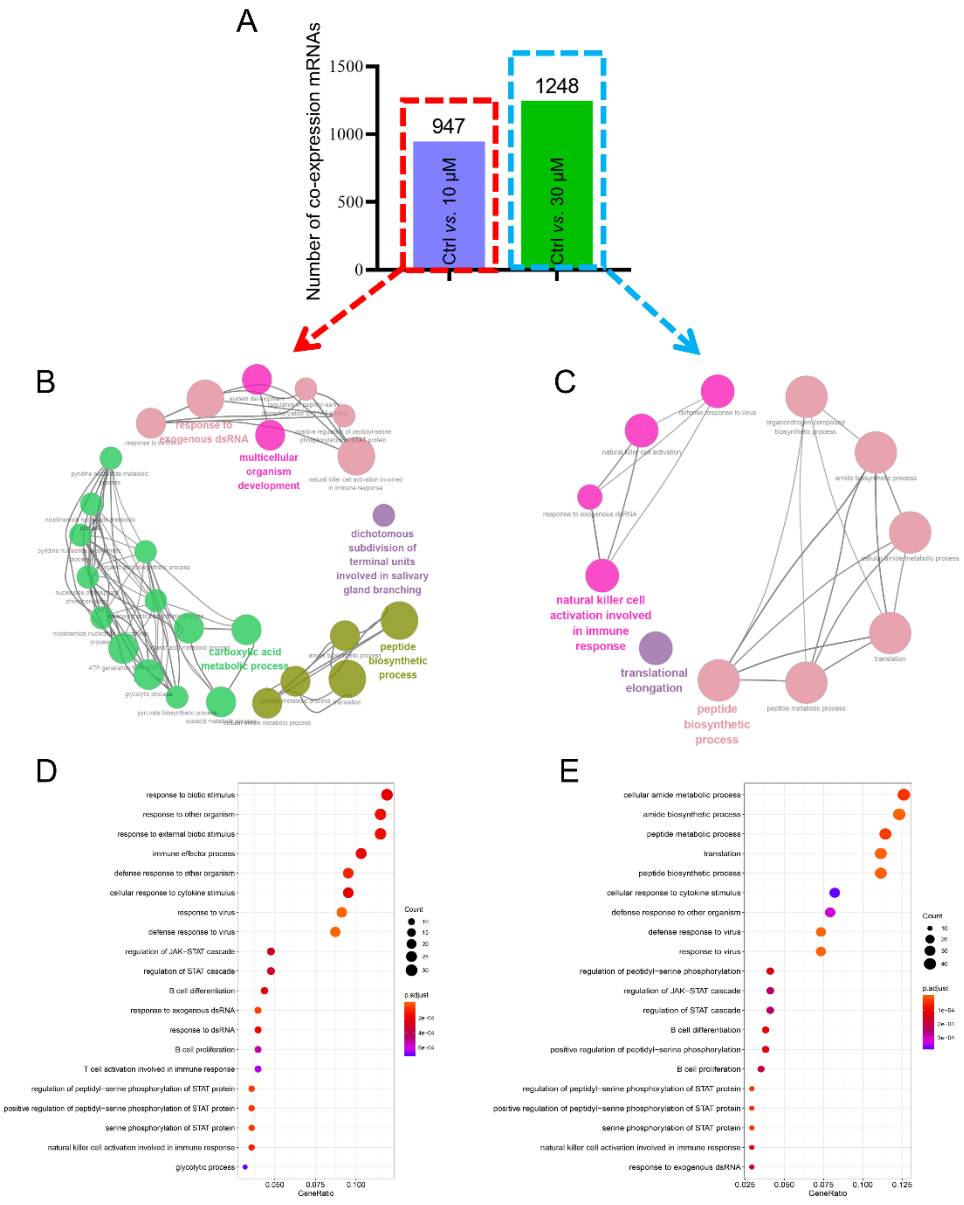
A
Number of co-expression mRNAs
1500
1000
500
0
947
1248
Ctrl vs. 10 μM
Ctrl vs. 30 μM
B
response to exogenous dsRNA
multicellular organism development
dichotomous subdivision of terminal units involved in salivary gland branching
carboxylic acid metabolic process
peptide biosynthetic process
C
natural killer cell activation involved in immune response
translational elongation
peptide biosynthetic process
D
response to biotic stimulus
response to other organism
response to external biotic stimulus
immune effector process
defense response to other organism
cellular response to cytokine stimulus
response to virus
defense response to virus
regulation of JAK-STAT cascade
regulation of STAT cascade
B cell differentiation
response to exogenous dsRNA
response to dsRNA
B cell proliferation
T cell activation involved in immune response
regulation of peptidyl-serine phosphorylation of STAT protein
positive regulation of peptidyl-serine phosphorylation of STAT protein
serine phosphorylation of STAT protein
natural killer cell activation involved in immune response
glycolytic process
GeneRatio
Count
p.adjust
E
cellular amide metabolic process
amide biosynthetic process
peptide metabolic process
translation
peptide biosynthetic process
cellular response to cytokine stimulus
defense response to other organism
defense response to virus
response to virus
regulation of peptidyl-serine phosphorylation
regulation of JAK-STAT cascade
regulation of STAT cascade
B cell differentiation
positive regulation of peptidyl-serine phosphorylation
B cell proliferation
regulation of peptidyl-serine phosphorylation of STAT protein
positive regulation of peptidyl-serine phosphorylation of STAT protein
serine phosphorylation of STAT protein
natural killer cell activation involved in immune response
response to exogenous dsRNA
GeneRatio
Count
p.adjust

650

Figure 4

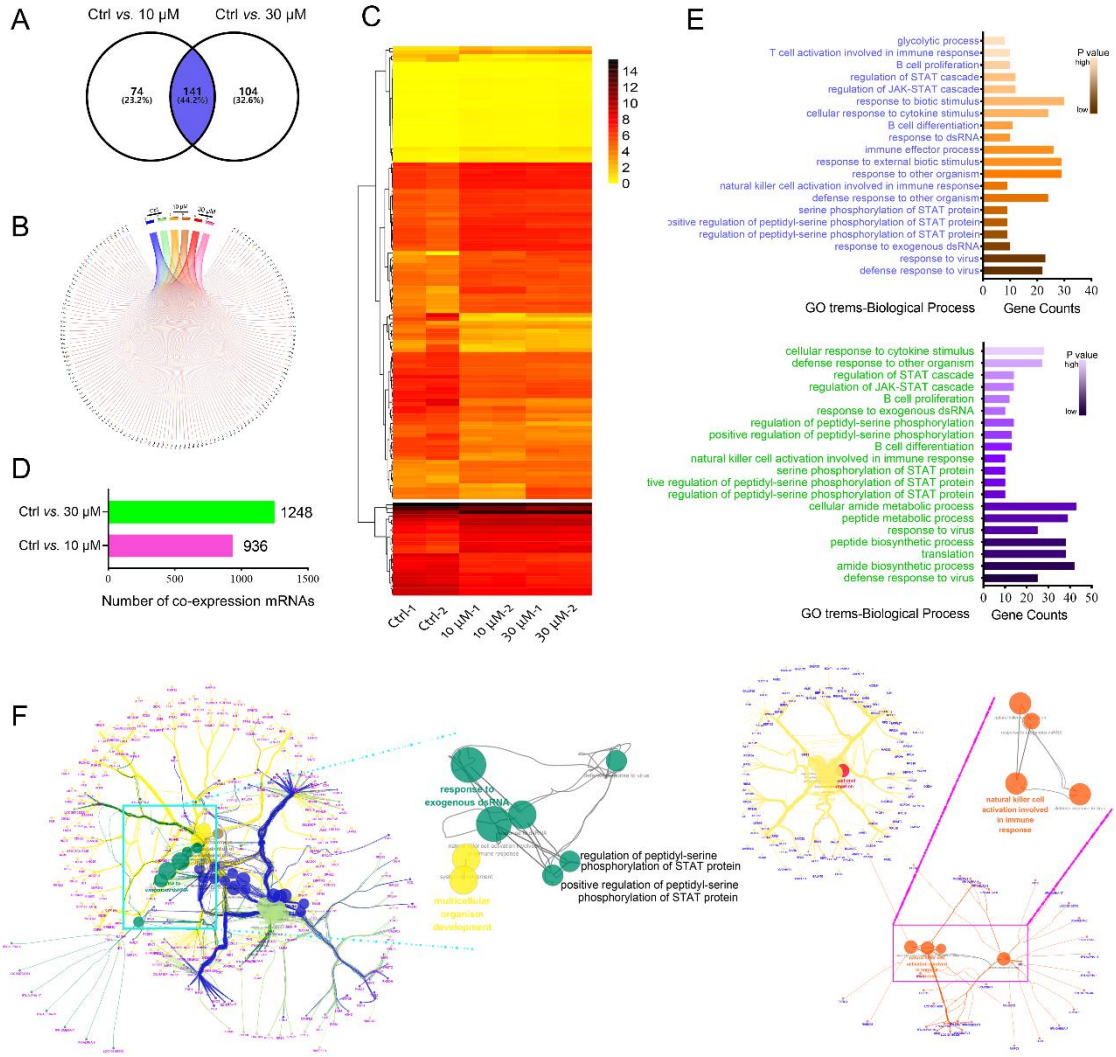
A
Ctrl vs. 10 μM
Ctrl vs. 30 μM
74 (23.2%)
141 (44.2%)
104 (32.6%)
B
C
14
12
10
8
6
4
2
0
Ctrl-1
Ctrl-2
10 μM-1
10 μM-2
30 μM-1
30 μM-2
D
Ctrl vs. 30 μM
1248
Ctrl vs. 10 μM
936
0
500
1000
1500
Number of co-expression mRNAs
E
glycolytic process
T cell activation involved in immune response
B cell proliferation
regulation of STAT cascade
regulation of JAK-STAT cascade
response to biotic stimulus
cellular response to cytokine stimulus
B cell differentiation
response to dsRNA
immune effector process
response to external biotic stimulus
response to other organism
natural killer cell activation involved in immune response
defense response to other organism
serine phosphorylation of STAT protein
positive regulation of peptidyl-serine phosphorylation of STAT protein
regulation of peptidyl-serine phosphorylation of STAT protein
response to exogenous dsRNA
response to virus
defense response to virus
P value
high
low
0 10 20 30 40
GO trems-Biological Process
Gene Counts
cellular response to cytokine stimulus
defense response to other organism
regulation of STAT cascade
regulation of JAK-STAT cascade
B cell proliferation
response to exogenous dsRNA
regulation of peptidyl-serine phosphorylation
positive regulation of peptidyl-serine phosphorylation
B cell differentiation
natural killer cell activation involved in immune response
serine phosphorylation of STAT protein
tive regulation of peptidyl-serine phosphorylation of STAT protein
regulation of peptidyl-serine phosphorylation of STAT protein
cellular amide metabolic process
peptide metabolic process
response to virus
peptide biosynthetic process
translation
amide biosynthetic process
defense response to virus
P value
high
low
0 10 20 30 40 50
GO trems-Biological Process
Gene Counts
F
response to exogenous dsRNA
multicellular organism development
regulation of peptidyl-serine phosphorylation of STAT protein
positive regulation of peptidyl-serine phosphorylation of STAT protein
natural killer cell activation involved in immune response

651

Figure 5

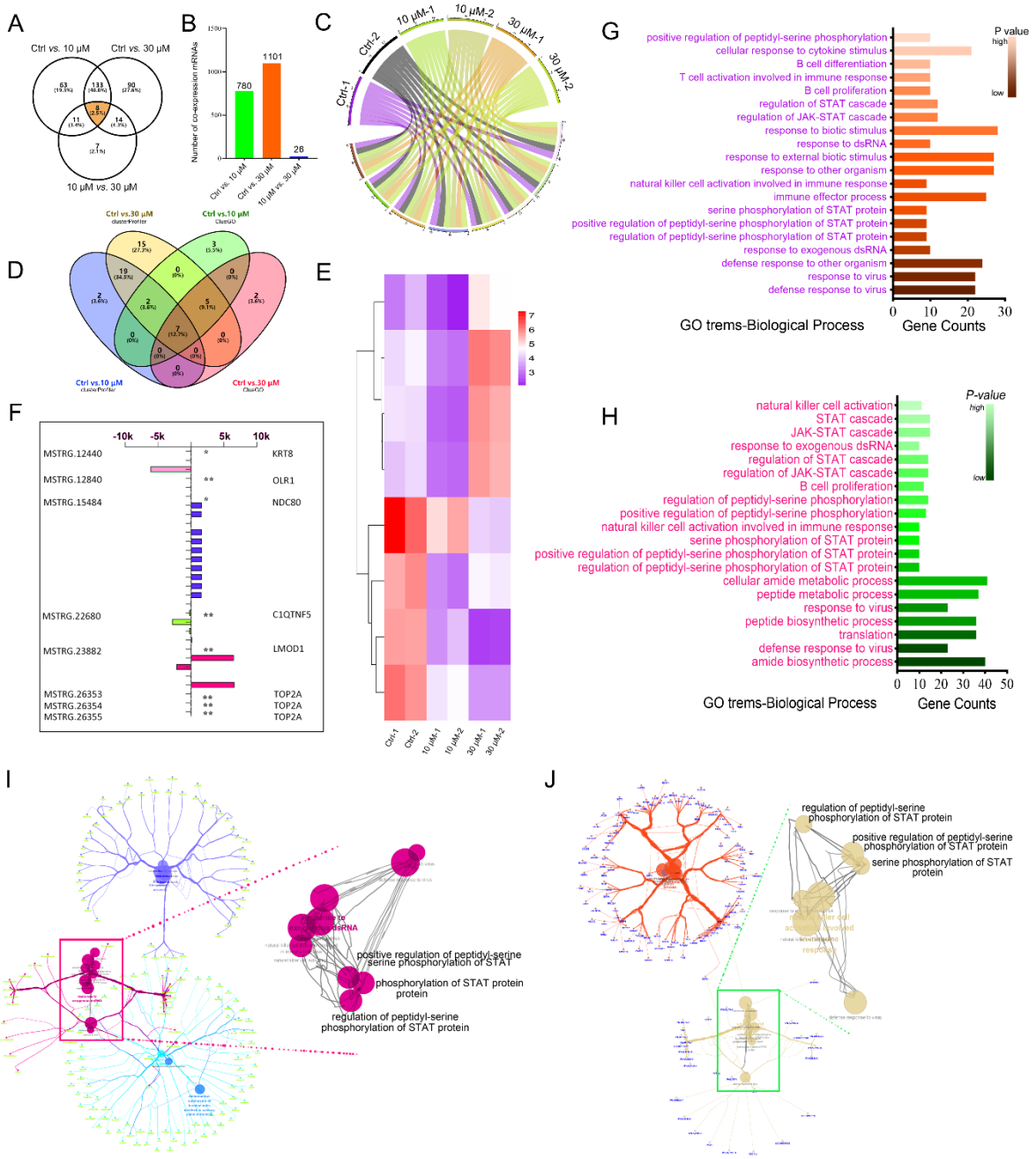
A
Ctrl vs. 10 μM
Ctrl vs. 30 μM
10 μM vs. 30 μM
B
Number of co-expression mRNAs
780
1101
26
C
Ctrl-1
Ctrl-2
10 μM-1
10 μM-2
30 μM-1
30 μM-2
D
Ctrl vs.30 μM
Ctrl vs.10 μM
E
F
-10k
-5k
5k
10k
MSTRG.12440
KRT8
MSTRG.12840
OLR1
MSTRG.15484
NDC80
MSTRG.22680
C1QTNF5
MSTRG.23882
LMOD1
MSTRG.26353
MSTRG.26354
MSTRG.26355
TOP2A
G
positive regulation of peptidyl-serine phosphorylation
cellular response to cytokine stimulus
B cell differentiation
T cell activation involved in immune response
B cell proliferation
regulation of STAT cascade
regulation of JAK-STAT cascade
response to biotic stimulus
response to dsRNA
response to external biotic stimulus
response to other organism
natural killer cell activation involved in immune response
immune effector process
serine phosphorylation of STAT protein
positive regulation of peptidyl-serine phosphorylation of STAT protein
regulation of peptidyl-serine phosphorylation of STAT protein
response to exogenous dsRNA
defense response to other organism
response to virus
defense response to virus
P value
high
low
GO trems-Biological Process
Gene Counts
H
natural killer cell activation
STAT cascade
JAK-STAT cascade
response to exogenous dsRNA
regulation of STAT cascade
regulation of JAK-STAT cascade
B cell proliferation
regulation of peptidyl-serine phosphorylation
positive regulation of peptidyl-serine phosphorylation
natural killer cell activation involved in immune response
serine phosphorylation of STAT protein
positive regulation of peptidyl-serine phosphorylation of STAT protein
regulation of peptidyl-serine phosphorylation of STAT protein
cellular amide metabolic process
peptide metabolic process
response to virus
peptide biosynthetic process
translation
defense response to virus
amide biosynthetic process
P-value
high
low
GO trems-Biological Process
Gene Counts
I
positive regulation of peptidyl-serine serine phosphorylation of STAT
phosphorylation of STAT protein protein
regulation of peptidyl-serine phosphorylation of STAT protein
J
regulation of peptidyl-serine phosphorylation of STAT protein
positive regulation of peptidyl-serine phosphorylation of STAT protein
serine phosphorylation of STAT protein

652

Figure 6

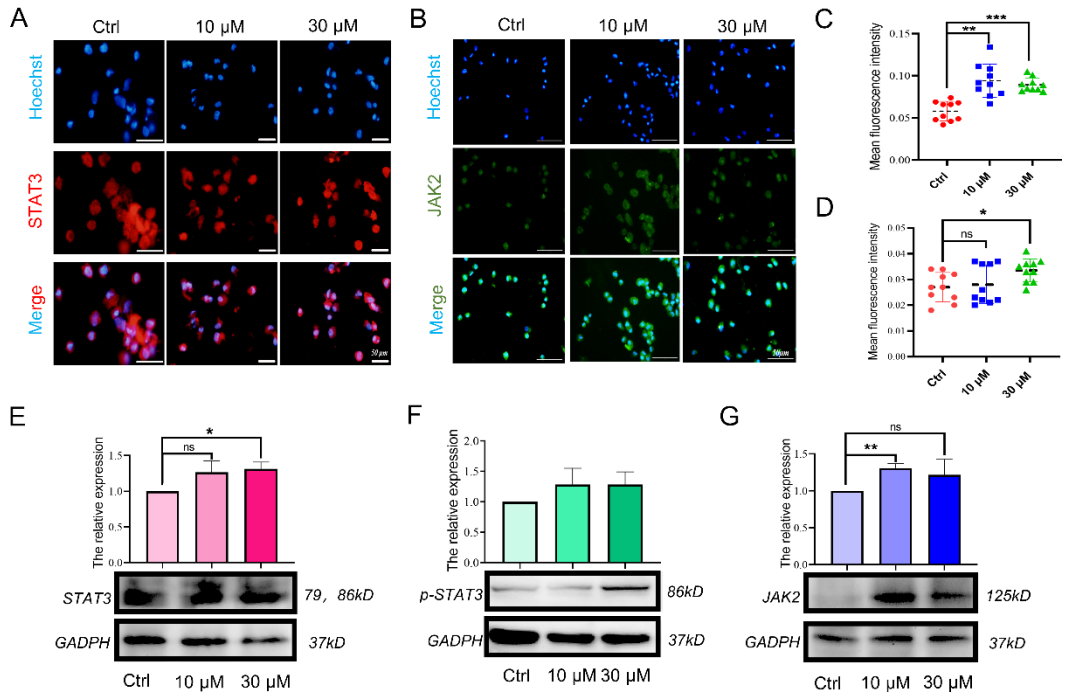
A
Ctrl
10 μM
30 μM
Hoechst
STAT3
Merge
B
Ctrl
10 μM
30 μM
Hoechst
JAK2
Merge
C
Mean fluorescence intensity
***
**
Ctrl
10 μM
30 μM
D
Mean fluorescence intensity
*
ns
Ctrl
10 μM
30 μM
E
The relative expression
*
ns
STAT3
79, 86kD
GADPH
37kD
Ctrl
10 μM
30 μM
F
The relative expression
p-STAT3
86kD
GADPH
37kD
Ctrl
10 μM
30 μM
G
The relative expression
ns
**
JAK2
125kD
GADPH
37kD
Ctrl
10 μM
30 μM

653

Figure 7

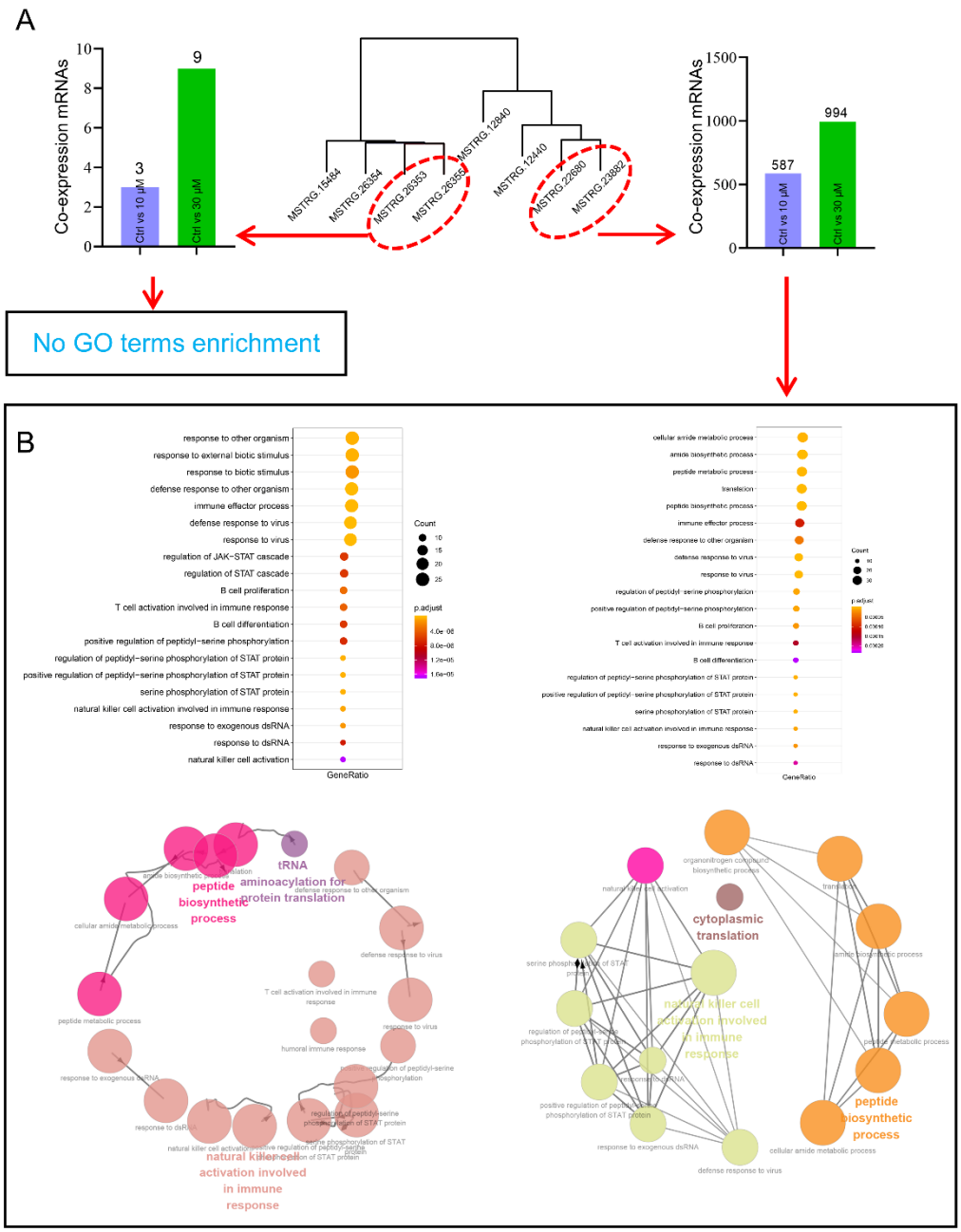
A
Co-expression mRNAs
Ctrl vs 10 μM
Ctrl vs 30 μM
3
9
MSTRG.15484
MSTRG.26354
MSTRG.26353
MSTRG.26359
MSTRG.12840
MSTRG.12440
MSTRG.22680
MSTRG.23882
587
994
No GO terms enrichment
B
response to other organism
response to external biotic stimulus
response to biotic stimulus
defense response to other organism
immune effector process
defense response to virus
response to virus
regulation of JAK-STAT cascade
regulation of STAT cascade
B cell proliferation
T cell activation involved in immune response
B cell differentiation
positive regulation of peptidyl-serine phosphorylation
regulation of peptidyl-serine phosphorylation of STAT protein
positive regulation of peptidyl-serine phosphorylation of STAT protein
serine phosphorylation of STAT protein
natural killer cell activation involved in immune response
response to exogenous dsRNA
response to dsRNA
natural killer cell activation
GeneRatio
Count
p.adjust
tRNA aminoacylation for protein translation
peptide biosynthetic process
natural killer cell activation involved in immune response
cytoplasmic translation
peptide biosynthetic process

Figure S1

A

Sample	Raw reads	Clean reads	Q20(%)	Q30(%)	GC contemt (%)
Ctrl-1	10677946	10559016	93.71	87.63	47.20
Ctrl-2	9792352	9668258	94.10	88.00	49.92
10 μM-1	10890598	10813977	94.56	88.92	49.52
10 μM-2	12625870	12532210	95.68	91.33	49.04
30 μM-1	11087387	11014287	95.94	91.81	49.37
30 μM-2	9090533	8999512	94.29	88.28	48.88

B

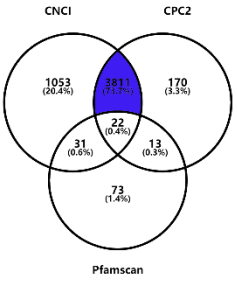

C

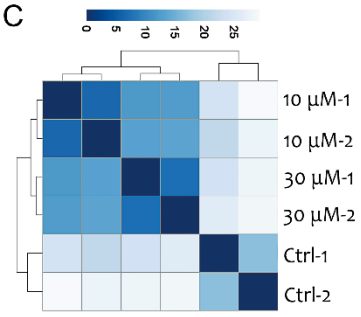

D

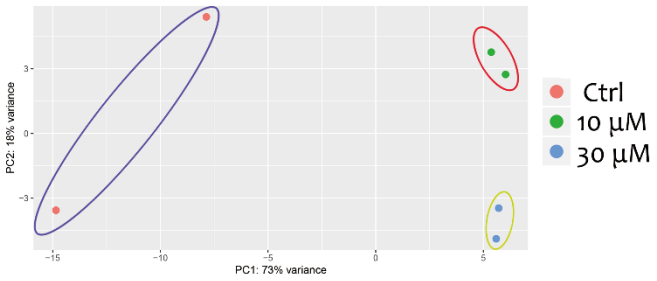

Figure S2

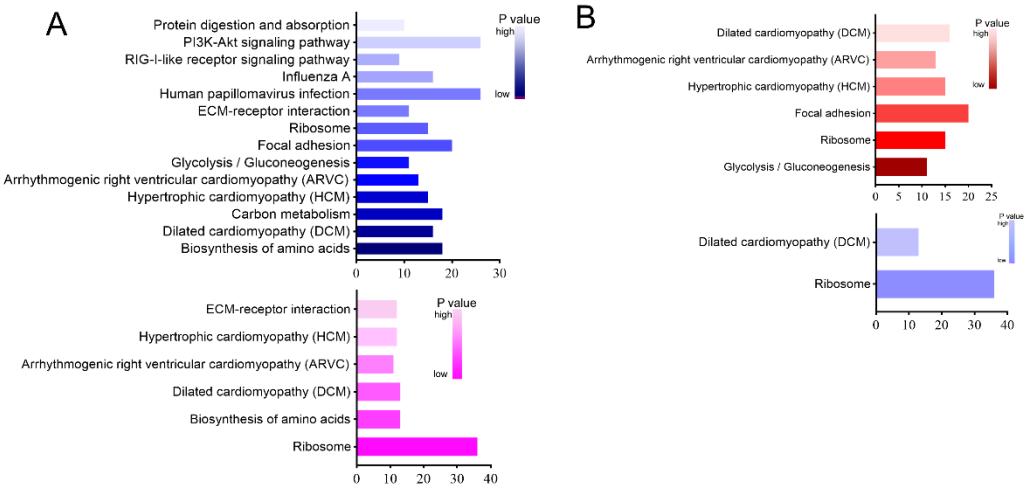

657

Figure S3

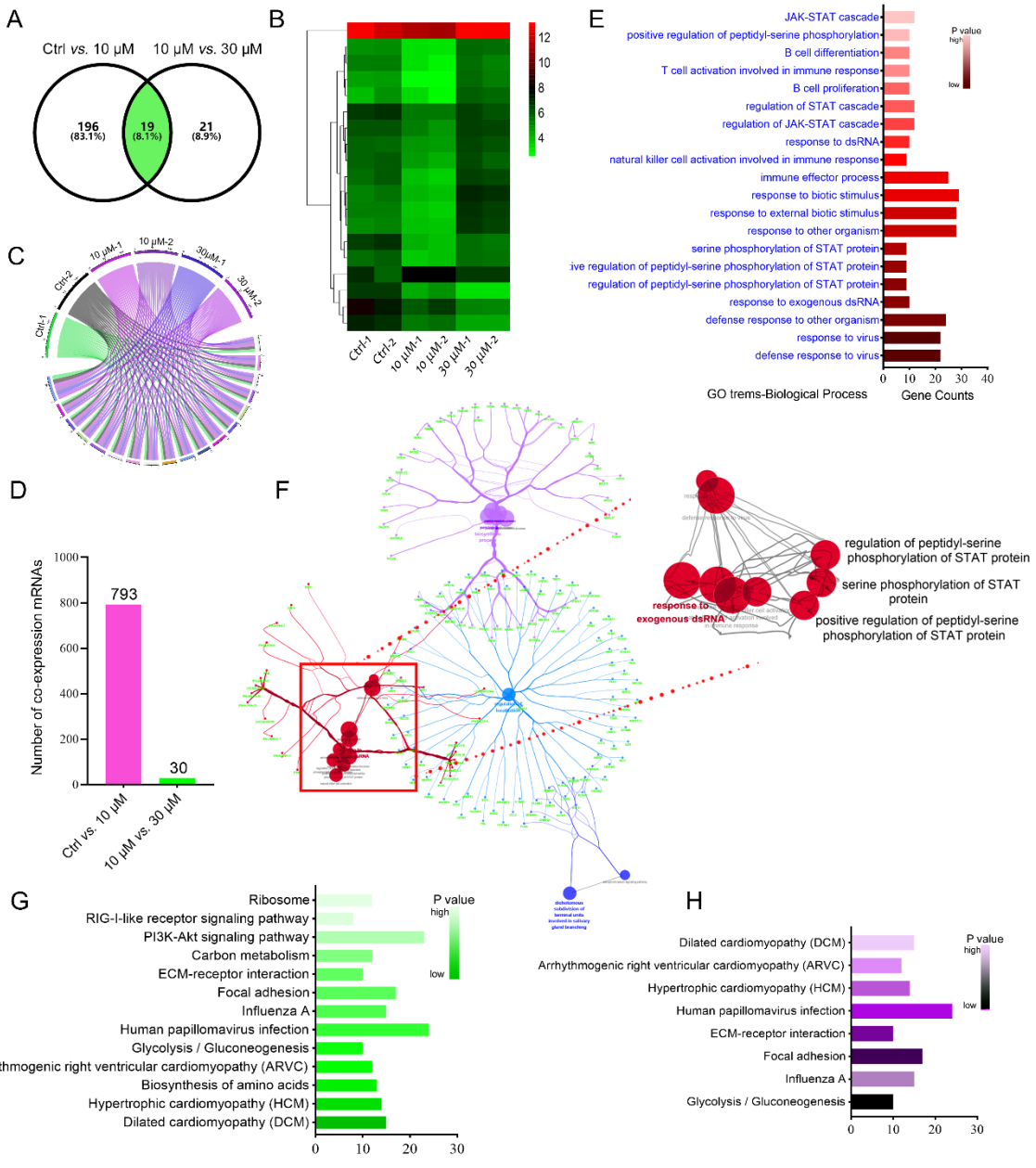

658

Figure S4

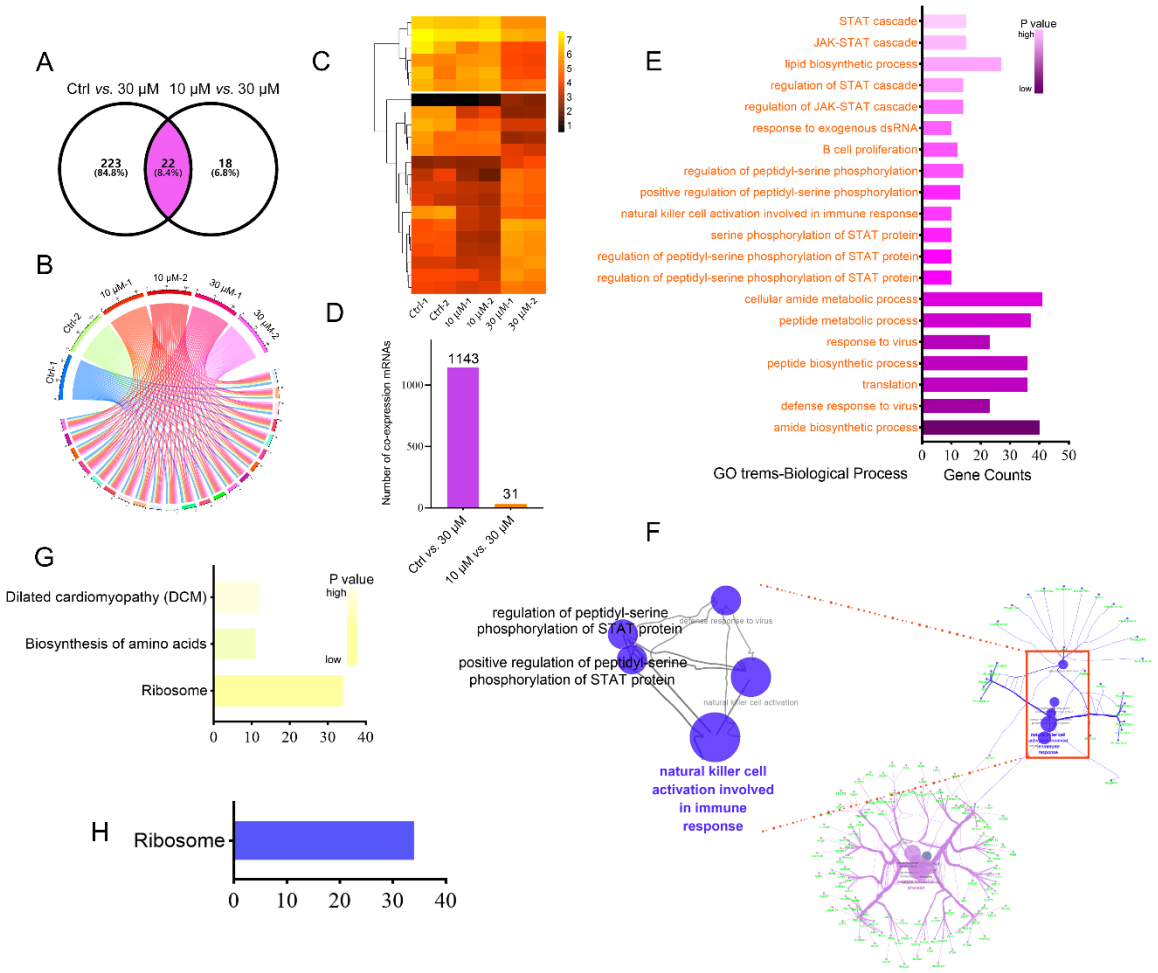
A
Ctrl vs. 30 μM
10 μM vs. 30 μM
223 (84.8%)
22 (8.4%)
18 (6.8%)
B
C
D
Number of co-expression mRNAs
1143
31
Ctrl vs. 30 μM
10 μM vs. 30 μM
E
STAT cascade
JAK-STAT cascade
lipid biosynthetic process
regulation of STAT cascade
regulation of JAK-STAT cascade
response to exogenous dsRNA
B cell proliferation
regulation of peptidyl-serine phosphorylation
positive regulation of peptidyl-serine phosphorylation
natural killer cell activation involved in immune response
serine phosphorylation of STAT protein
regulation of peptidyl-serine phosphorylation of STAT protein
regulation of peptidyl-serine phosphorylation of STAT protein
cellular amide metabolic process
peptide metabolic process
response to virus
peptide biosynthetic process
translation
defense response to virus
amide biosynthetic process
P value
high
low
GO trems-Biological Process
Gene Counts
F
regulation of peptidyl-serine phosphorylation of STAT protein
positive regulation of peptidyl-serine phosphorylation of STAT protein
natural killer cell activation involved in immune response
G
Dilated cardiomyopathy (DCM)
Biosynthesis of amino acids
Ribosome
P value
high
low
H
Ribosome

Figure S5

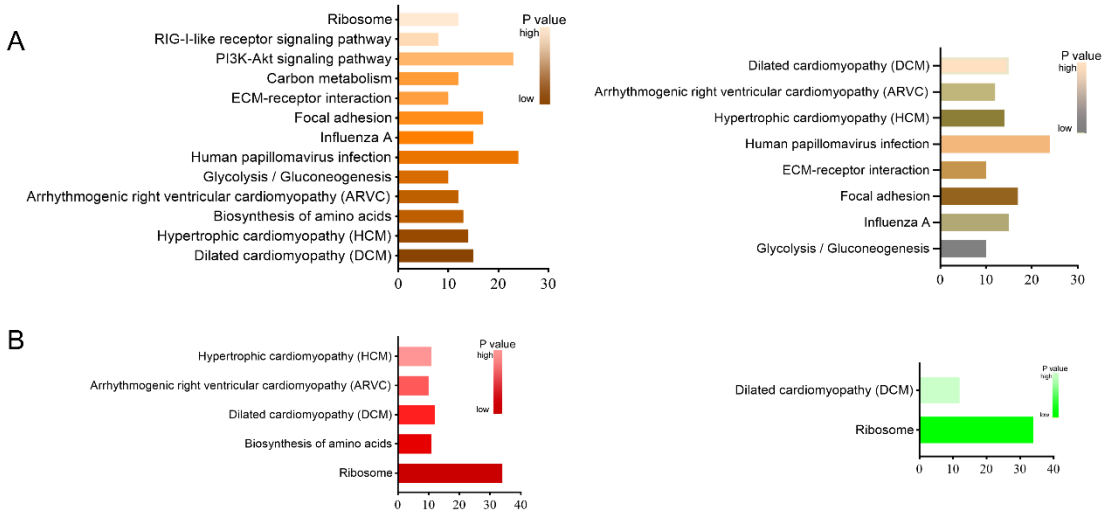
A
Ribosome
RIG-I-like receptor signaling pathway
PI3K-Akt signaling pathway
Carbon metabolism
ECM-receptor interaction
Focal adhesion
Influenza A
Human papillomavirus infection
Glycolysis / Gluconeogenesis
Arrhythmogenic right ventricular cardiomyopathy (ARVC)
Biosynthesis of amino acids
Hypertrophic cardiomyopathy (HCM)
Dilated cardiomyopathy (DCM)
P value
high
low
0 10 20 30
Dilated cardiomyopathy (DCM)
Arrhythmogenic right ventricular cardiomyopathy (ARVC)
Hypertrophic cardiomyopathy (HCM)
Human papillomavirus infection
ECM-receptor interaction
Focal adhesion
Influenza A
Glycolysis / Gluconeogenesis
P value
high
low
0 10 20 30
B
Hypertrophic cardiomyopathy (HCM)
Arrhythmogenic right ventricular cardiomyopathy (ARVC)
Dilated cardiomyopathy (DCM)
Biosynthesis of amino acids
Ribosome
P value
high
low
0 10 20 30 40
Dilated cardiomyopathy (DCM)
Ribosome
0 10 20 30 40

663 **Table S1.** Primary antibody of IF

Primary antibody	Art.No.	Manufacturers
STAT3	#9139	Cell Signal Technology, US
JAK2	#3230	Cell Signal Technology, US

664

665 **Table S2.** Primary antibody of WB

Primary antibody	Art.No.	Manufacturers
STAT3	#9139	Cell Signal Technology, US
p-STAT3	#9134	Cell Signal Technology, US
JAK2	#3230	Cell Signal Technology, US

666

Figure 1

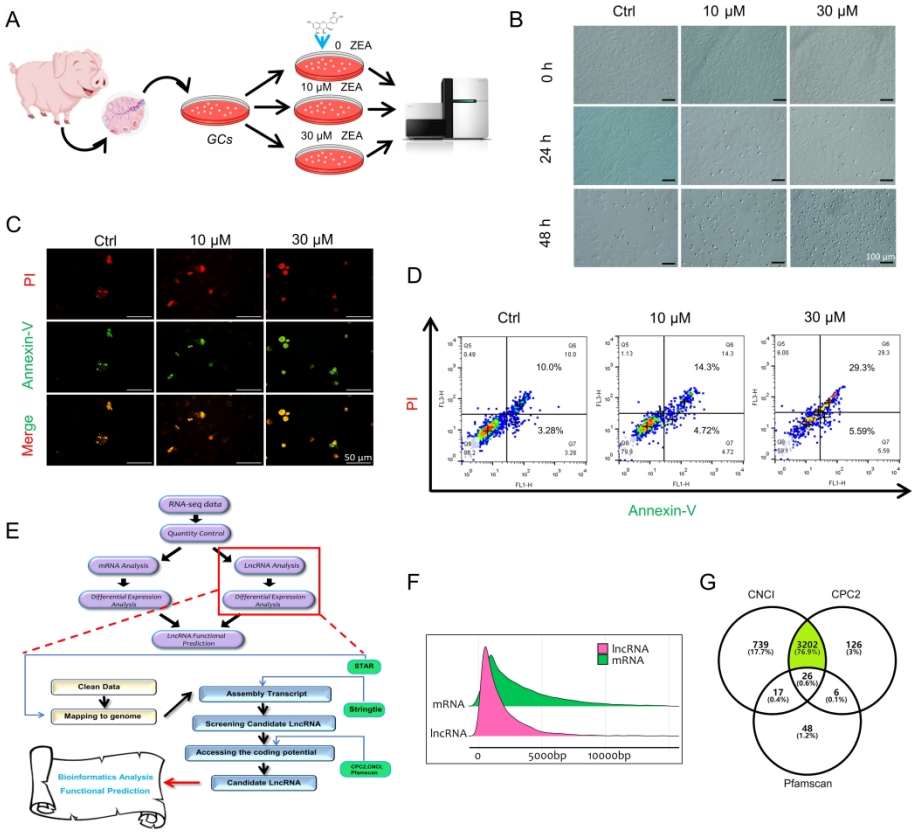

190x179mm (600 x 600 DPI)

Figure 2

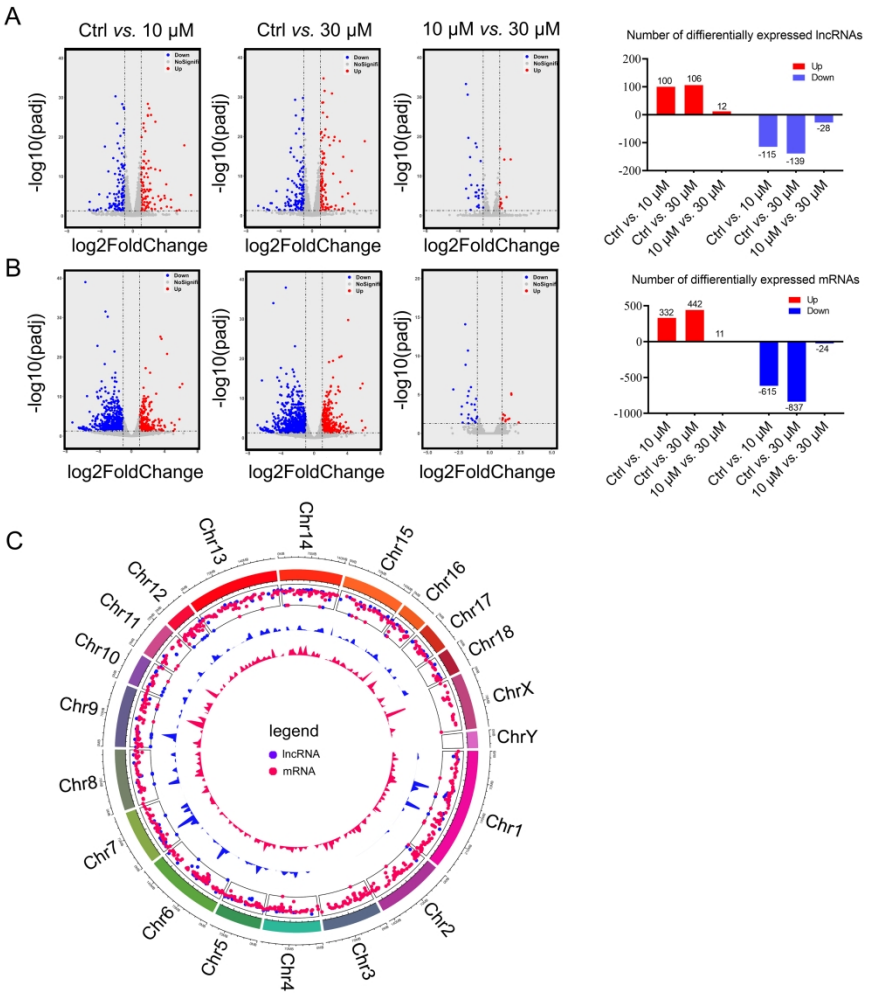

169x188mm (600 x 600 DPI)

Figure 3

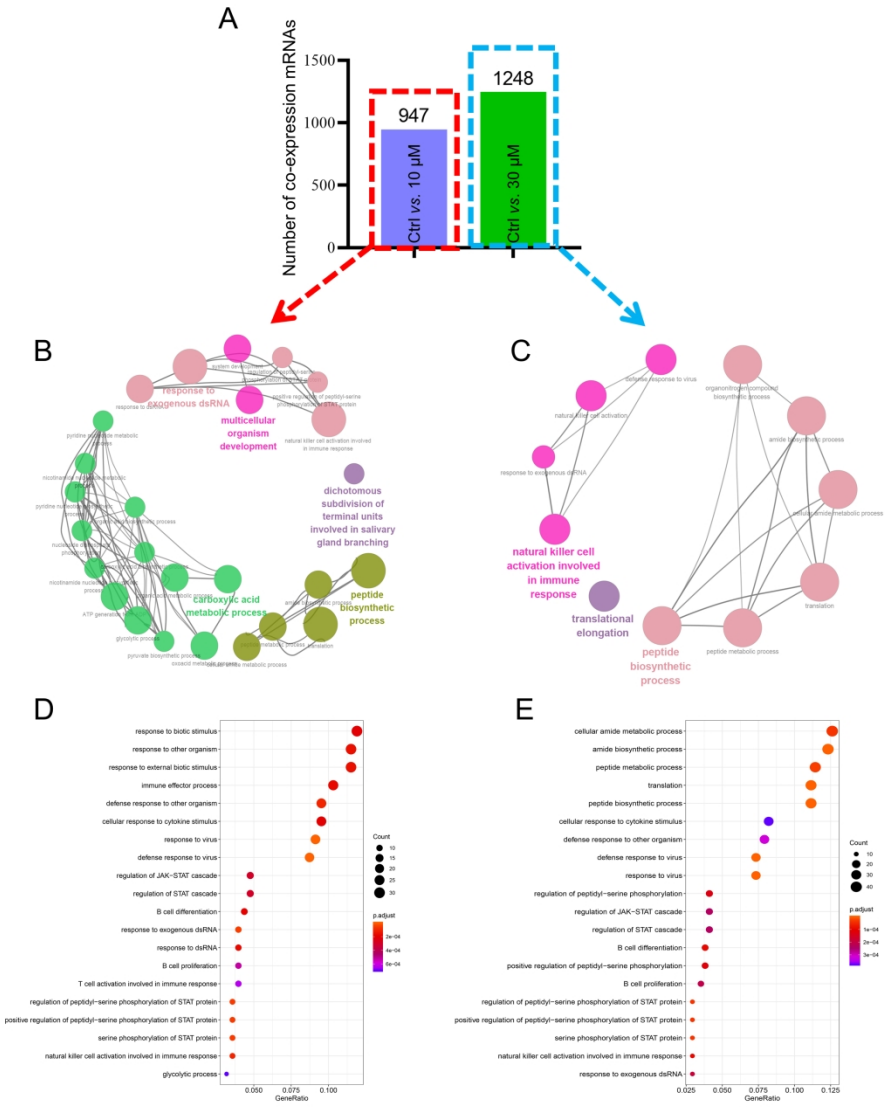

136x172mm (600 x 600 DPI)

Figure 4

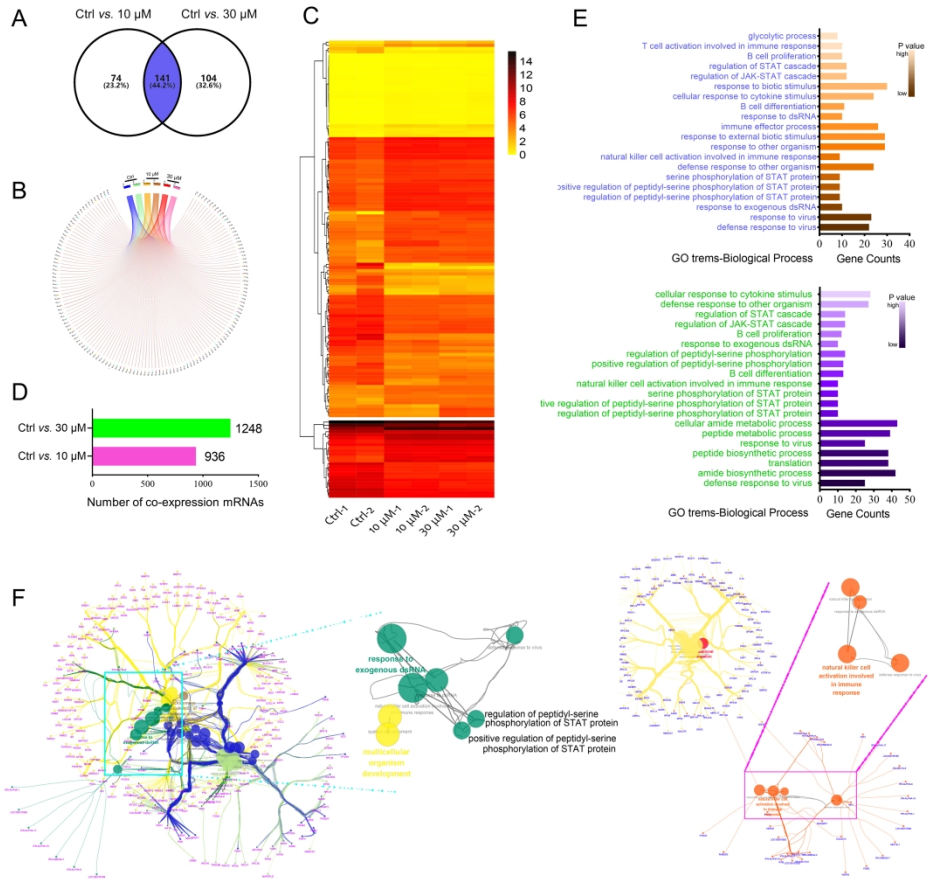

178x180mm (600 x 600 DPI)

Figure 5

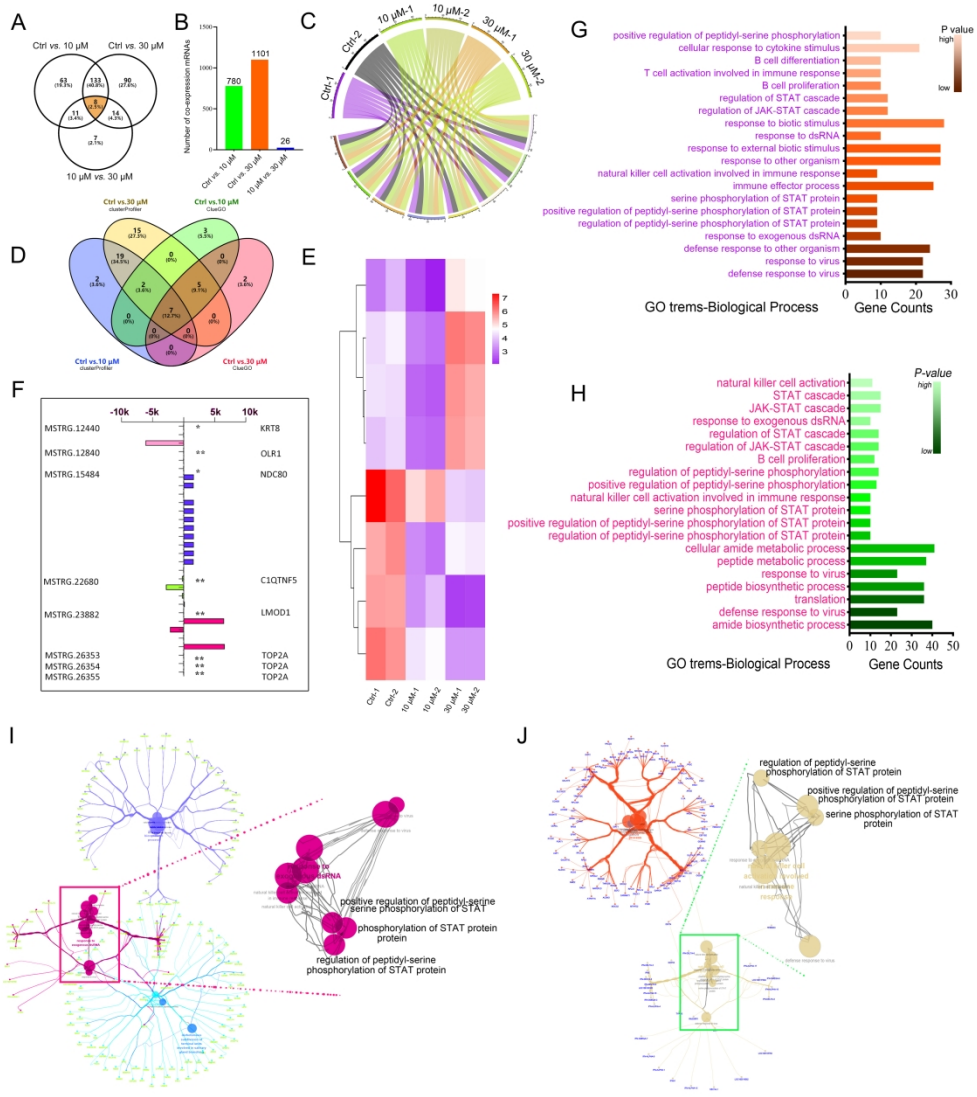

186x220mm (600 x 600 DPI)

Figure 6

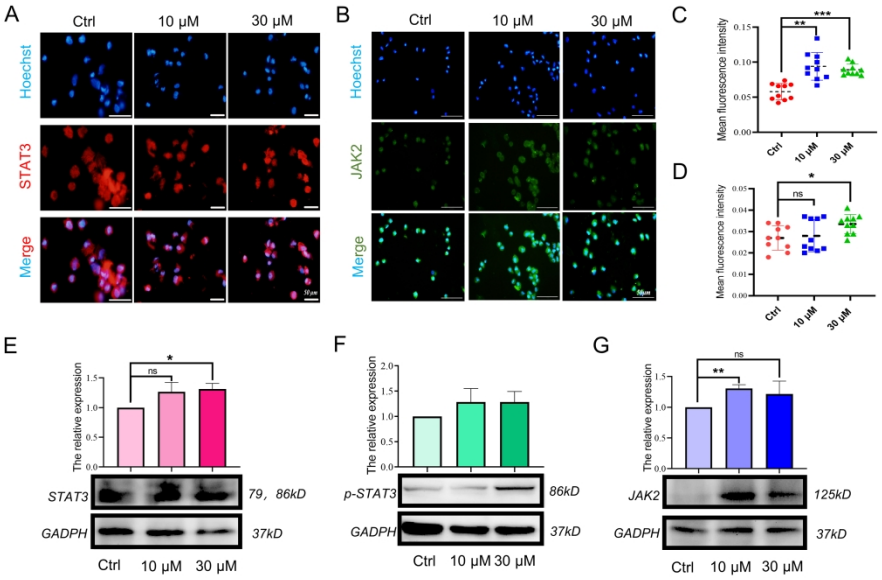

190x123mm (600 x 600 DPI)

Figure 7

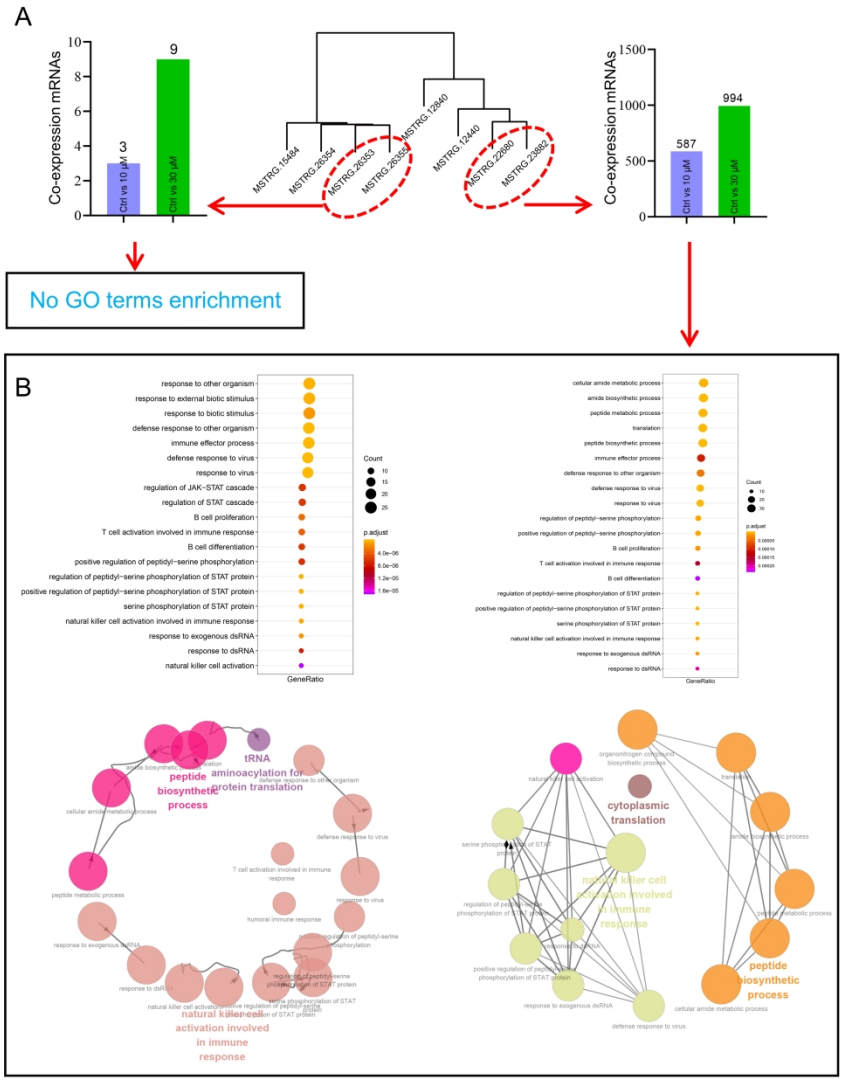

163x194mm (600 x 600 DPI)